Universidade de Aveiro
2021

Departamento de Engenharia de Materiais e Cerâmica

Cristiana Barbosa Lopes Fernandes

Estruturas tridimensionais eletro-estimuláveis à base de nanoestruturas de carbono/hidrogel para engenharia de tecido neuronal

Three-dimensional electro-responsive carbon-reinforced hydrogels for neural tissue engineering

Universidade de Aveiro
2021
Departamento de Engenharia de Materiais e Cerâmica

Cristiana Barbosa Lopes Fernandes

Three-dimensional electro-responsive carbon-reinforced hydrogels for neural tissue engineering

Dissertação apresentada à Universidade de Aveiro para cumprimento dos requisitos necessários à obtenção do grau de Mestre em Materiais e Dispositivos Biomédicos, realizada sob a orientação científica do Doutor Gil Alberto Batista Gonçalves, investigador do Centro de Tecnologia Mecânica e Automação (TEMA) da Universidade de Aveiro, e co-orientação do Professor Doutor Rui Ramos Ferreira e Silva, Professor Associado do Departamento de Engenharia de Materiais e Cerâmica da Universidade de Aveiro, e da Doutora Nathalie Braz Barroca, investigadora do TEMA da Universidade de Aveiro.

This work was supported and financed by the FCT grant UIDB/0048/2020 and UIDP/0048/2020 – Fundação para a Ciência e a Tecnologia; and CENTRO-01-0145-FEDER-022083 - Centro Portugal Regional Operational Programme (Centro2020), under the PORTUGAL 2020 Partnership Agreement, through the European Regional Development Fund.

o júri

presidente	Prof. Doutor João André da Costa Tedim professor auxiliar em Regime Laboral da Universidade de Aveiro
vogal	Doutor Nuno Miguel Franco dos Santos investigador doutorado da Universidade de Aveiro
vogal	Doutor Gil Alberto Batista Gonçalves Investigador auxiliar da Universidade de Aveiro

agradecimentos

Expresso o meu profundo agradecimento ao meu orientador Doutor Gil Gonçalves pela possibilidade que me deu em realizar este trabalho, tornando-o sempre entusiasmante e desafiante tanto a nível pessoal como científico, pela sempre disponibilidade e por toda a sua orientação. Ao co-orientador Professor Doutor Rui Silva, pela orientação, motivação e disponibilidade para fazer mais, que manifestou ao longo deste percurso. À co-orientadora Doutora Nathalie Barroca pela sua disponibilidade na partilha de conhecimento e discussão ativa dos problemas e soluções que foram surgindo ao longo do trabalho.

Ao Doutor Ricardo Silva e à Inês Oliveira por toda a contribuição no processo de crescimento das amostras de VA-CNTs, bem como o bom ambiente de trabalho, amizade, aconselhamento e a constante discussão proativa, que sempre me incentivou a trabalhar. À Daniela Silva e à Ângela Semitela por todos os ensinamentos, ajuda e incansável disponibilidade na execução dos estudos biológicos e a total disponibilidade para discutir os resultados, que enriqueceram este trabalho.

A todos os responsáveis pela ajuda nas demais caracterizações utilizadas neste trabalho.

À Universidade de Aveiro, ao Departamento de Engenharia de Materiais e Cerâmica e ao Centro de Tecnologia Mecânica e Automação.

Aos meus amigos, com quem pude sempre contar com apoio incondicional, uma gargalhada certa e longas conversas, aliviando momentos mais stressantes.

Ao meu namorado e melhor amigo Henrique, por todas as melhores e piores horas, garantindo sempre a sua constante e incansável disponibilidade em tudo o que precisasse, motivando-me e trazendo-me o equilíbrio necessário para continuar a trabalhar pelos meus objetivos.

À minha família, por todo o amor e carinho, pela paciência e apoio que me prestaram, não só no decorrer deste percurso, mas também ao longo de toda a minha vida.

A todos,
muito obrigada!

palavras-chave

Nanotubos de carbono verticalmente alinhados, micropilares, densificação, hidrogéis, células estaminais neurais, eletroestimulação, lesão da medula espinal

resumo

O principal objetivo do presente trabalho constituiu na otimização da produção de estruturas tridimensionais eletro-estimuláveis à base de nanoestruturas de carbono/hidrogel, estudando a sua citocompatibilidade com células estaminais para engenharia de tecido neuronal.

Nesse sentido foram primeiramente preparados dois padrões de nanotubos de carbono verticalmente alinhados (VA-CNTs) por deposição química em fase vapor (T-CVD): (1) floresta densa de VA-CNTs e (2) micropilares de VA-CNTs. Além disso, foram também estudados os substratos anteriormente descritos após tratamento por vapor de acetona, resultando na formação de VA-CNTs e micropadrões colapsados, apresentando uma morfologia com um padrão celular e uma semelhante a uma "flor", respetivamente. As respetivas amostras foram caracterizadas por microscopia eletrónica de varrimento (SEM), de transmissão (TEM) e foi medido o ângulo de contacto com a água (WCA). As diferentes amostras estudadas foram exploradas na integração com hidrogéis à base de gelatina metacrilada (GelMA).

A influência dos diferentes padrões de VA-CNTs preparados foi estudada através da avaliação do comportamento celular com o recurso a células estaminais neurais (NSCs). Por ensaios de imunocitoquímica, viabilidade celular e SEM, foi observada a afinidade das células para com as diversas estruturas de carbono, em comparação com o substrato de silício (Si). Para além disso foi também verificada a aptidão das diversas estruturas baseadas em VA-CNTs como plataformas para proliferação e diferenciação de NSCs. Os substratos de VA-CNTs colapsados evidenciaram uma propensão para induzir a diferenciação celular em neurónios, possivelmente devido à sua rugosidade superficial à nanoescala favorecer este mecanismo biológico.

Os resultados obtidos demonstraram que as estruturas baseadas em VA-CNTs favorecem a proliferação e diferenciação das células estaminais neurais, podendo futuramente ser aplicados como estruturas tridimensionais eletro-estimuláveis com elevado desempenho para engenharia de tecido neural.

keywords

Vertically aligned carbon nanotubes, micropillars, densification, hydrogels, neural stem cells, eletro-responsive, spinal cord injury

abstract

The main objective of the present work consists of the optimization of the production of three-dimensional electro-responsive carbon-reinforced hydrogels, to study their cytocompatibility with neural stem cells (NSCs) for neural tissue engineering.

For that matter, initially vertically aligned carbon nanotubes (VA-CNTs) with two different patterns were prepared by thermal chemical vapor deposition (T-CVD): (1) VA-CNTs dense forest and (1) VA-CNTs micropillars. Furthermore, the substrates previously described were studied after acetone vapor treatment, resulting in a cellular and “flower-like” pattern morphology, respectively. Structural characterization of the respective samples was made using scanning electron microscopy (SEM), transmission electron microscopy (TEM) and the measurement of the water contact angle (WCA). The integration with gelatin-methacryloyl (GelMA) -based hydrogels were explored in the different studied samples.

The influence of the different VA-CNTs prepared patterns was studied by the evaluation of the cell behavior with resort to NSCs. By immunocytochemical staining, cell viability assays and SEM, it was observed the cells affinity for the diverse carbon structures, in comparison to the silicon (Si) substrate. Besides, it was also verified the suitability of the VA-CNTs platforms for cell viability and proliferation. The collapsed VA-CNTs substrate made evident the tendency for cell differentiation into neurons, possibly due to their superficial roughness at the nanoscale, which favors this biological mechanism.

The results obtained demonstrated that VA-CNTs based structures favors the proliferation and differentiation of NSCs, making them promising as future three-dimensional electroresponsive structures with excellent performances for neural tissue engineering.

Content

List of Figures

List of Tables

Abbreviations and Acronyms List

3D - three-dimensional

AFM - atomic force microscopy

Anti-Tuj1 - anti-tubulin β 3

ATCC - american type culture collection

ATR-FTIR - attenuated total reflectance fourier-transform infrared

BSA - bovine serum albumin

BSE - back-scattered electrons

CBN - carbon based nanomaterial

CNS - central nervous system

CNT - carbon nanotube

CVD – chemical vapor deposition

DAPI - 4’,6-diamidino-2-phenylindole

DC - direct current

DPBS - Dulbecco's phosphate buffer saline

EAD - electric arc discharge

ECM - extracellular matrix

EDS - energy dispersive X-ray spectroscopy

EDTA - ethylenediamine tetraacetic acid

EMEM - Eagle's minimum essential medium

ESC - embryonic stem cell

Eth D-1 - ethidium homodimer-1

f-CNT - functionalized-carbon nanotube

FBS - fetal bovine serum

GelMA - gelatin-methacryloyl

GFAP - glial fibrillary acidic protein

GIXRD - grazing incident X-ray diffraction

GO – graphene oxide

HDMS – hexamethyldisilazane

ITS - insulin-transferrin-selenium

LA - laser ablation

LAP - lithium phenyl-2,4,6-trimethylbenzoylphosphinate

MAA - methacrylic anhyhidride

MSC - mesenchymal stem cell

MWCNT - multi-walled carbon nanotube

NSC - neural stem cell

O.D.f - final optical density

P/S - penicillin/streptomycin

PBS - phosphate buffer saline

PCL - poly-ϵ-caprolactone

PEG - polyethylene glycol

PET - positron emission tomgraphy

PGA - poly-glycolic acid

PLA - poly-lactic acid

PLGA - poly-lactic-co-glycolic acid

PNS - peripheral nervous system

PVD - physical vapor deposition

RA - retinoic acid

RF - radio frequency

rGO – reduced graphene oxide

RMS - roughness

RT - room temperature

SCB - sodium cacodylate buffer

SCI - spinal cord injury

SD - standard deviation

SE - secondary electron

SEM - scanning electron microscopy

SWCNT - single-walled carbon nanotube

T-CVD - thermal-chemical vapor deposition

TEM - transmission electron microscopy

VA-CNT - vertically aligned carbon nanotube

WCA - water contact angle

YM – Young’s modulus

Chapter 1- Framework and objectives

The development of three dimensional (3D) arrays of vertically aligned carbon nanotubes (VA-CNTs) with controllable lengths and physicochemical properties remains a topic that generates interest from a broad range of applications across different research fields. In cell culture and tissue engineering applications, the VA-CNTs microstructures can mimic the 3D environment of native tissues and stimulate cell growth.

The most common method for fabricating VA-CNTs, the so-called "forests", is by thermal-chemical vapor deposition (T-CVD) using a continuous or patterned metallic catalyst films deposited by a physical vapor deposition (PVD) process. The T-CVD approach enables vertical self-organization of carbon nanotubes (CNTs) on a silicon (Si) substrate, and this mechanically favorable configuration facilitates the growth of VA-CNTs whose length can reach up to several micrometers. In this work, we present a deposition-growth-densification process to produce high density VA-CNT forests and micropatterned VA-CNT forest. The catalyst preparation process employs alumina (Al_2O_3) and iron (Fe) as the multilayer catalyst, conventional T-CVD to grow VA-CNTs forests and the liquid-induced densification process to increase the density of VA-CNTs forests. During the densification process, cellular pattern or "flower-like" pattern of the VA-CNTs forests are formed by strong capillary force during solvent evaporation and Van der Waals interaction between the nanotubes.

The following objective is to incorporate a hydrogel onto the grown VA-CNTs patterns to better mimic the *in vivo* environment for the seeded neural stem cells (NSCs). The hydrogel is the outcome of the modification of gelatin with methacrylic anhydride (MAA), resulting in gelatin-methacryloyl (GelMA), that can photopolymerize by the presence of the water-soluble lithium phenyl-2,4,6-trimethylbenzoylphosphinate (LAP) under visible light. To obtain the biohybrid, GelMA deposition was carried by spin coating and solvent cast onto the surface of VA-CNTs.

Simultaneously, the cytocompatibility of the different CNTs based platforms is investigated in view of using them as electroresponsive platforms (see Figure 1). NSCs, namely NE-4C cells are seeded onto the various CNTs structures with different patterning

and their viability, proliferation and differentiation are analyzed over a 14 days culture period.

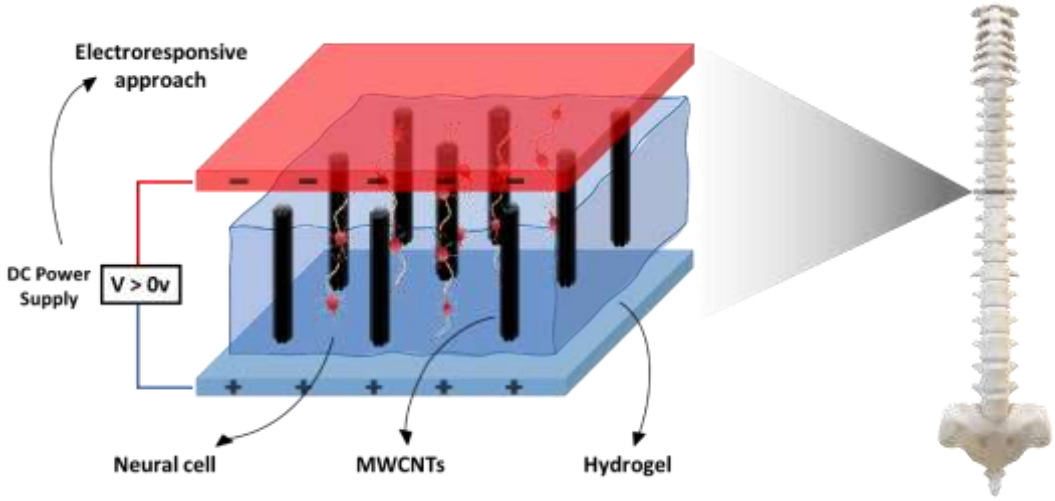

Figure 1 - Conceptual illustration of the VA-CNTs application in neuro-prosthetic field.

The present dissertation is divided in six chapters, including this one.

On chapter 2, a literature review is presented about the general issues on the structure and synthesis of the main components of the scaffold in study, CNTs, hydrogel and NSCs, as well as their application on tissue engineering. On chapter 3, the experimental procedure of the production of the CNTs substrates is described, namely the multilayer catalyst preparation, synthesis and micro-patterning of VA-CNT, and the capillary driven process. There is also a description of the characterization techniques used and their results. On chapter 4, the preparation of the hydrogel is described, along with its experimental results. On chapter 5, the cell culture and assays required to test cell viability and the CNTs cytocompatibility are reported, and the results obtained discussed. Finally, chapter 6 presents the main conclusions obtained during this work and future work.

Chapter 2 – Literature Review

1. Nanotechnology

Nanotechnology has flourished into the most progressive field of research as a result of the various applications and possibility to custom-design the properties of a material, by changing their composition, size and shape [1]. As this new concept is considered to be the future, with the most advanced manufacturing technology today, it was first introduced in 1959 by the Nobel acclaimed Richard Feynman, which stated "*The principles of physics, as far as I can see, do not speak against the possibility of maneuvering things atom by atom*". Later, the Nanotechnology National Initiative defined nanotechnology as the "*understanding and control of matter at the nanoscale, at dimensions between approximately 1 and 100 nm*" [2][3][4].

The main approach that characterizes this field of research can be divided in two concepts. The "bottom up" that consists of the precise arrangement of individual atoms or molecular building blocks where they are needed, by scanning probe microscopy or self-assembling to create objects at nano, micro and macroscale. The second concept, on opposition to the previously mentioned, lies on the conversion of macro-scale systems into nanoscale, by a continuous of reduction operations to discard undesired elements of the system. For this reason, the concept is termed "top down" [2][3].

Nanotechnology has been and will continue to affect people's lives. With the prodigious discovery of the carbon nanostructures, carbon nanotechnology became a significant part of the field of research for the development of Hi-Tech applications. Indeed, the relevance of carbon nanotubes for the scientific community was already recognized by the attribution of two Nobel prizes by The Royal Swedish Academy of Sciences: The Nobel Prize in Chemistry 1996 attributed to Robert F. Curl Jr., Sir Harold W. Kroto and Richard E. Smalley "*for their discovery of fullerenes*" [5] and The Nobel Prize in Physics 2010 attributed to Andre Geim and Konstantin Novoselov for "*groundbreaking experiments regarding the two-dimensional material graphene*" [6]. The versability of carbon materials can either be found on nature [7] as well as synthetic approaches, which allows this technology to be applied in different areas [8].

2. Carbon Nanomaterials

Carbon is an element of superior importance, not only for life but as a functional material for many applications. Depending on the arrangement assumed by the carbon atoms, different allotropic structures with completely different properties can be expected [9]. The most typically studied carbon-based nanomaterials (CBNs) are fullerenes, graphene, and CNTs (Figure 2) [10]. These nanoparticles are not only appealing considering their high electrical conductivity, chemical stability, great mechanical properties, and light weight, but also owing to their unique optical, electronic, mechanical, thermal, and chemical properties [11][12]. Depending on the properties already mentioned and the structural arrangement, carbon nanomaterials can assume multiple classifications according to their dimensionality.

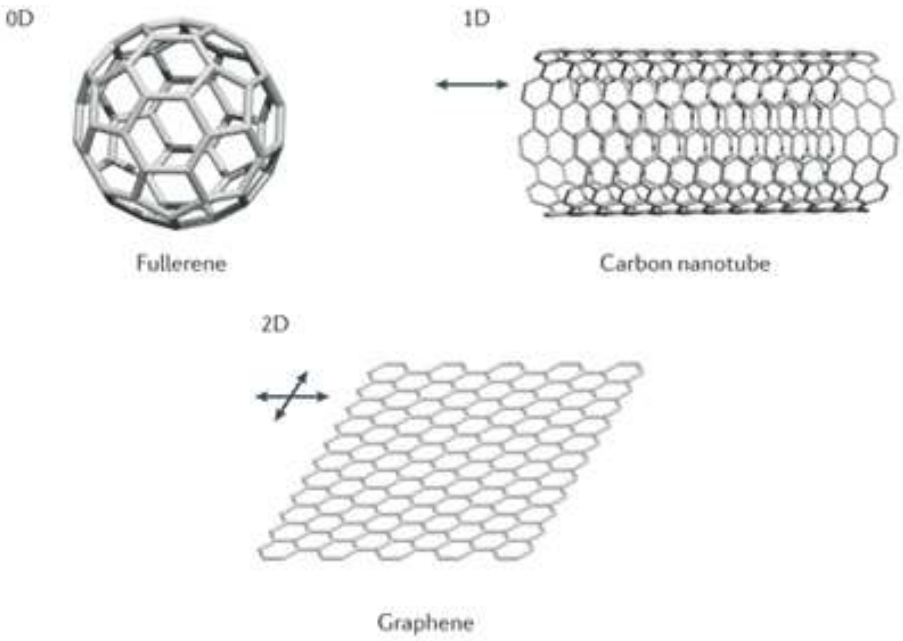

Figure 2 - Fullerenes, carbon nanotubes, graphene represent 0D, 1D, 2D nanocarbons, respectively.[13]

Fullerene is a polyaromatic, symmetrical, and hollow spherical cage with 60 carbon atoms (C_{60}), constituted by pentagons and hexagons only, resulting in a trivalent convex polyhedron with exactly three sp^2 hybridized carbon bonds joining every vertex [14]. They can be obtained by synthetic methods, carbon-arc synthesis from solid graphite, or found in nature or even in the interstellar space [7]. An almost infinite number of fullerenes isomers

can be obtained with many different shapes depending on the distribution of the pentagons and the number of carbon atoms [15]. Fullerenes have been explored in numerous applications, namely energy production and semiconductors, but also in antiviral and photodynamic therapies, antibacterial agents, and drug carriers in the medical field [9][5][16].

Graphene is another allotropic carbon nanomaterial composed of an atomic sheet of sp^2 carbon arranged in a honey-comb pattern, being the first 2D crystal isolated under room conditions [17]. The pioneer studies were correlated to its peculiar electronic behavior under magnetic field at low temperature. Since the early report, many interesting properties have been reported for graphene, including high charge carrier mobilities of 200 000 cm^{-2}/V s, high optical transparency of 97.7%, a high thermal conductivity of 5000 W m^{-1} K^{-1}, a high Young's Modulus (YM) of ∼1 TPa and a large specific surface area of 2630 m^2 g^{-1} [18]. It was considered a versatile building block for energy storage, biosensing, and anticancer therapies [16]. Depending on number of layers, graphene can assume different properties, varying from a single to multiple graphene layers [19].

Nowadays, a large number of graphene derivatives have been reported in the literature, that consist of the heteroatom doping of the 2D aromatic structure [20], namely graphene oxide (GO) and reduced graphene oxide (rGO), that founded interesting potential applications for longer-lasting batteries, more efficient solar cells, corrosion prevention, bending electronics and advanced medicinal technologies [18].

CNTs are cylindric nanostructures resulting from rolled-up in single-walled (SWCNTs) or multi-walled (MWCNTs) concentric graphene layers, with tunable physical characteristics, depending on the length, diameter, chirality, and number of layers [21]. SWCNTs are characterized by a diameter in the range of 0.4–2.0 nm and few μm in length, while MWCNTs diameters is up to 100 nm and the length from 1 to several μm. Their extraordinary structural, electronic, mechanical and chemical properties have been explored by the scientific community for applications in field emission, energy storage and electronics [22], as well recently showed their potential uses for the development of quantum-photonic devices [23].

A growing field for exploring the CNTs outstanding properties is related to their inclusion in new biomaterials for medical applications, for instance: *in vivo* imaging systems,

drug delivery and advanced scaffolds for tissue engineering, namely bone, cardiac and nerve regeneration [24].

However, there are still some concerns about the poor understanding on how to safely expand and apply engineered nanomaterials, which includes CNTs, that could lead to unknown threats to the human health and environment [25]. For this reason, the biocompatibility and toxicity of the nanomaterials are the most important matter when it comes to the use of CNTs as a biomaterial for implantation in the human body [26].

2.1.Carbon Nanotubes

2.1.1. Structure

CNTs are an allotropic form of carbon arranged in a cylindrical structure made of graphene sheets [27]. According to the number of walls, they can be characterized as SWCNTs and MWCNTs. The SWCNTs (Figure 3a) exhibit solely one rolled up graphene layer, while MWCNTs (Figure 3b) can present two or more graphene tubes, with diameters in the order of few to many nanometers [28]. The cylindrical structure is made of a hexagonal arrangement of sp^2 hybridized carbon network that can provide singular properties to the nanostructure.

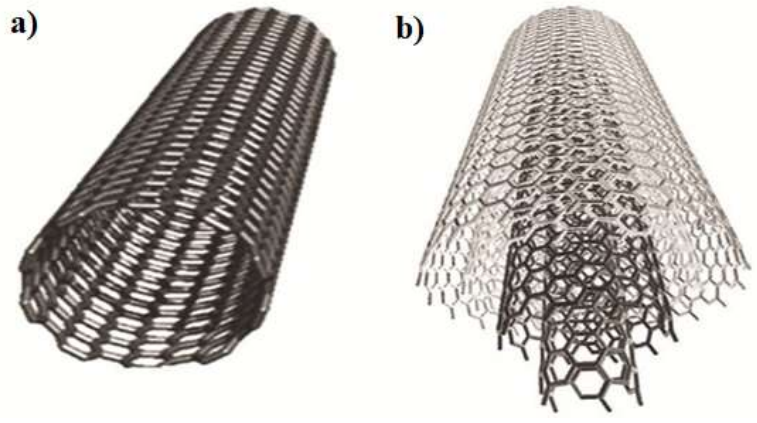

Figure 3 - Diagram of a) SWCNT and b) MWCNT.[28]

2.1.2. Properties and Applications

Depending on the rolling up direction, the CNTs properties can alter between a metal like conductor, with relatively high conductivity, typical for armchair tubes structures, or semiconductor, distinctive of zigzag and chiral structures (Figure 4) [29]. Besides the high conductivity of the CNTs, the nanostructure offers outstanding properties that make it a very interesting approach for research. Along with their excellent electrical potential, the material also retains superior YM with high tensile strength, exceptional thermal conductivity, and chemical stability [30][31]. Due to their properties, CNTs revealed themselves has an adaptable application for different fields of engineering such as: structural reinforcement in composites, coatings (considering their hydrophobic nature), nanoelectronic devices, batteries, sensing devices, among other examples [32]. Taking into account their carbon purity and length [26], CNTs show high biocompatibility, low toxicity, and immunogenicity, fitting them as an ideal candidate for biomedical applications. In this context, the biocompatibility can be defined as "*the ability of a material to perform with an appropriate host response in a specific application*" [33]. Biosensors, drug delivery systems, growth substrate, and composites for implants or scaffolds, are given as application examples [34][35]. Nevertheless, it should be stressed out that the success of CNTs technology in biomedical field is dependent upon the continuation of research into the toxicology of CNTs and their related biomaterials.

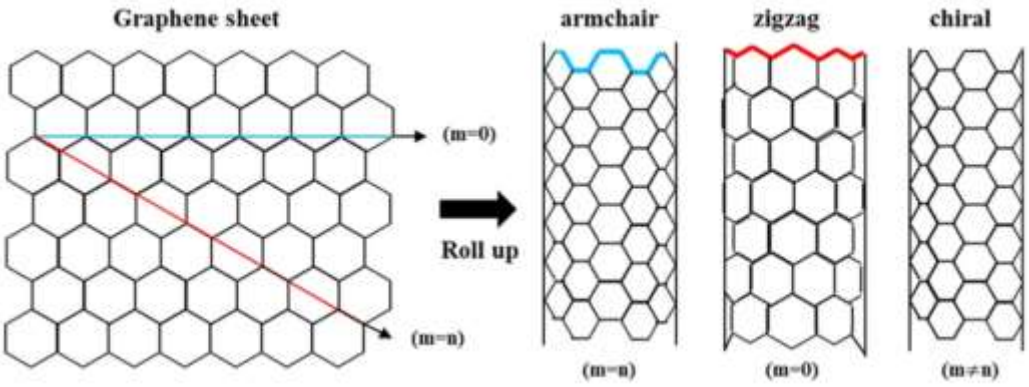

Figure 4 - CNT configurations: zigzag, armchair, and chiral.[29]

2.1.3. Synthesis of VA-CNTs

Vertically aligned CNTs also known as VA-CNTs forests or arrays, present outstanding properties and a great potential for a wide variety of applications such as functional material benefiting from the vertical alignment morphology. The CNTs can be grown by different preparation methods, in particular high-temperature methods. For the growth of high-quality VA-CNTs on solid substrates a catalytically driven T-CVD process is the most often used approach, allowing tunability of the resulting VA-CNTs material properties [3]. To this end, a catalyst composed of metallic element combined with a buffer layer, which should be deposited on a solid substrate before the deposition of the metallic catalyst thin film, such as iron, nickel, or cobalt (Fe, Ni or Co). The buffer layers are used to prevent the diffusion of the metallic catalyst into the substrates (e.g., Si wafer), in order to improve the CNTs yield growth process. In this way, it is very important to produce high-quality buffer layers, such as alumina, titanium nitride or titanium dioxide (Al_2O_3, TiN or TiO_2) [36]. The catalyst composition containing a dedicated combination of elements ranging from metallic to oxide ceramics thin films, which is commonly classified as multilayer or binary catalyst. The synthesis of CNTs is divided into three main methods such as electric arc discharge (EAD), laser ablation (LA) and chemical vapor deposition (CVD). Therefore, each method will grant CNTs distinctive yield, morphology and degree of purity [37].

i. Electric Arc Discharge: an electric arc discharge is caused by two cylindrical graphite electrodes inside a steel chamber with inert gas. As the electrodes get closer, the current starts to flow and generates plasma between them. The temperature reached is on the range of 3000 to 4000ºC, which leads to the graphite sublimation at the electrodes [38]. This technique has been explored for the synthesis of both, SWCNTs and MWCNTs, and present as a main advantage the simple setup, the possibility to obtain high product yields with fewer structural defects in comparison with other methods. As main advantages, it requires high temperature and purification steps of the final products (tangled nanotubes).

ii. Laser ablation: the process is resultant of vaporizing a graphite electrode through a high-powered laser. When the graphite inside the quartz involucre

reaches temperatures on the order of 1200ºC, the tube is filled with an inert gas. Then, the laser sweeps across the graphite surface, vaporizing it and forming CNTs [38]. The main advantages of this technique consist of a relatively high production yield and relatively low metallic impurities on final structure of CNTs. On other hand, the main disadvantage is the heterogeneity of the produced CNTs and is considered an expensive process that have been limiting their application mostly to the lab scale.

iii. Chemical vapor deposition (depending on the activation source of the reactant gases *i.e.*, thermal- or plasma enhanced-CVD): this method needs a set of metallic catalyst particles (Fe, Ni, Co) on a furnace with temperatures varying between 500 and 700ºC. The nanotubes are formed by the decomposition of the carbon gas precursors on a substrate previously coated with a catalyst [38]. This method presents as main advantages, the economically viable and large-scale production of high purity CNTs and easy control of the reaction parameters and possibility for aligned growth. Nevertheless, the synthesis products usually consist in MWCNTs and the catalyst particles can remain inside of the nanotube structure, after their growth.

2.1.4. Synthesis of VA-CNTs by CVD

From the practical point of view the CVD growth of CNTs can be divided mainly into four steps: *(i)* initially, the chamber goes through the heating phase, followed by the argon (Ar) flow, in order to stabilize synthesis temperature, *(ii)* the pre-treatment of the catalyst begins. This step operates in a reducing gas environment, with Ar and hydrogen (H_2) flow where de Ar is used as a carrier gas [39]. The pre-treatment phase is responsible for the formation of active catalysts nanoparticles (Fe, Ni or Co) over the substrate, so that later CNTs can nucleate and grow [40]. *(iii)* The CNTs growth process initiates, with the presence of Ar, H_2 and acetylene (C_2H_2). The C_2H_2 is used as the carbon source, that leads to the formation of metastable carbon molecules, which diffuse down for the growth of the CNTs. The CNTs growth process is divided into two main chemical mechanisms (Figure 5):

(a) the ‘tip-growth’, that occurs when the catalyst particles are not well fixed on the substrate, leading to its lift upon the CNT growth; and (b) the ‘base-growth’ that consist of the remaining of the particle attached to the substrate [40]. *(iv)* The last step consists of the decrease of the furnace temperature while filled with Ar, for cooling stage and removal of reaction by-products.

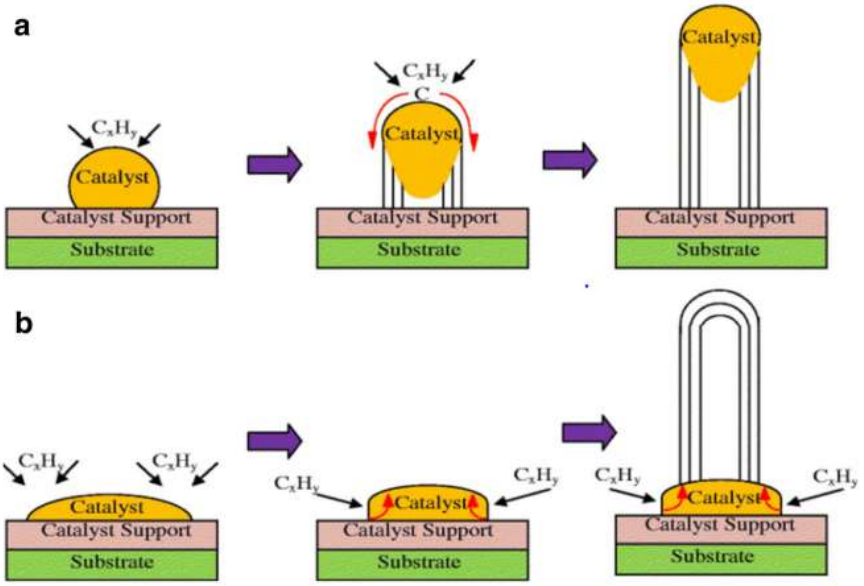

Figure 5 - Different growth mechanisms of CNTs using T-CVD. a) Tip-growth model, b) Base-growth model.[41]

2.1.5. Exohedral Funcionalization of CNTs

The CNTs surface takes a relevant part on the interaction of the nanostructures with their involving environment. The properties responsible for this behavior are the hydrophobic nature of the nanotubes, that makes them insoluble in water as well as in the most common organic solvents and the agglomeration of the CNTs is a consequence of the strong Van der Waals forces between the nanotubes [42]. On the other hand, the functionalization of the nanotubes induces the weaken of the strong hydrophobicity, leading to increased dispersibility on water solutions, allowing the bond with the graphene surface, enabling the creation of hybrid materials [37]. Hereby, to obtain a versatile structure, with tuned electrical and chemical properties while preserving its intrinsic properties, prone to be used in the diverse scientific and technological areas, therefore the CNTs functionalization must be considered towards the intended application [39]. From the practical point of view,

exohedral functionalization consists on the attachment of functional groups or molecules on their external surface walls [43].

The external surface functionalization of the CNTs can be explored using two different approaches according to the type of the chemical bond stablished: covalent and non-covalent. The typical covalent functionalization involves the linkage of functional groups to the main body of the CNTs, by covalent bonds (Figure 6). The defective carbon atoms present on the walls or at the tips of the CNTs, can be oxidized by strong oxidants, generating carboxylic acid groups. The functional group can then be converted into acid chloride and esterified, to increase the CNTs reactivity, and allow the attachment of hydrophilic molecules [29]. However, many other approaches have been developed so far for the chemical covalent functionalization of CNTs surface or inner cavity [44].

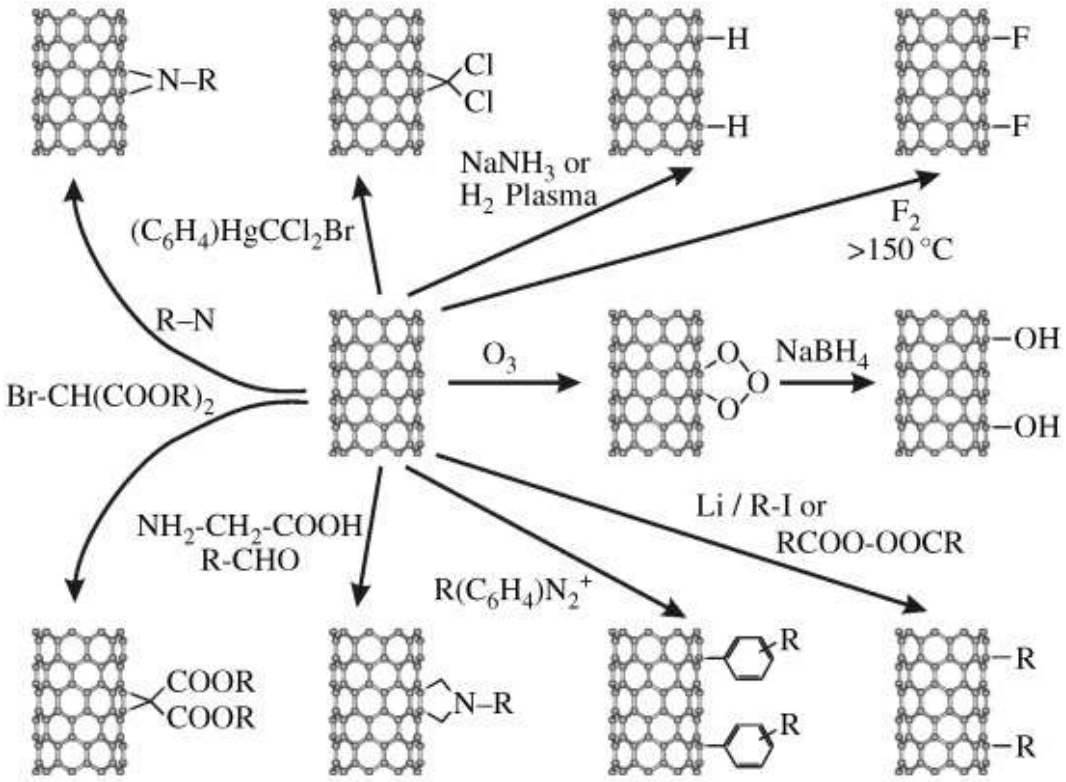

Figure 6 - Schematic representation of the different approaches for CNTs covalent surface functionalization.[44]

The non-covalent strategy is based on physical bonding, as it involves Van der Walls forces, hydrogen bonds, electrostatic forces and π-π interaction, to attain the physical

adsorption of molecules in the CNTs sidewalls. Non-covalent functionalization can be divided into two main methods that takes advantage of the aromatic nature of the CNTs surface (Figure 7). The first approach lies on the wrapping of surfactants or polymer chains on the nanotube's walls, and the other one is accomplished by π- π stacking interactions between aromatic rings of grafted materials and π-electrons of graphitic sheets on the surface of the nanostructures. The grafted surfactants and the polymer act as dispersing agents in order to increase the CNTs solubility in aqueous solutions or increment their compatibility for integration in many different polymeric, metallic or ceramic matrices. This non-covalent strategy have been widely explored in biomedical applications, due to the high affinity between the nanostructures and biomolecules, like DNA, RNA, peptides and enzymes [29][45].

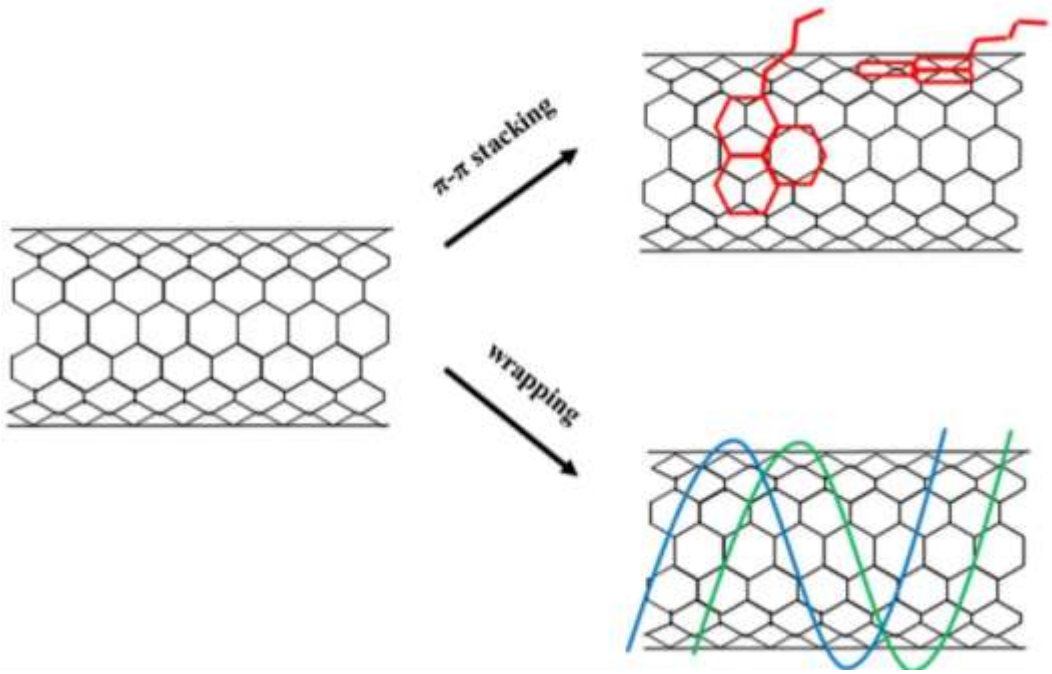

Figure 7 - Two non-covalent approaches to functionalize the CNTs.[29]

In summary, the covalent functionalization of the nanotubes enhances their processability and functionality, acting as a more stable and robust approach in comparison to the non-covalent strategy. Nonetheless, the disruption of the π networks on the nanotubes structure can strongly affect their physical and chemical properties [29].

2.2.Carbon Nanotubes in Tissue Engineering

The use of CNTs becomes relevant for tissue engineering as a nano-filler, not only due to its advantageous properties, as cellular uptake, high stability, and electromagnetic behavior, but also owing to the crosslinking of these nano structures to hydrogels [46]. Hydrogels are characterized as a biocompatible and biodegradable polymeric network, complemented with a hydrophilic environment, capable to mimic the architecture and properties of the soft tissue [47].

Therefore, these hybrid systems have been gaining great importance in tissue engineering, as scaffolds for organ growth, 3D printing and bio-sensing applications [46]. It is important that certain properties are maintained to ensure the recolonization and proper function of cells and tissues, exhibiting high mechanical strength and significant conductivity of the material, along with the mechanical resistance, biocompatibility, good cell adhesion and cross-linked networks. However, the use of CNTs demands the regulation of the cytotoxicity and nanotubes purity, by means of their concentration, which may affect cell viability [46].

Many studies have indicated and concluded about the potential toxicity of CBNs and CNTs, on either single- or multi-walled CNTs [48][49]. The groups most affected by this possible hazardous material are the ones that generate and handle it, as they are susceptible to the material inhalation, ingestion, or cutaneous absorption [50]. However, in the particular study case, the CNTs are fixed to a substrate, which means that the possible danger brought by the material occurs once it is implanted.

Early reports showed that histopathological studies determined that SWCNTs induce acute and chronic pulmonary pathologies [51], systematic damage in the blood chemistry [52], liver [53] and cardiovascular system [54], further MWCNTs exposure has led to oxidative stress on cells [55][56], development of pulmonary fibrosis [57] and lung tumors [58], inhibition of growth, viability, photosynthetic properties, decreased metabolic activity [56], increase in cell death rate [59].

However, the toxicity of the CNTs depends on various parameters such as their size, length, shape, surface area, tendency for agglomeration, as well as the presence and nature of catalyst residuals generated during the fabrication process of CNTs [29]. Interestingly,

the high aspect ratio of CNTs makes them unusual for toxicological investigation in that they share shape characteristics with both nanoparticles and fibers [60]. Studies showed that not only the nanostructure morphology was a factor, but the low toxicity of the MWCNTs could also be related to their hydrophobic properties, which affected the contact between MWCNTs and cells [59][50]. These characteristics are schematically represented in Figure 8.

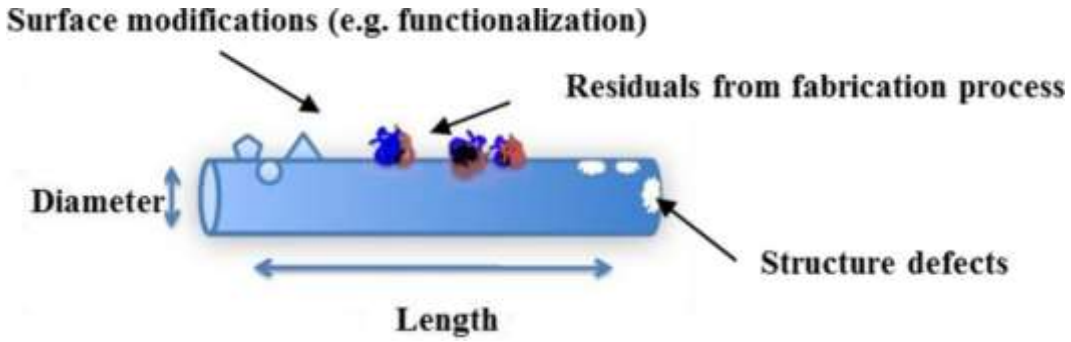

Figure 8 - Schematic illustration of several factors that might cause CNTs toxicity.[29]

Prato *et al.* reported that the introduction of hydrophilic moieties to CNTs allows the formation of less biologically active nanostructures, with easier transport along the organism (*e.g.* circulatory system, tissue parenchyma), therefore reaching the CNTs biocompatibility. Another aspect to take into consideration is the CNTs biodegradability which can be facilitated by their chemical functionalization and structural defects. In fact, it has been shown that functionalized CNTs can be degraded by oxidative enzymes [26]. S. Alidori *et al.* [61] studies demonstrates that the biological effects of ammonium-functionalized carbon nanotubes (f-CNT) were recently conducted in nonhuman primates using quantitative whole body positron emission tomography (PET). The data obtained revealed almost full elimination of the injected activity (>99.8%) from the primate within 3 days ($t_{1/2}$ = 11.9 hours). These results revealed that when CNTs are accurately nanoengineered they can present a significant potential for the design of sophisticated nanomedicines to aid late-stage development and human clinical use [61]. However, Xuefei Lu *et al.* recently reported that a single dose (60 μg) of long CNTs (20–50 μm), per mouse, introduced to the lungs via intratracheal instillation 120 days before breast cancer induction, enhanced metastasis of the

breast cancer cells compared to control mice [62]. In fact, it is important to notice that the application of CNTs for biomedical invasive applications remain a research topic of big debate in the scientific community [63]. In addition, CNTs safety should be evaluated by subjecting them to toxicity tests for implantation, cytotoxicity, carcinogenicity, genotoxicity, and accumulation in organs [24]. The electrical properties of the f-CNTs can be explored in the elaboration of scaffolds for electrically sensitive tissues applications. The f-CNTs with the intended functionalization, are able to mimic the behavior of certain tissues, such as the cardiac muscle and the neural tissue [16][37][64]. These being the ones with the maximal application, as tissues that perform the propagation of electrical signals. Correa-Duarte *et al*. also demonstrated that cell proliferation and differentiation are enhanced considering the ability of CNTs to reproduce a 3D architecture that resembles the natural morphology of the tissues [65].

2.2.1. Patterned CNTs

Surface properties and morphology of scaffolds were given great importance considering the cell response to the biological material, owing to their environment capable of stimulating cell adhesion, proliferation, and orientation. Recent studies have shown the promising effects of topographical patterns on cell viability, when complemented with the use of a support material as CNTs, on the study of cell growth in tissue engineering [66]. In this regard, patterning of VA-CNTs into a micro/nanometer scale structure has shown to be a promising tool [66][67]. Therefore, arranging VA-CNTs in arrays of bundles creates free space between the bundles allowing a high contact guiding ability for cell growth onto nanotube surface of the biohybrid [67]. For instance, the capillary driven method is a good alternative to modify the VA-CNTs micropillars obtained by micro-patterning the metallic catalyst assisted by shadow-mask. In this simple approach the densification of VA-CNTs micropillars is accomplished by exposing them to acetone vapors. The use of locally directed actions, such as mechanical stresses, capillary forces, along with their interactions with templates, offers opportunity to create novel self-organized geometries and to design fabrication processes that achieve attractive combinations of dimensional control and throughput (Figure 9).

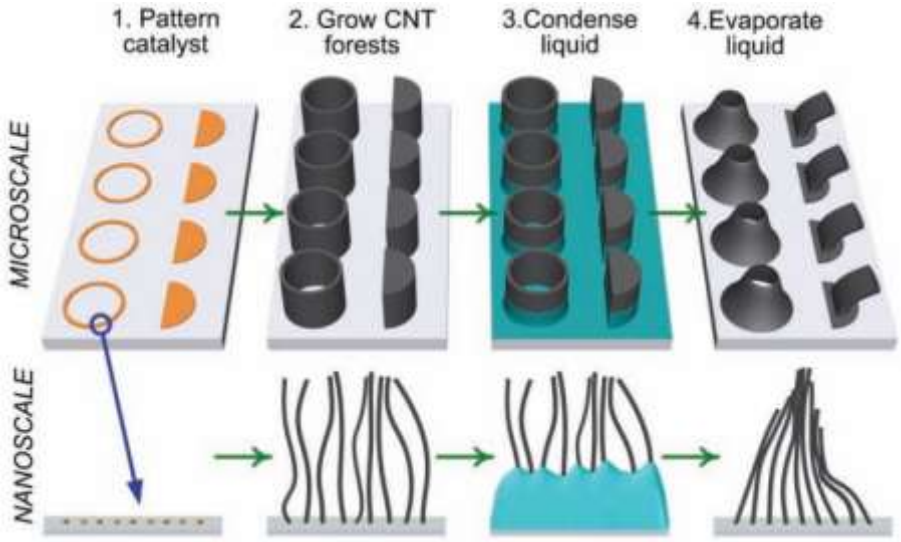

Figure 9 - Illustration of CNT forest growth and capillary forming.[68]

3. Biohybrid

Biomaterial-based scaffold hold great potential for tissue engineering and regenerative medicine as a result of their morphological porous architecture which grants cell ingrowth and matter transport, facilitating new tissue formation and the biomaterial degradation. The envisaged biohybrid is composed of three complementary components: CNTs that appear as a supporting structure able to provide conductivity to the biomaterial; an hydrogel responsible for the soft tissue-like properties, creating an aqueous microenvironment simulating the extra cellular matrices (ECM) structure; and the cells that combined with this scaffold will support axonal regrowth, reinstate the neural circuitry and regenerate growth potential by scaffold integration [69][70].

3.1.Hydrogel

Hydrogels can be broadly classified as water swollen crosslinked polymer network, having ≥ 90% of water content by weight [47][69]. This biomaterial can be categorized into two classifications: the naturally and synthetically obtained hydrogels. Either type has its benefits and applications.

Hydrogels obtained from natural polymers possess natural ligands which contributes to increased adhesion to the cells, typical from ECM. Besides, various hydrogels made of natural proteins are biodegradable and biocompatible, complemented with a supportive nature during cell attachment. Nevertheless, this type of hydrogel still has some downsides, like the properties irregularities on the preparation of every batch, and the difficulty to synthesize and process [47]. Natural polymers are divided into proteins and polysaccharides. Protein-based hydrogels, made of ECM-derived proteins, include for instance collagen, gelatin, Matrigel® and GelMA. Polysaccharides includes chitosan, alginate, agarose, hyaluronic acid, and methylcellulose, and are extensively used in neural tissue engineering applications [71].

Otherwise, synthetically obtained hydrogels have the benefit of being chemically customized in order to match the needs of application and usage of the material, however they lack the natural polymer characteristic, cellular adhesion which can be enhanced via functionalization with ECM proteins [47]. The mostly used synthetic polymers are poly-lactic acid (PLA), poly-ϵ-caprolactone (PCL), poly-lactic-co-glycolic acid (PLGA), poly-glycolic acid (PGA) and polyethylene glycol (PEG), widely used in neural tissue engineering [69][72].

The features that make hydrogels such an appealing biomaterial for this field of research are not only the characteristics already mentioned, both by natural and synthetic polymers, but their morphological, chemical, and mechanical properties which allow them to be used for neural tissue engineering. The most relevant features include: (*i*) biocompatibility to enhance cell adhesion, proliferation and differentiation; (*ii*) biodegradability at a close-matched rate of the new tissue formation and its final removal from the system; (*iii*) neural transmission to support neurite growth and neural regeneration; (*iv*) appropriate mechanical properties in order to relief stress from the lesion region, stabilize the material for culture and influence cellular mechanotransduction (the conversion of mechanical information from the microenvironment into biochemical signaling); and (*v*) porosity, enabling a similar scaffold to the ECM of the natural tissue, permitting vascularization, cell dispersion and exchange of waste and nutrients (Figure 10) [69][70].

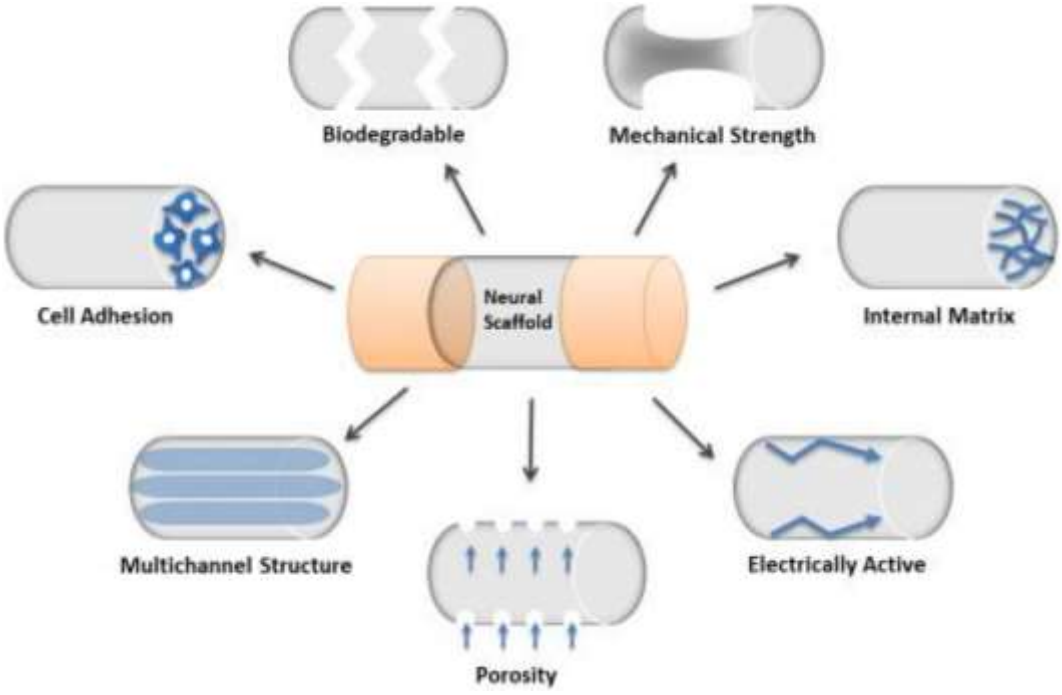

Figure 10 - Schematic illustration of neural scaffold relevant features.[69]

3.1.1. GelMA

Gelatin as a biomaterial used for the manufacturing of hydrogels is derived from the parent protein collagen via heat denaturation and partial hydrolysis procedures, maintaining the bioactive sequence of collagen and consequently retaining its capacity to promote cell functions as adhesion, migration, proliferation and differentiation [73]. This natural polymers is also very important because of its degradability, biocompatibility *in vitro* as well as during implantation, and its integrin recognition RGD (Arg-Gly-Asp) motif along its backbone, relevant for the effective interaction of biomaterial with cells [47]. Furthermore, gelatin is less immunogenic than collagen, as it presents less aromatic groups [74].

Owing to the facile access to gelatin, as it can be obtained from different by-products of animals. To create a physical hydrogel, raw gelatin must be at specific concentrations and temperatures, and still shows low mechanical strength [74]. It is possible to improve this property by a number of crosslinking strategies, including the use of crosslinking and chemical modification to support photo-crosslinking [75].

The selected technique is the chemical modification by the use of MAA to support photo-crosslinking, as this method provides faster and uniform *in situ* curing. MAA is the most vastly used and for this reason, the product GelMA has been used in distinct bio-applications, inclusively with different types of cells and composite materials [74]. GelMA can assume a chemically crosslinked hydrogel stage by visible or UV irradiation, depending on the photoinitiator used.

The photopolymerization process is expressed by the irradiation of a polymeric solution with the appropriate light wavelength, causing the photoinitiator to produce free radicals, ions or photoinduced step-growth polymerization, that will initiate polymerization with the monomer and lead to the crosslinked hydrogel. Nonetheless, the reaction rate of photopolymerization and the hydrogel biocompatibility can still vary with the light intensity, concentration and efficiency of the photoinitiator, such as the choice of materials which require good biocompatibility, biodegradability and functionality, as the material properties affect the network structure and mechanical properties of the hydrogels. By this means, the selection of appropriate photoinitiators and materials can reduce or avoid these problems once applied to a practical application [76].

For MAA, the photo-crosslinking is reactive to visible light, as shown in Figure 11.

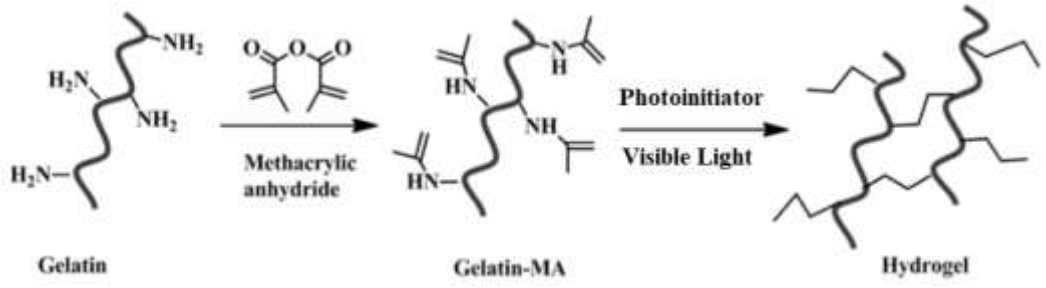

Figure 11 - Illustration of the synthesis of GelMA and hydrogel formation under visible light.[77]

3.2.Neural Stem Cells

Stem cells, which have the ability to replenish and multi-potently, under proper conditions, differentiate into various cell types with distinct biological functions, have been considered a major part in the field of regenerative medicine. Advances in nanomedicine and

the crucial impact in neurological research, are the reasons that led great interest into developing strategies to promote and control cell proliferation and differentiation, in order to further comprehend the central nervous system (CNS) [78].

In biology it is know that all cells originate from undifferentiated stem cells that can renew themselves or rise to more specialized cell types. Therefore, cell selection is vital for tissue engineering since they must imitate the physiological situation of the cells *in vivo* and maintain their functions under optimized conditions [69]. Very relevant for tissue engineering, mesenchymal stem cells (MSCs), NSCs and embryonic stem cells (ESCs) can be differentiated into various cells. However, the most relevant cell line in this study case are the NSCs. This can be specialized into the neuronal or glial progenitors, and consequently neurons or astrocytes and oligodendrocytes, respectively, as represented in Figure 12.

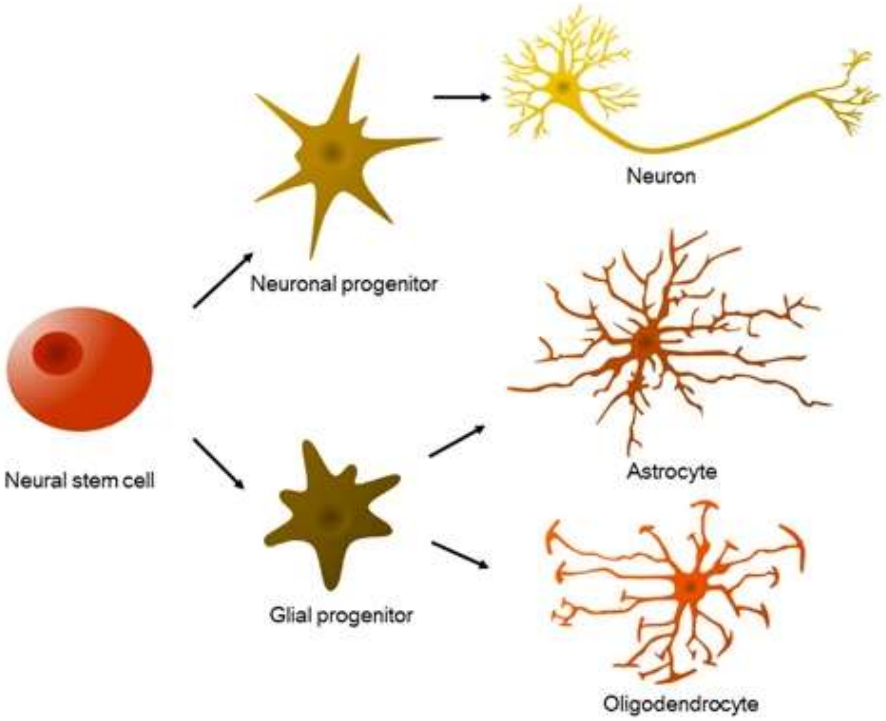

Figure 12 - Neural stem precursor cells (NSPCs) differentiation into neural cells of the CNS.[79]

Hence, the main ambition on using this cell line is to enable their use conjugated with a specific patterned substrate (CNTs) into damaged tissues, to achieve the tissue regeneration [80].

3.2.1. Neuronal Growth

The nervous system, as mentioned previously, forms a vastly complex cellular communication network with an elaborate morphology of extending neurites (axons and dendrites) across great distances. The neurites growth and synapses formation is achieved and controlled by a highly specialized structure on the tip of the neurite (growth cone) [81]. The neuron cell morphology can be observed in Figure 13.

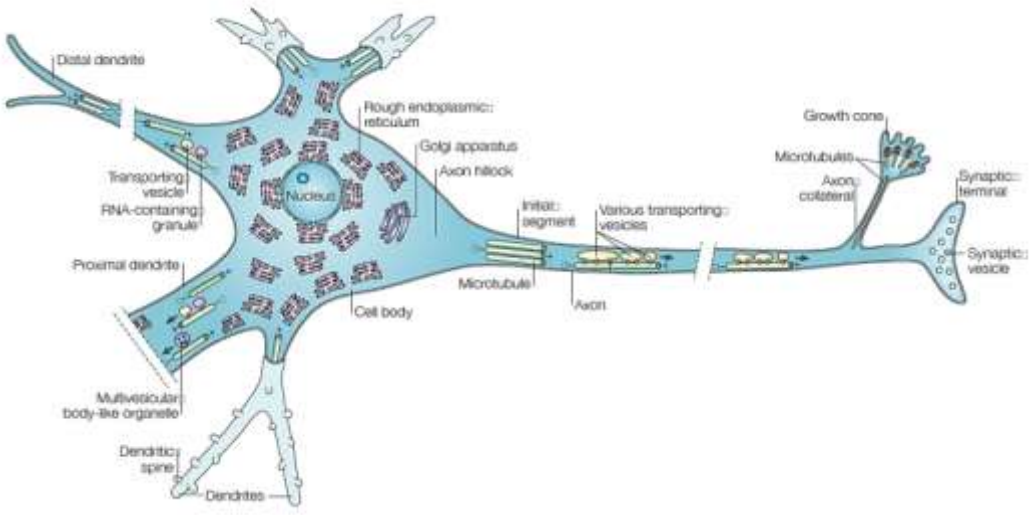

Figure 13 - Illustration of the typical dendrites (left) and single axon (right) from the neuron cell.[82]

In order to use neural stem cells for spinal cord repair, the promotion of axonal growth and the achievement of long-distance regeneration are the two main factor in experimental strategies. Some of the existing techniques are pharmacological intervention, functional electrical stimulation and physiotherapy. Besides, the substrate properties have also an important role on cells structure and function, granting the capability to direct and guide live cells. Previous studies have demonstrated that the correlation between CNTs and cells caused diverse cell behavior alterations, like a decrease on astrocyte formation and

macrophage density, an increased on neuronal electrical signaling, and an enhanced NSCs differentiation into neurons [78]. Also, it was also demonstrate that the interaction between CNTs and cells is greatly dependent of the surface roughness of the substrate, since it affects the anchoring to the neuronal cells [83].

For this reason, the use of patterned CNTs substrates emerged as an novel alternative for forming scaffolds to guide neurite outgrowth, with the supplementary potential to ensure electrical signal transmission through the neurons, to stimulate cell proliferation and neurite extension, but also endorse cellular migration and intracellular connection [84][85].

3.3.Integration of the Bioink into VA-CNTs

The integration of the bioink into the VA-CNTs is a very challenging step. The hydrogels, as explained in previous sections have proven relevant on cell culture applications, as it can regulate their behavior and provide an appropriate biocompatible and biodegradable environment for cell attachment, expansion, and differentiation. Therefore, hydrogel faculties for tissue engineering are similar to those presented by the natural ECM [47]. Bioinks are for this reason, a biomaterial containing biologically active components, acting as a cell-laden medium during its formulation and printing, as it is differentiated in Figure 14. Bioinks used for bioprinting usually contain hydrogel or hydrogel precursors, decellularized matrices, separate cells, cell/tissue spheroids, bioactive molecules, growth factors, proteins among other [73].

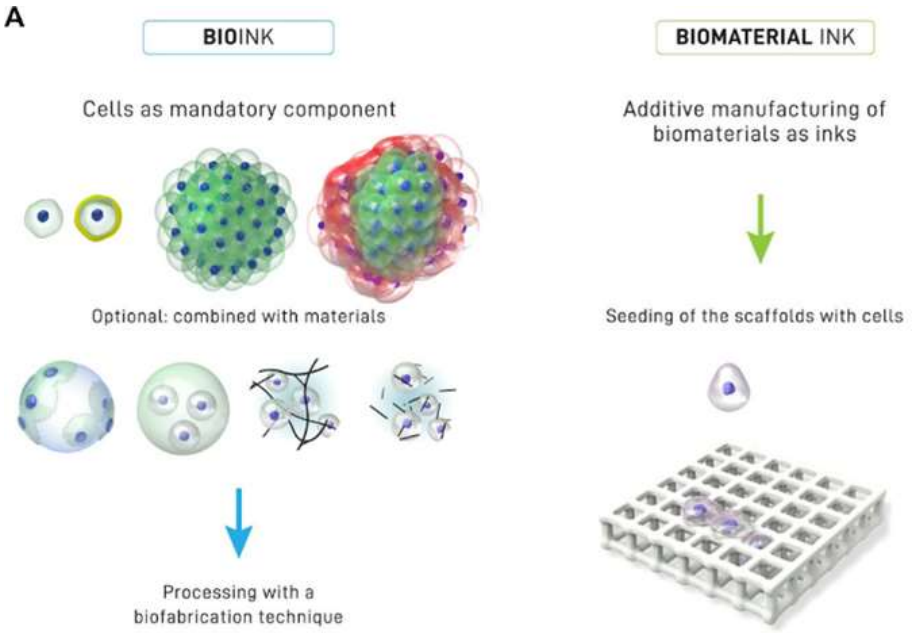

Figure 14 - Distinction between a bioink (A), where cells are a mandatory component of the printing formulation in the form of single cells, coated cells and cell aggregates (of one or several cell types), or also in combination with materials (for example seeded onto microcarriers, embedded in microgels, formulated in a physical hydrogel, or formulated with hydrogel precursors), and a biomaterial ink (B), where a biomaterial is used for printing and cell-contact occurs post-fabrication [86]. The images in this scheme are not displayed in scale.

As the field of biomaterials is continuously improving, the complexity of the cell culture systems increases with it. Therefore, the development of a bioink and its arrangement on a substrate, in order to accomplish cell growth support and conductive properties for the scaffold on development, is one of the ambitions of tissue engineering [70]. However, bioprinting of bioinks is still a challenge to overcome because of the inadequate shear tinning behavior and viscosity of bioinks, such as GelMA. The techniques used to address this issue will be aboard next.

3.3.1. Cell Seeding

The production of 3D scaffolds, either made of natural or synthetic polymers have been accomplished by multiple methods like gas foaming, melt molding, electrospinning, and phase separation, but still the scaffold morphology (shape, inner channel configuration, pore size, …) cannot be totally modulated by these methods. Furthermore, the techniques

mentioned are not suitable to produce scaffolds with cells, as a consequence of their rough processing conditions [69].

From a printability point of view, the scaffold and hydrogel must show the following properties: *(i)* shear thinning behavior (viscosity drop) to prevent the cells from high shear stress during extrusion and therefore improve cell viability; *(ii)* high viscosity restorability, once the bioink is printed; *(iii)* high self-supporting behavior to retain the spreading of the printed bioink and support the weight of the top layers; *(iv)* biodegradable, with minimum toxicity (hydrogel and by products); and *(v)* cross-linking ability to offer stability. To assure the permanent network of the hydrogel, the bioink can be submitted to two strategies, the photo and ionic cross-linking [73].

Therefore, new methods have been accessed to easily arrange the dimension and shape of the scaffold to allow cells integration.

3.3.2. Conventional Deposition Techniques

The conventional methods to deposit the biohybrid into the CNTs substrate are solvent-casting and spin-coating. These are techniques have the advantages of low cost. The same functional potential as other methods and the formation of a uniform thin layer on the support surface [87][88].

In the solvent-casting method, a drop of liquid containing the suspension of interest, this mean, the neural stem cells embedded into GelMA, is deposited on the carbon-based nanostructure, ideally until full coverage and spread on the CNTs surface.

As alternative, in the spin-coating technique, a small amount of bioink is deposited onto the center of the substrate, and afterwards it is rotated at high speed in order to spread the coating polymer by centrifugal force. In general, the higher the rotation speed, the thinner the coating layer.

The last approached method consisted of the confluence of the two methods aforementioned, starting by the spin-coating of a thin layer of bioink into the CNTs substrate and later the deposition of the same bioink solution drop by solvent-casting. On both of the techniques, the bioink is submitted to physical gelation under visible light right after the

deposition and spread of the GelMA embedded with the NSCs, enabling the formation of a complex 3D matrix. The schematic illustration of the two methods can be observed on Figure 15.

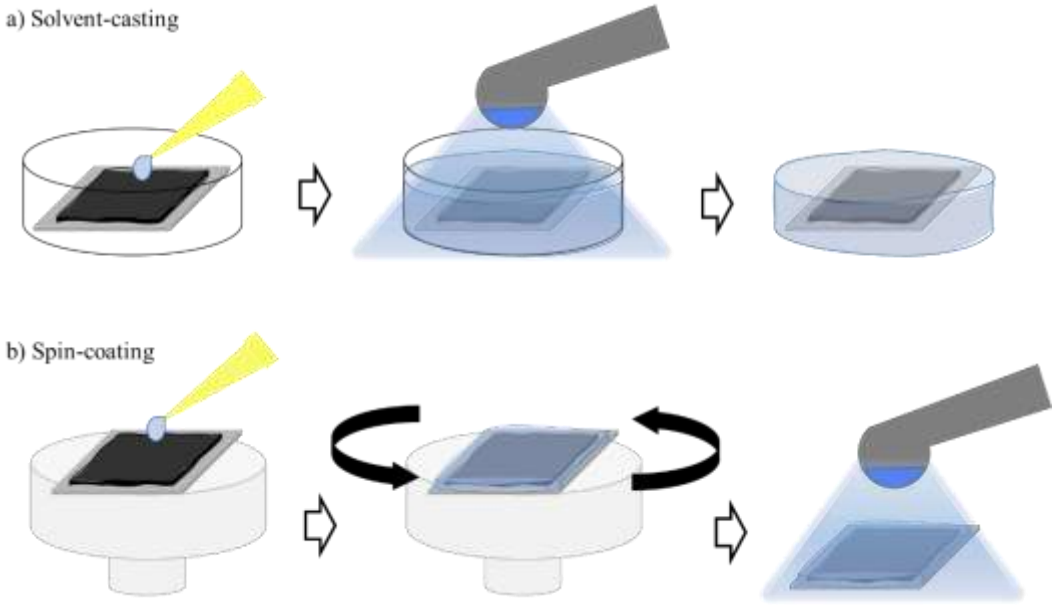

Figure 15 - Schematic illustration of the a) solvent-casting and the b) spin-coating method.

3.3.3. 3D Bioprinting

Nowadays, 3D printing has been growing and gaining significance as a tool for tissue engineering. This is mostly due to the advances in this technology, when dealing with cell biology and material science, allowing the fabrication of personalized, and programable scaffolds. Owing to this, 3D bioprinting is an alternative to the construction of tissue-like biomimetic biohybrids, capable of reproduce the precise anatomy of the site of regeneration [89][90].

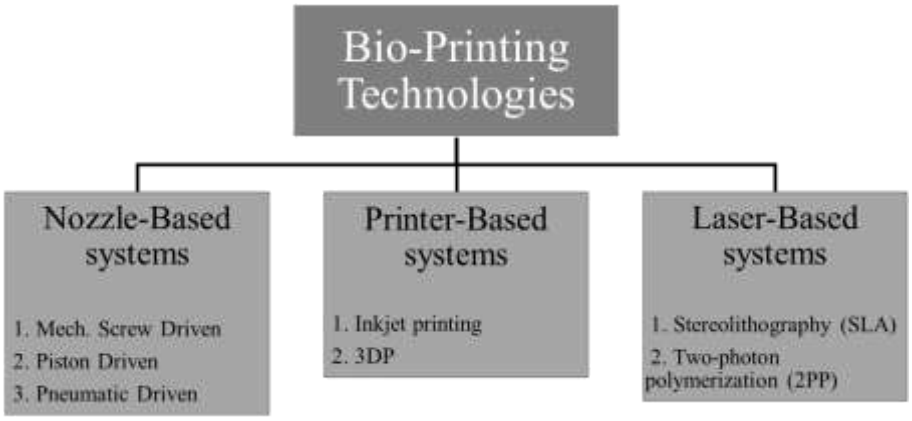

Figure 16 - Overview of different types of bioprinting techniques.[47]

Bioprinting can be divided into three main categories: inkjet bioprinting, robotic dispersion and laser-assisted bioprinting on the basis of printing processes as illustrated in Figure 16 [75]. The method approached in this work study is the pneumatic driven as a result of robotic dispensing, as seen in Figure 17. The extrusion of the continuous bioink filament is assisted by pressurized air on a layer-by-layer deposition, through a movable nozzle acting as the print head of the bioink into the CNTs substrate [91].

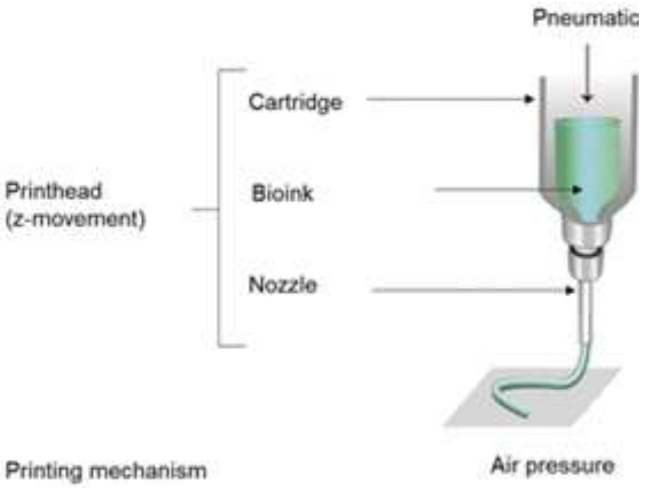

Figure 17 - Schematic demonstration of the pneumatic driven extrusion system.[92]

3.4.Spinal Cord Injury

The reason that led CNTs biohybrids to show great potential in tissue engineering is their favorable surface for cellular growth, neural signal transmission and great environment for cell proliferation and differentiation [93]. These main properties are crucial since neural cells are in control of the transmission of information of stimuli, such as touch, sound or light, as electrical and chemical signals throughout the nervous system up to the spinal cord and brain. Thus, the strategy to aboard with the application of nanomaterials to neuroscience is to assemble a scaffold capable to regrowth, restoration, or repair degenerated neurons and nervous tissues.

Along these lines, the nervous system can be divided in two groups, the CNS, and the peripheral nervous system (PNS). CNS is responsible for conducting signals between the brain and the spinal cord, and the rest of the body. However, opposite to PNS, the CNS has a low capacity to self-repair, due to its complexity, which can lead to the loss of function. This CNS disease is named spinal cord injury (SCI), and it causes the loss of neural cell bodies, axons, and glia support, in response to physical damages or neurodegenerative diseases.

Hence, CNTs biohybrids and their derivatives have been used in research for the formation of scaffolds capable of promoting neuronal growth and functionalization, calling upon their electrical conductivity, overcoming the traditional nerve grafts [94][95].

Caleresu *et al.* and Pampaloni *et al.* have studied the use of nanostructured materials and nanosized-topographies made of polystyrene/CNTs nanocomposites and CBNs as components of neuroregenerative film interfaces, respectively, on the performance of implantable biodevices, to increase sensitivity and selectivity, while reducing tissue reactivity. The authors could successfully prove the predisposition of the platforms/carpets to integrate neuronal circuits, cultured networks, reduce neuroglia formation and assume high network activity, demonstrating promising results for the implementation of the structures on neuro-prosthetic or neurostimulation devices, and enhance the recovery of lesioned brain cultures for devices in regenerative medicine and tissue engineering [96][97].

On other studies, Imani *et al.* showed the possibility to develop a CNT/Nafion nanocomposite to promote regeneration of axons into the lesion cavity and achieve functional recovery after SCI, of hind limbs in a rat model [98].

However, on a more similar perspective to this work, recent studies have explored the use of 3D micropatterned CNTs templates to direct neurite stem cell growth, taking advantage of the mechanical flexibility, electrical conductivity and texture of the CNTs micropillars, leading to enhanced therapeutic effects within injured spinal cord or peripheral nerves [99]. Vasconcelos *et al.* has also coupled the use of CNT to a photopolymerizable hydrogel and an anti-inflammatory molecule to be used *in situ* on SCIs, resulting on a CNTs functionalized safe scaffold with photopolymerization compatible with cell viability [43].

In this work, the ECM analogue is achieved by the existence of the CNTs embedded on the cell proliferation environment [100][101], to develop conductive nerve conduits for SCI treatment (Figure 18) [102].

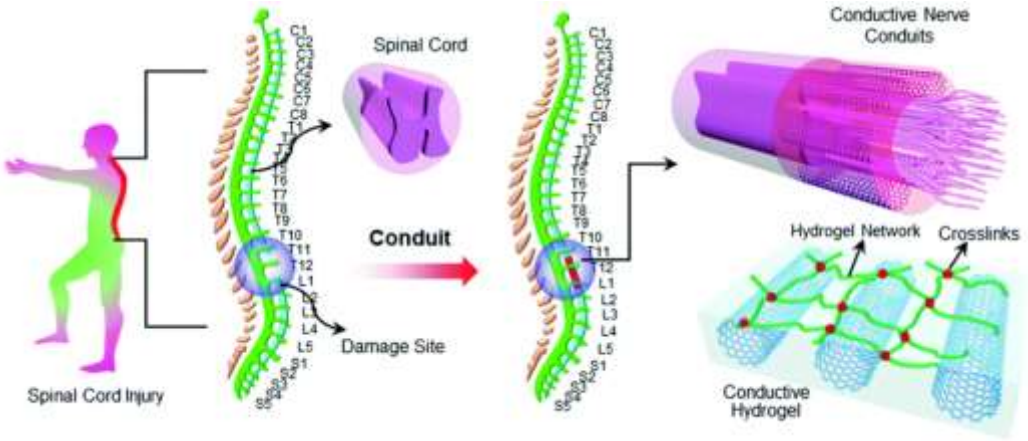

Figure 18 - a) Schematic demonstration of the spinal cord in the human body. b) Conductive nerve conduits for spinal cord injury treatment. c) Structure of the conductive hydrogel.[102]

Besides its mechanical reinforcement, the nanostructures can also boost neuronal signaling, by the application of an electrical stimulation to it, enhancing neuronal performance, regeneration, and outgrowth [103].

Chapter 3 – Synthesis of 3D micropatterned VA-CNTs

1. Experimental

1.1. Multilayer catalyst preparation

Figure 19 provides a generic schematic illustration of the VA-CNTs synthesis process via T-CVD, and prior to the nanotubes growth process there is a need to prepare a multilayer catalyst supported on solid substrate. In this way, polished silicon (Si (100)) wafers from SILTRONIX with 300 nm thermally grown silica (SiO_2) were used as substrates which had been sequentially coated by ~10 nm Al_2O_3 and ~17 nm (10 min of deposition time) Fe films by PVD from an oxide ceramic Al_2O_3 target and from a metallic Fe solid target, respectively. In particular, radio frequency (RF-) was used for the ceramic and direct current (DC-) magnetron sputtering for the metallic film materials.

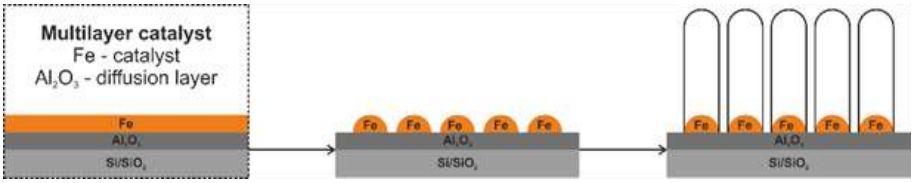

Figure 19 - Schematic illustration of the VA-CNTs growth via T-CVD.

The Fe deposition occurs when a DC power is applied to the target in an inert atmosphere of Ar (10 sccm). The surface of the target is eroded by high-energy ions (Ar^+) within the plasma, and the released atoms travel through high vacuum atmosphere and deposit onto $Si/SiO_2/Al_2O_3$ substrate to form a thin film, while the Al_2O_3 diffusion or buffer layer was previous deposited by using a RF power supply and a reactive atmosphere comprised of Ar (10 sccm) and oxygen (O_2; 3 sccm). Here, the combined oxide layers (SiO_2/Al_2O_3) act as diffusion barriers, avoiding the formation of catalytic inactive iron silicides. The experimental parameters are summarized in Table 1. Additionally, the PVD-process allows the deposition of patterned Fe thin films via shadow masking. This mask simply stops material from being deposited onto a Si wafer substrate in a desired pattern

overlay, creating a ‘shadow’ area on the substrate on which no material is deposited, in order to achieve the desired Fe catalyst pattern. The shadow masking technique consists of a circular hole array metallic mask with 500 µm diameter holes and a constant interspacing distance of 400 µm.

Table 1 - PVD (RF- and DC-magnetron sputtering) experimental parameters.

	Al_2O_3	**Fe**	**TiN**
Base pressure (kPa)		3.0×10^{-4}	
Working pressure (kPa)	6.0×10^{-3}	4.8×10^{-3}	
Current (A)	-	0.06	0.02
Power input (W)	70	30	20
Flux of Ar (sccm)		11	
Flux of O_2 (sccm)	3	-	-
Deposition time (min)	30	2, 4, 8, 10	90

1.2.Synthesis of VA-CNTs

The VA-CNTs growth was carried out on a home-made tubular T-CVD reactor (horizontal quartz tube with an outer diameter of 5 cm) equipped with various gas delivery lines and standard mass flow controllers, connected to PC station for automatic operation (controlled by DAYSLab software), to control the flow of the different reaction gases, as shown in Figure 20.

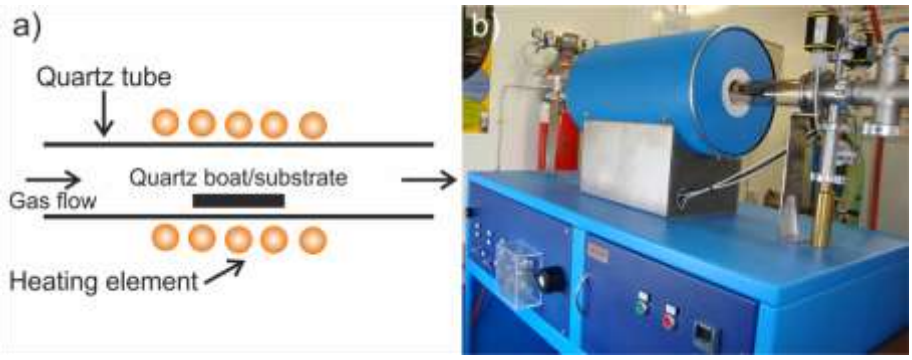

Figure 20 - Schematic illustration a) and digital image b) of the T-CVD used for the VA-CNTs growth.

In a typical T-CVD run (Figure 21), the as-prepared Fe substrate is placed into quartz tube chamber of the reactor and evacuated with rotary pump ($3.0x10^{-2}$ kPa). Afterwards, the chamber is refilled with Ar up to atmospheric pressure. Then, the substrate is pulled to the center of the reactor and the annealing step is initiated. First, in Ar flow (1000 sccm; step I) and then, in a reductive flow of Ar (200 sccm) and H_2 (500 sccm) for 1 min (step II). In this stage of the growth process the Fe thin film is broken into catalyst nanoparticles from where the nucleation will take place. Subsequently, the VA-CNTs synthesis (step III) is undertake with a gas mixture of C_2H_2 (10 sccm), H_2 (100 sccm) and Ar (400 sccm), at 725 °C and during 8 min or 15 min followed by a cooling stage until reaching room temperature (step IV). The total gas flow is fixed at 510 sccm, for all the experiments.

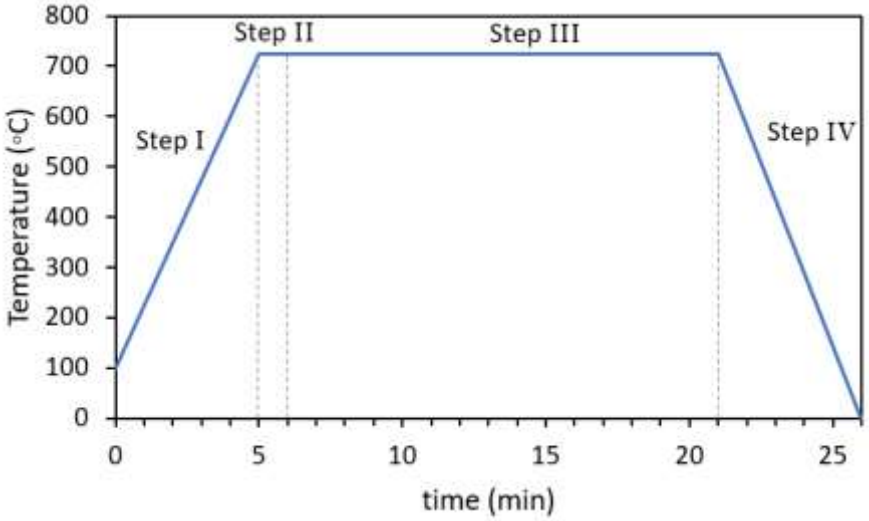

Figure 21 - Schematic illustration of the different process steps for growing VA-CNTs by T-CVD.

1.2.1. Micro-patterning of VA-CNTs

The micro-patterning of VA-CNTs was carried out by a shadow mask method. As mentioned above, the VA-CNTs growth by T-CVD process initiates through the catalyst preparation on a solid support (Si wafer) through the deposition of metallic thin films (*i.e.*, Fe) by means of PVD technique. Moreover, the PVD offers the possibility of deposition continuous thin films or patterned thin films with a shadow mask (stencil) on the top of the Si substrate (Figure 22a). The aim of the patterning the Fe catalysts thin film is to produce

VA-CNTs bundles arrays that occupied a circular area of around 500 µm diameter and from 450 µm to 1000 µm spacing (Figure 22b). In Figure 23 can be observed a schematic illustration of the different morphologies obtained by CNTs growth.

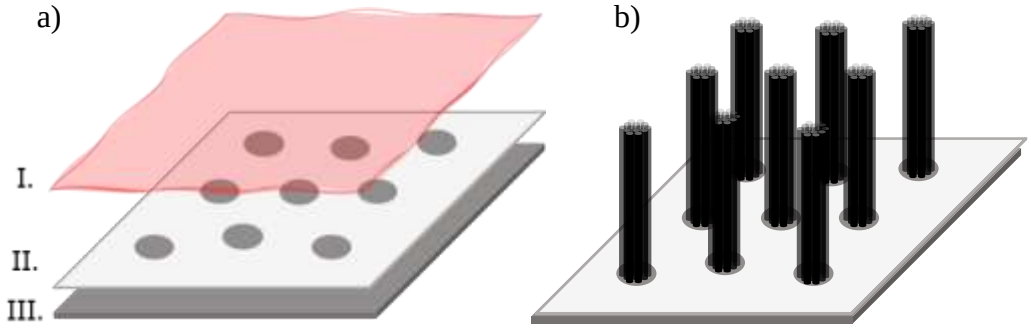

Figure 22 - Schematic illustration of the fabrication of micropatterned VA-CNTs by shadow mask. a) I. Fe layer catalyst thin film by PVD, II. Mo shadow patterned masking and III. Si/SiO_2 substrate with a thin film of Al_2O_3 by PVD: polished Si wafer. b) Micropatterned VA-CNTs growth.

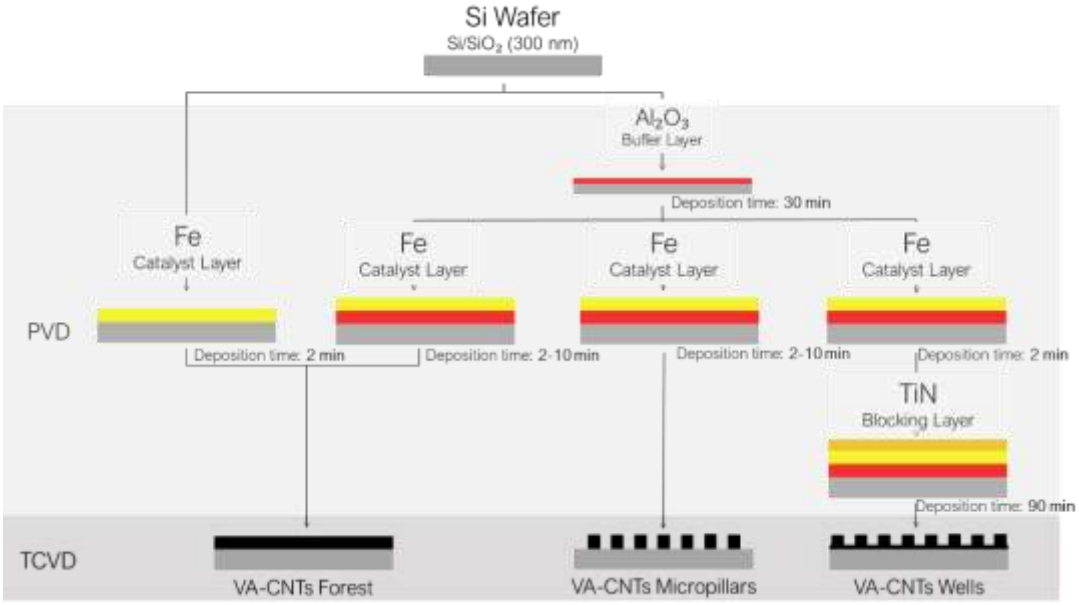

Figure 23 - Schematic representation of the various VA-CNTs morphologies.

1.2.2. Capillary driven patterning

An alternative method to obtain the patterned CNTs substrate is by capillary forming, proposed by De Volder *et al* [68], which consists of the collapse of the nanostructures on

themselves. The VA-CNTs substrate are grown on the conditions aforementioned on Table 1, and afterward the nanotubes are collapsed, as acetone is condensed on the substrate. This process is done by placing the substrate inverted (CNTs facing down) on the top of a beaker containing boiling acetone. The solvent vapor rises and condenses on the substrate, merging into the CNTs structure. After the substrate has been exposed to the vapor for 60 seconds, the substrate is removed from the beaker. A schematic illustration of the technique is shown in Figure 24**.** The resulting substrate architecture exhibits CNTs locally aggregate by the elastocapillary mechanism, and the formation of open cellular-like structures [104][105]. The resulting substrate exhibits the nanotubes in a dense structure and unique shape, consequence of the capillary action.

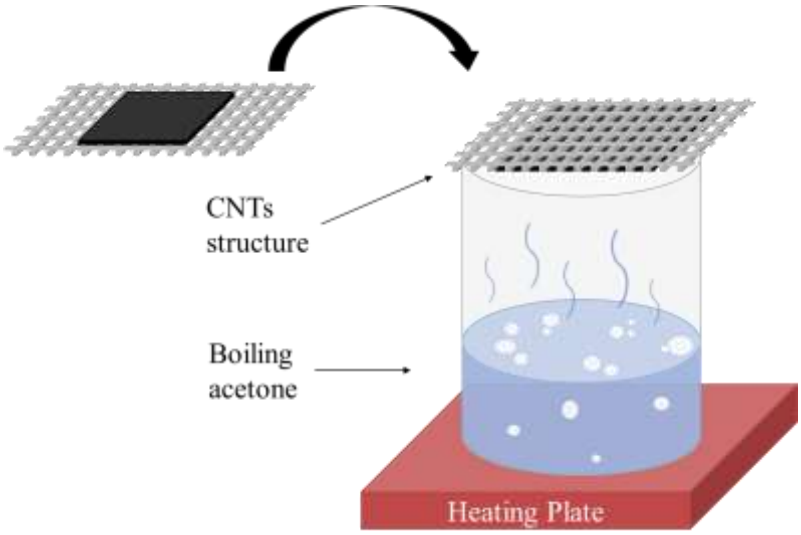

Figure 24 - Schematic illustration of capillary driven patterning method. The VA-CNTs forests were glued to a Mo mesh.

1.3.Characterization

Structural and morphological properties of the multilayered catalyst and the VA-CNTs were characterized by scanning electron microscopy (SEM, Hitachi SU70 microscope) operated in secondary electron (SE) mode at 15 kV, equipped with energy dispersive X-ray spectroscopy (EDS). Grazing incident X-ray diffraction (GIXRD) was carried out using a Rigaku Geigerflex D Max-C Series diffractometer on glass substrate coated with manganese oxide. The radiation used was Cu Kα (λ=1.5418 Å), with a scan time

of 100 s and step size (2θ) of 0.02°. The internal structure investigated by transmission electron microscopy (TEM, JEOL JEM-2200FS microscope), operated at 200 kV. The samples for HRTEM measurements were prepared by dry adhesion of the CNTs to a holey carbon film supported on a copper grid. Raman spectroscopy (Jobin Yvon T64000) was carried out at a 532 nm excitation wavelength at room temperature (RT). Atomic force microscopy (AFM) measurements were performed with an Ntegra Prima setup (NT-MDT) in tapping mode under ambient conditions. A silicon cantilever (Nanosensor PPP-NCHR) with the spring constant of k ≈ 42 N m-1 and tip radius less than 10 nm was used. AFM observations were taken on scanned area of 5 µm x 5 µm or 1 µm x 1 µm. The water contact angle (WCA) was carried out with ultrapure water with OCA 20 (DataPhysics Instruments, Germany).

2. Results and Discussion

2.1.Multilayer catalyst for VA-CNTs synthesis

The multilayer catalyst is comprised of Al_2O_3 and Fe thin films on Si/SiO_2 substrate by PVD technique. From Figure 25a it is possible to observe the cross-sectional SEM image of the 435 nm thick Fe film with the corresponding EDS mapping confirming the presence of the Fe on the substrate. This long Fe deposition allows the determination of the film thickness and consequently the Fe growth rate. On the other hand, the Figure 25b shows the GIXRD pattern acquired from the deposited Fe film. Interestingly, the reflections observed in the GIXRD pattern are related to the Si/SiO_2 substrate, however it is expected the deposition of metallic Fe.

As aforementioned, the Al_2O_3 buffer layer acts as diffusion barrier between the Fe film and the Si/SiO_2 substrate, averting the formation of catalytic inactive $FeSi_2$, assuring the preservation of catalytic particles for the CNTs growth. Coupling to this property, the buffer layer also inhibits the attachment of the Fe particles to the substrate surface, allowing the distribution of the Fe particles, limiting their mobility, and avoiding the coalescence of smaller particles into larger ones, which would diminish the activity of the catalyst.

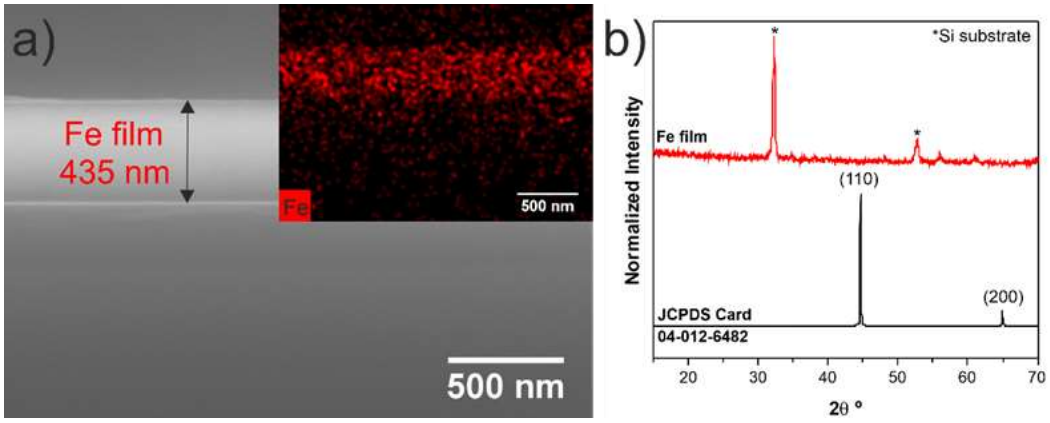

Figure 25 - Cross-sectional view SEM image a) and GIXRD pattern b) of the Fe thin film deposited by PVD for 240 min. The inset in a) shows the EDS elemental mapping identifying the presence of the Fe.

Before the VA-CNTs growth step, Figure 26, the continuous Fe film is broken into Fe nanoparticles from where the nanotubes growth takes place, owing to the heating of the catalyst until 725°C temperature and the presence of H_2 on the film during the pre-treatment step. H_2 has the fundamental role of reducing the oxidized Fe particles to an active catalytic stage for the VA-CNTs growth. The produced nanoparticles exhibit an average size of 13 nm with a standard deviation of 1 nm.

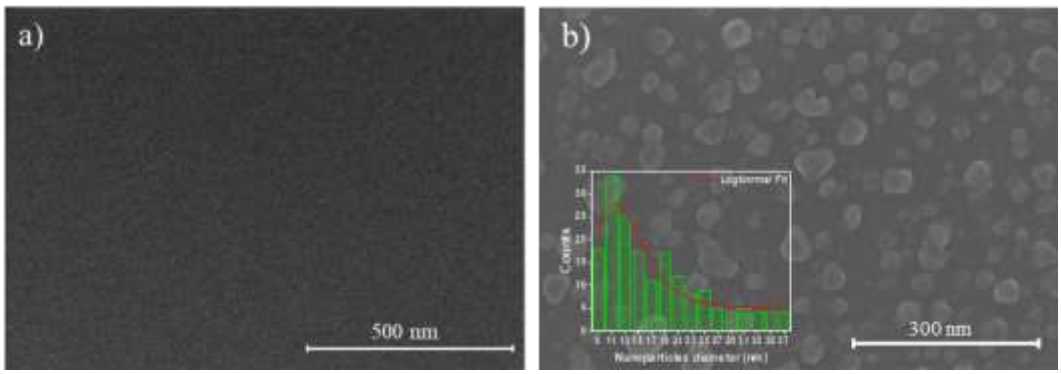

Figure 26 - Top-view SEM image of the multilayer catalyst film before a) and after b) the pre-treatment. Inset shows the typical particle size distribution histogram, red line is log-norm fit of the bin center points.

On the other hand, the Figure 27 shows the AFM images of the pattern Fe film before (a) and after (b) the pre-treatment step. The roughness (RMS) increases from 1 nm to 9 nm pointing out the effect of this step on the surface features of the Fe film.

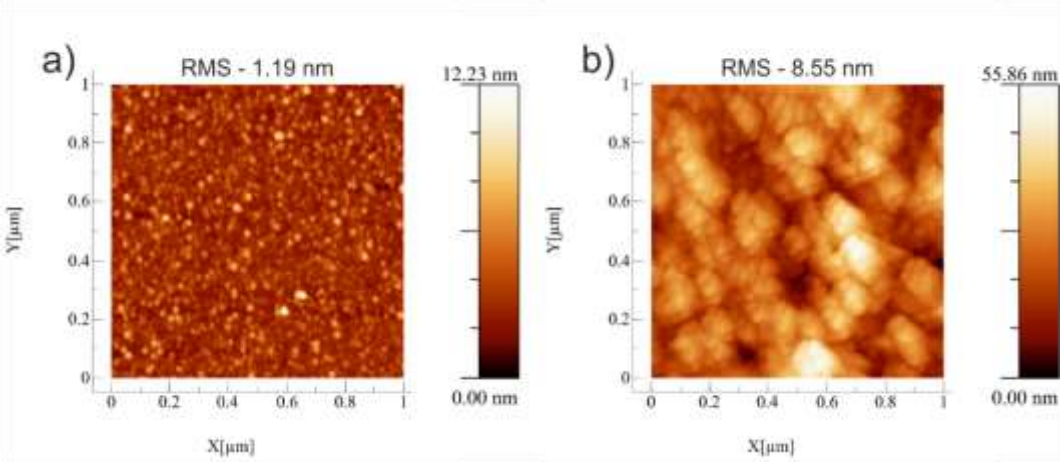

Figure 27 - Patterned Fe film after a) and before b) the pre-treatment step.

2.2.Micro-patterning VA-CNTs assisted by shadow mask

The results of the T-CVD experimental conditions on the height of the VA-CNTs are depicted in a collection of SEM images at different magnifications (Figure 28). The control over the VA-CNTs height was accomplished by the introduction of Al_2O_3 buffer layer to the Si/SiO_2 substrate and the growth time duration.

The VA-CNTs forest presented in Figure 28a and b is grown on Fe/SiO_2 substrate revealing the vertically alignment with a very dense morphology and uniform with approximately 189±4 µm in height. In opposition, the introduction of the Al_2O_3 buffer layer to the Si/SiO_2 substrate led to an enhancement of the VA-CNTs height ca. 499±6 µm, as shown in Figure 28c and d.

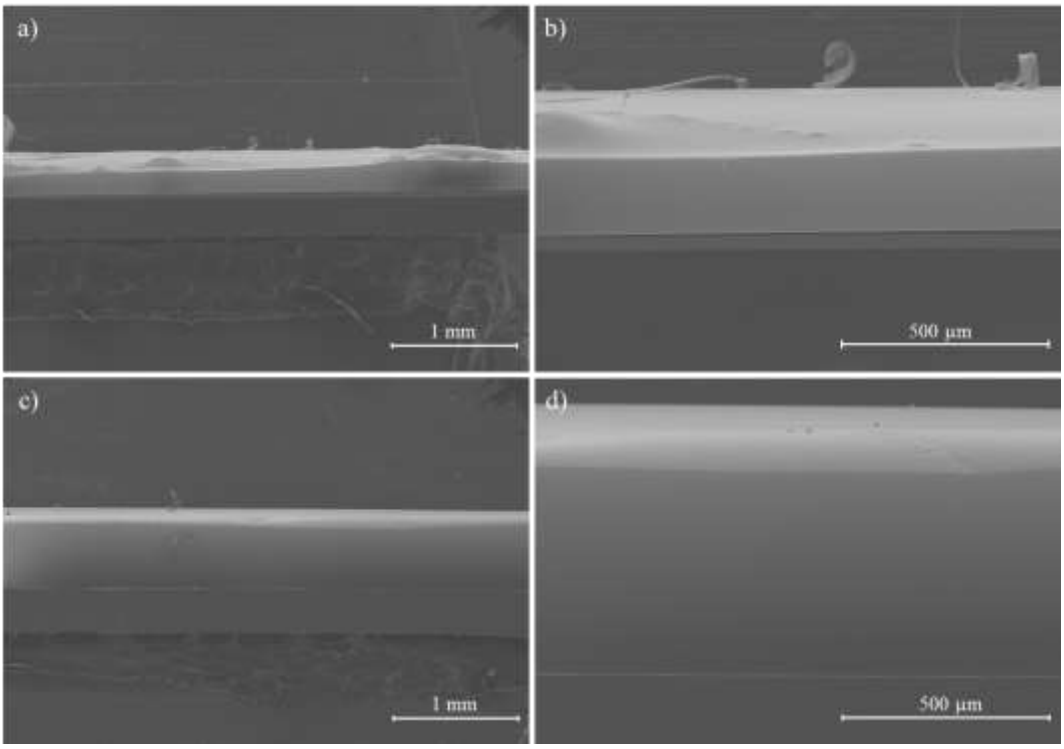

Figure 28 - Side-view SEM images of the (a and b) VA-CNTs forest grown on Fe (2 minutes)/SiO_2/Si substrate; and (c and d) VA-CNTs forest grown on a Fe (2 minutes)/Al_2O_3 multilayer substrate.

BF-HRTEM images of the nanotubes showing their internal structure can be observed on Figure 29. The nanotubes are MWCNTs, the walls are seen as dark contrast in the HRTEM images. On the other hand, the formation of amorphous carbon during the VA-CNTs growth is not unusual and it can be seen on the outermost surface of the nanotube (marked with the black arrow, in Figure 29a). Raman features makes Raman spectroscopy a general and common tool for characterizing structures of VA-CNTs. The stretching of the C−C bond in graphitic materials gives rise to the so-called G-band Raman feature which is common to all sp^2 carbon systems while the D-band is related to the presence of a defects on the hexagonal sp^2 network [106]. Representative Raman spectrum of the nanotubes depicting the D-band and G-band characteristic of the multiwalled nanotubes, which is in good agreement with the HRTEM results, presenting I_D/I_G ratio value of 0.49. This result suggests the presence a low degree of disorder or defects on the surface of the CNTs [107].

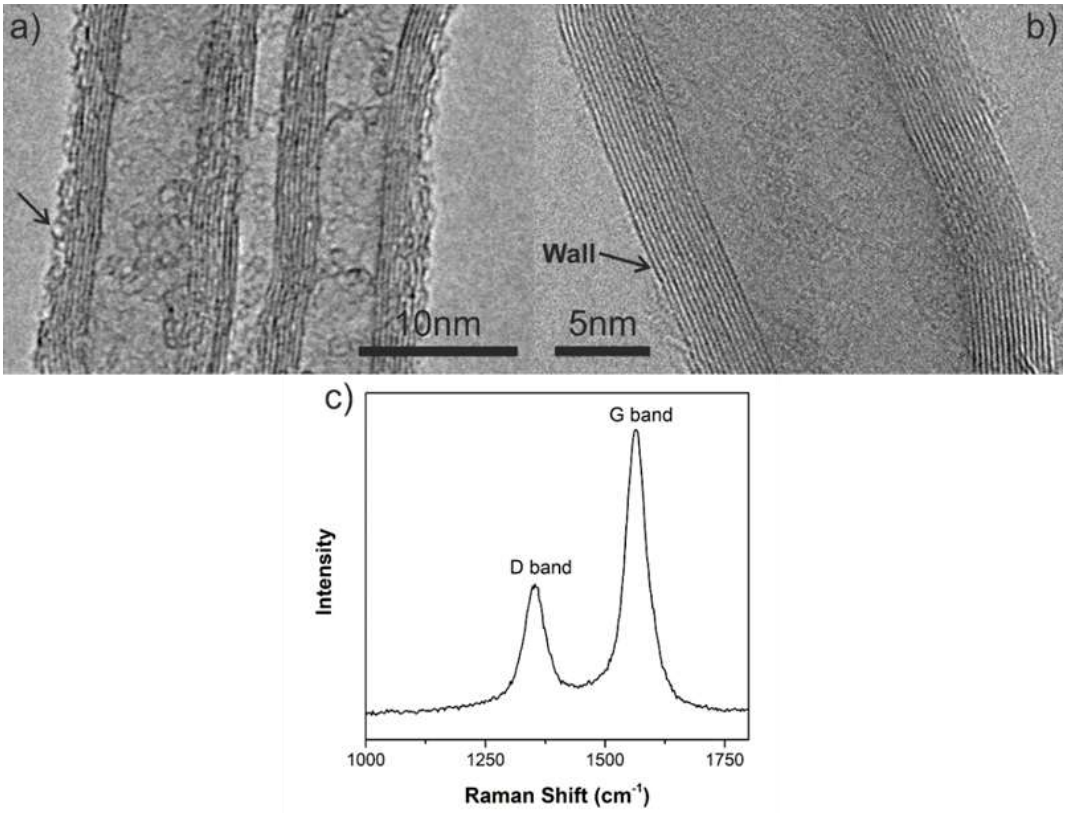

Figure 29 - BF-HRTEM images (a and b) and Raman spectrum c) of the VA-CNTs. MWCNTs have interlayer (*i.e.*, distance between walls) separation of 0.34 nm.

The VA-CNTs grown from the use of a shadow mask during the Fe catalyst layer deposition, after the deposition of the Al_2O_3 layer are shown in Figure 30a and b, and Figure 30c and d, after 8- and 15-minutes growth. As a result, circular VA-CNTs micropillars with 279±14 and 454±11 µm in height are obtained.

In order to achieve a pattern height of 454±11 µm similar to the continuous VA-CNTs forest while keeping constant the growth time, the Fe deposition time was increased from 2 min to 10 min, *i.e.*, the Fe thin film thickness. This finding can be related with use of the shadow masking that led to a deposition of a thinner Fe catalyst.

In alternative to the micropillars pattern morphology, the deposition of a blocking layer such as TiN layer over the Fe catalyst thin film, resulted on the growth of VA-CNTs with an inverted pattern to the previously presented samples, as can be seen in Figure 30e and f. The VA-CNTs forest with inverted pattern present a height of 549±13 µm, under the same growing conditions of the previous samples.

The highest VA-CNTs forests were selected for the application of the capillary driven method. These forests are shown in Figure 28c and d continuous VA-CNTs forests and as well as in Figure 30e and d micropillars pattern VA-CNTs forests.

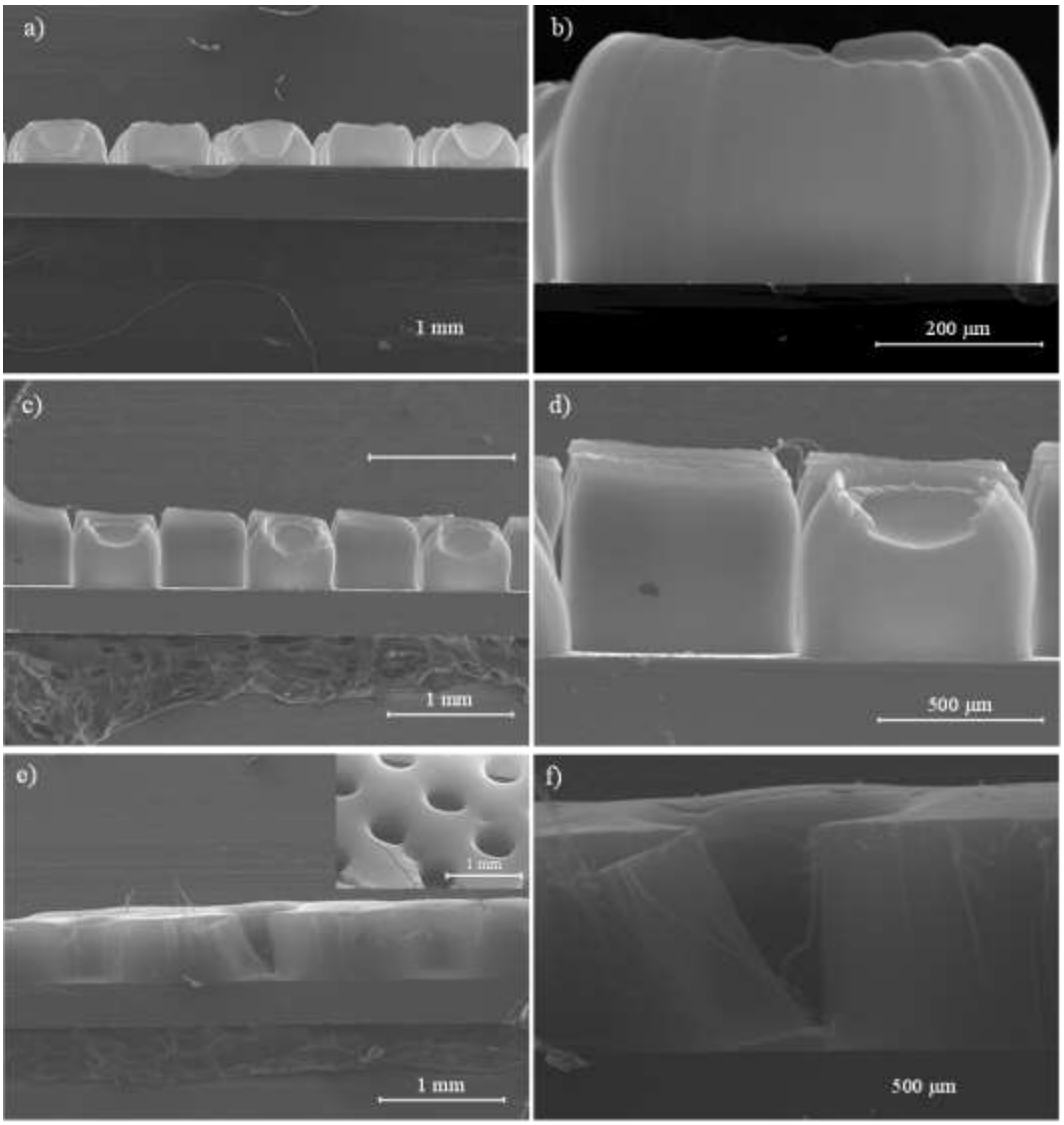

Figure 30 - Side-view SEM images of the (a and b) VA-CNTs micropillars after 8 minutes growth on a Fe (2 minutes)/Al_2O_3 multilayer substrate; (c and d) VA-CNTs micropillars after 15 minutes growth under the same conditions; and (e and f) VA-CNTs inverted micropillars grown for 15 minutes on the multilayer substrate.

2.3.Micro-patterning assisted by capillary driven VA-CNTs

By means of SEM analysis (Figure 31), it is possible to compare the resulting morphologies features after the capillary driven patterning caused by the acetone vapor. In both the obtained patterns, the CNTs behavior is similar as it is possible to identify a densification of the VA-CNTs forest and micropillars. It is possible to denote in Figure 31 (d to f) the structural arrangement observed on Figure 31 (a to c), with the CNTs presenting their alignment even though they show a collapsed morphology, which appears as long, stretched walls on a honeycomb-like structure. However, it can be observed the presence of what it appears to be an amorphous layer on the site where the VA-CNTs gather without collapsing. The capillary driven results observed on the micropillars VA-CNTs substrate (Figure 31 (j to l)) presents a similar stacking behavior in comparison to the forest substrate although not preserving the aligned morphology.

As already mentioned, this performance is resultant of the collapse of the nanostructure on themselves, caused by the condensation of the acetone on the substrate. This patterning step on the VA-CNTs morphologies synthesized by CVD method in order to create a suitable so-called nest for cells, promising for cell encapsulation and proliferation [61][77].

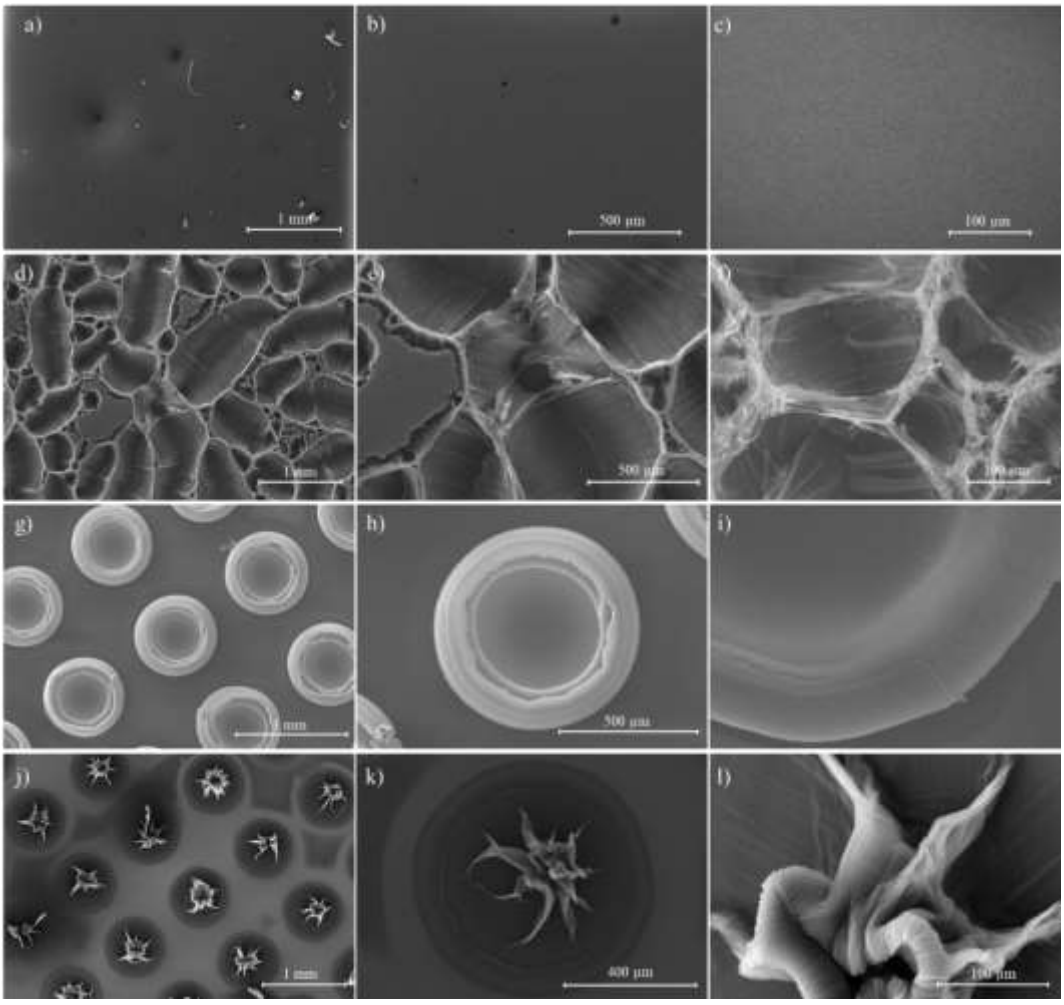

Figure 31 - SEM images of the morphology surface of (a to c) VA-CNTs forest; (d to f) VA-CNTs forest assisted by capillary driven features; (g to i) VA-CNTs micropillars; and (j to l) VA-CNTs micropillars assisted by capillary driven morphology.

The WCA was determined to assess the hydrophobic nature of the VA-CNTs surface, by static contact angle using the sessile drop method (drop volume 3 µL) and the shape of the liquid-vapor interface was determined by the Young-Laplace equation. From the Figure 32, it is possible to observe the water drop on the as-prepared VA-CNTs forest (a) and on the micro-patterned capillary driven VA-CNTs forest (b). The non-micro-patterned VA-CNTs presents a WCA of 160±7º which is super hydrophobic, as expected for the untreated VA-CNTs surface [108][109]. On the other hand, the micro-patterned VA-CNTs assisted by the acetone vapors induced the collapse of the vertical alignment of the nanotubes changing the WCA for 119±4º, indicating this processed film has a more hydrophilic surface, suggesting the possibility for some important biological activities, such as cell attachment

and neurite growth. The measurement of the WCA was also performed on the VA-CNTs micropillars, however the results obtained were not adequate for the study of the hydrophobic nature of the patterned material. The angle of the water drop could not be obtained as it showed no adherence to the patterned surface.

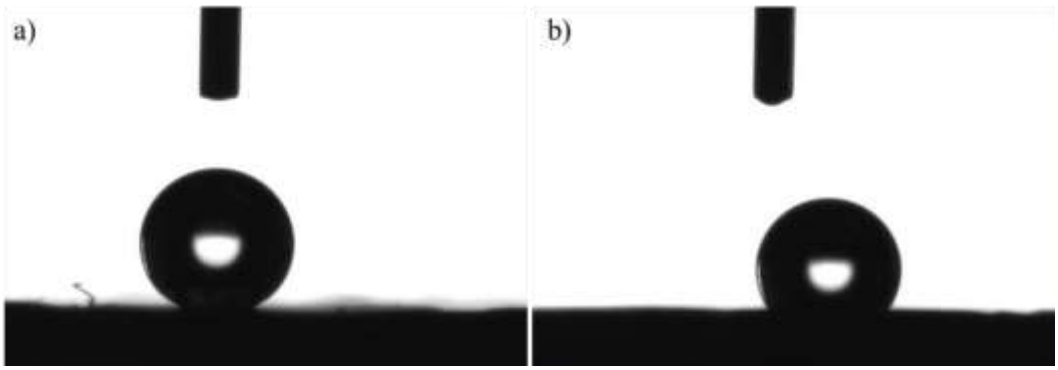

Figure 32 - WCA of the a) VA-CNTs – 160±7º and b) capillary driven VA-CNTs – 119±4º.

3. Conclusion

In conclusion, VA-CNTs were successfully grown from a multilayer catalyst comprised of Fe/Al_2O_3 deposited on Si/SiO_2 substrates via T-CVD. The introduction of a buffer layer (Al_2O_3) lead to an increasement of the VA-CNTs arrays height, improving the T-CVD growth process yield. This finding allows the controlling of the VA-CNTs arrays height, either by the addition of a buffer layer or by the CNTs growth time variation, where the maximum length of 499±6 µm was reached for 15 min of growth time. The HRTEM studies revealed that the obtained nanotubes are MWCNTs in accordance with the Raman study. The fabrication of micro-patterning and capillary driven patterning of VA-CNTs were also successfully achieved. First, a film of Fe catalyst was patterned by shadow mask on Al_2O_3/ SiO_2/Si substrate. Second, the micropillar made of VA-CNTs were grown by T-CVD. Next the capillary driven patterning was carried out by introducing solvent vapor into the array causing an overall shrinkage of the VA-CNT micropillars. Finally, various patterns were achieved by modification of the experimental parameters, namely the VA-CNTs deposition time and bocking layer (TiN).

Chapter 4 – VA-CNTs Biohybrid Materials

1. Experimental

1.1.Hydrogel Preparation

1.1.1. GelMA Synthesis

Gelatin methacrylamide was prepared by reaction of gelatin with methacrylic anhydride.

After dissolution of type A porcine skin gelatin (Sigma-Aldrich) in phosphate buffer saline (PBS, ITW Reagents) at 50 °C, the solution was stirred for 1 hour until fully dissolved. The gelatin temperature was lowered to 40 °C, and the MAA (Sigma Aldrich) was added at a rate of 0.5 mL/min under stirring conditions. After 1 h of reaction, the reaction mixture was parceled into four containers and centrifuged at 4200 rpm for 10 minutes. The solution was then diluted and dialyzed for 5 days against distilled water at 40°C, at continuous stirring, to remove salts and methacrylic acid. The reaction product was then freeze-dried leading to a white solid, stored at about -80°C until further use.

1.1.2. Hydrogel Synthesis

Cross-linking of the methacrylamide modified gelatin was performed in aqueous medium in the presence of a watersoluble photoinitiator, LAP (Sigma Aldrich).

Freeze dried gelatin-methacrylamide was dissolved in Dulbecco's PBS (DPBS, ITW Reagents) containing 0.5% of LAP as a photoinitiator at 50 °C, until entirely dissolved. To obtain the GelMA hydrogel, the mixture needs to be irradiated by visible light.

The lamp used to cure the samples was VALO® Grand Curing Light with 385 to 515 nm wavelength, considering LAP has a maximum absorbance at 365 nm and a certain absorption in the visible range of 400-420 nm (Figure 33). This distinctive feature allows an effective photopolymerization of the hydrogel in the visible light, averting any possible mutagenicity or oxidative stress on the cells, caused by UV light [76].

Photoinitiator	λ_{abs} (nm)
LAP	365, 405

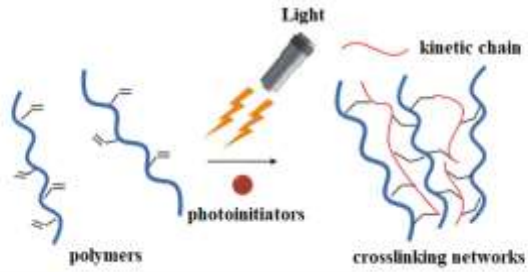

Figure 33 - LAP for photopolymerized hydrogels.[76]

1.2.Biohybrid Preparation

Biohybrid films were deposited on the VA-CNTs substrate by multiple casting methods.

(*i*) The biohybrid prepared by solvent-casting was obtained by the drop of 30 µL of the GelMA solution onto the surface of the substrate so that all the surface of the CNTs is coated.

(*ii*) Otherwise, on the spin coating method, a drop of 30 µL GelMA was fixed on the spin coater and the spin rate set as 900 rpm for 30 seconds. After both techniques, the biohybrid was submitted to visible light (1000 mW/cm^2) for 60 seconds, to obtain a crosslinked hydrogel.

(*iii*) The third method used to coat the CNTs substrate with the hydrogel was the combination of the two techniques mentioned above. Firstly, the substrate was subject to spin coating and exposed to 20 seconds of cross-linking time. Secondly, the sample is coated by solvent-casting, under the conditions cited.

All the samples were then stored in PBS at 37 °C for a selected period of time in order to access their dimensional stability.

1.3.Characterization

1.3.1. Scanning Electron Microscopy (SEM)

The hydrogel dimensional stability on the CNTs substrate was analyzed by the preparation of three sample morphologies by the solvent-casting method (30 μL/60 s UV exposition). The samples were collected for evaluation on day 0 (before immersed in PBS), and on the 1st, 4th and 14th day after kept immersed in PBS in an oven at 37 °C. Before SEM observation, the samples were freeze dried for 24 hours. The morphology and distribution of GelMA on the CNTs substrates was investigated by tabletop SEM (Hitachi TM4000Plus, Japan) operated in SE mode at 15 kV, equipped with EDS.

1.3.2. Fourier-transform infrared (ATR-FTIR) spectroscopy

To investigate the chemical interaction between VA-CNTs and GelMA, FTIR spectroscopy was performed by attenuated total reflectance -FTIR (ATR-FTIR, Perkin Elmer Spectrum BX, USA) from 4000-500 cm^{-1} with a resolution of 8 cm^{-1} and 64 scans.

2. Results and Discussion

2.1.Analysis of the dimensional stability of the biohybrids under simulated biological conditions

In order to validate the production of the biohybrid, the interfacial interaction between VA-CNTs and GelMA was accessed by using simplest synthetic methodologies. The produced GelMA hydrogel was proceeded by two different methods, the solvent-casting and spin-coating, which exhibited good compatibility.

The strong adhesion of the hydrogel upon deposition to the substrate was not equally verified, given the deposition method and the different patterns. On the spin-coating method it was easily verified the homogenous dispersion of the polymer on the surface of the substrate, forming a thin layer on its surface, as shown on Figure 34. However, the lack of a suitable hydrogel thickness on the hybrid would not grant support for the cells during the 14

cell culture days, on their proliferation and regeneration process, taking into account the fast degradation rate of the hydrogel, as observed on the next studies.

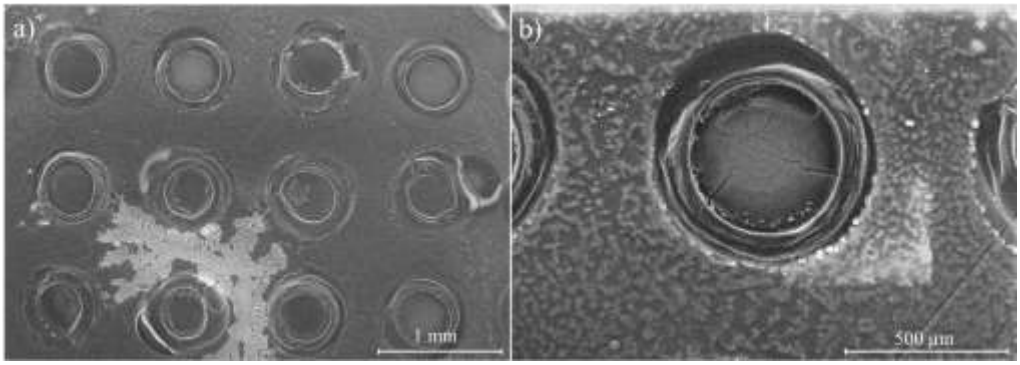

Figure 34 - Top-view SEM images of the VA-CNTs micropillars coated with GelMA by the spin-coating method.

On the solvent-casting method it was possible to observe a smooth adhesion of the GelMA to the VA-CNTs forest substrate, in contrast to the initial hydrophilic behavior revealed by the patterned CNTs micropillars surface, against the hydrogel. Nonetheless, after cross-linked the polymer showed good adherence to the CNTs substrate.

Therefore, to characterize the VA-CNTs morphologies coated with hydrogel was used SEM. Images of the prepared biohybrid showed a rapid decrease on the presence of GelMA coating the carbon materials under simulated biological conditions.

The morphology and distribution of hydrogel in the VA-CNTs forest, obtained by SEM imaging (Figure 35), demonstrates the presence of the hydrogel onto the forest before its immersion in PBS (day 0) and the degradation of the polymer over 14 days, referring to the time required for cell study. In this way, it is possible to denote the degradation of hydrogel after the first day. While the VA-CNTs forest exhibits a uniform coating of its surface on day 0, the sample removed from PBS after 1 day shows a still remarkable coating but notable GelMA degradation as the morphology of the forest begins to be exposed. However, on the 4^{th} and 14^{th} day the surface morphology of the forest does not change in the 3 samples collected, not showing the presence of a thin layer of hydrogel, as opposed to the samples of day 0 and 1.

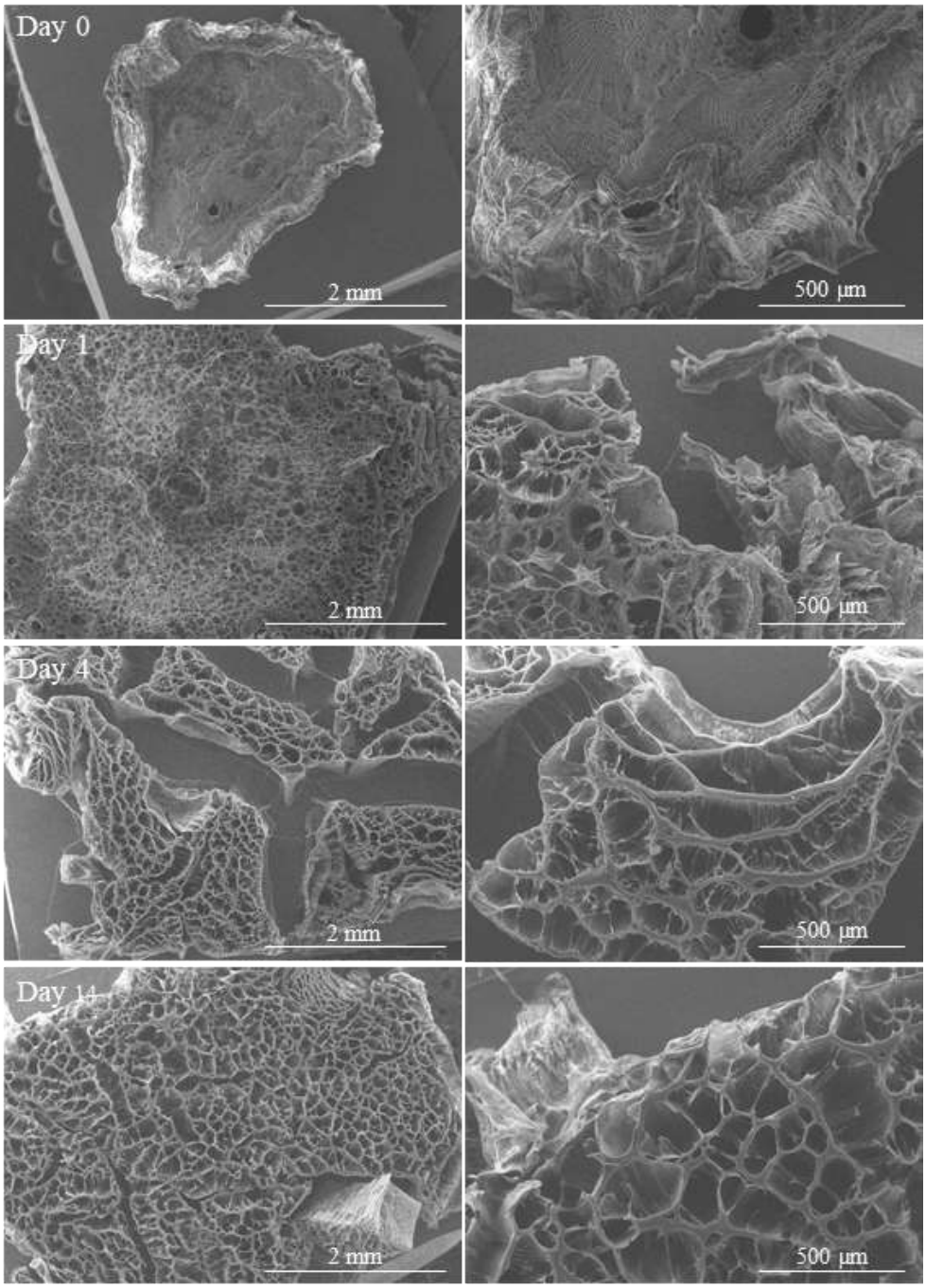

Figure 35 - SEM images show the morphology of porous surfaces of VA-CNT forest-GelMA layer. The image shows nanofibrous networks of CNTs involved on a gelatin thin layer, over 14 days.

As an alternative morphology to verify the hydrogel degradation behavior, Figure 36 and Figure 37 represent the VA-CNTs micropillars before and after being subjected to capillary driven process, respectively. In this morphology, can be observed a major discrepancy of the polymer concentration on the substrate surface, from the 1st to the 4th day.

Although there is an aggregation of the polymer on day 1, it is completely degraded by day 4, resulting on a thin film involving the external micropillars walls, from day 4 to 14 days of incubation. Therefore, there is no relevant difference between the hydrogel and the carbon nanostructures interaction on the patterned substrates subjected to the capillary driven process.

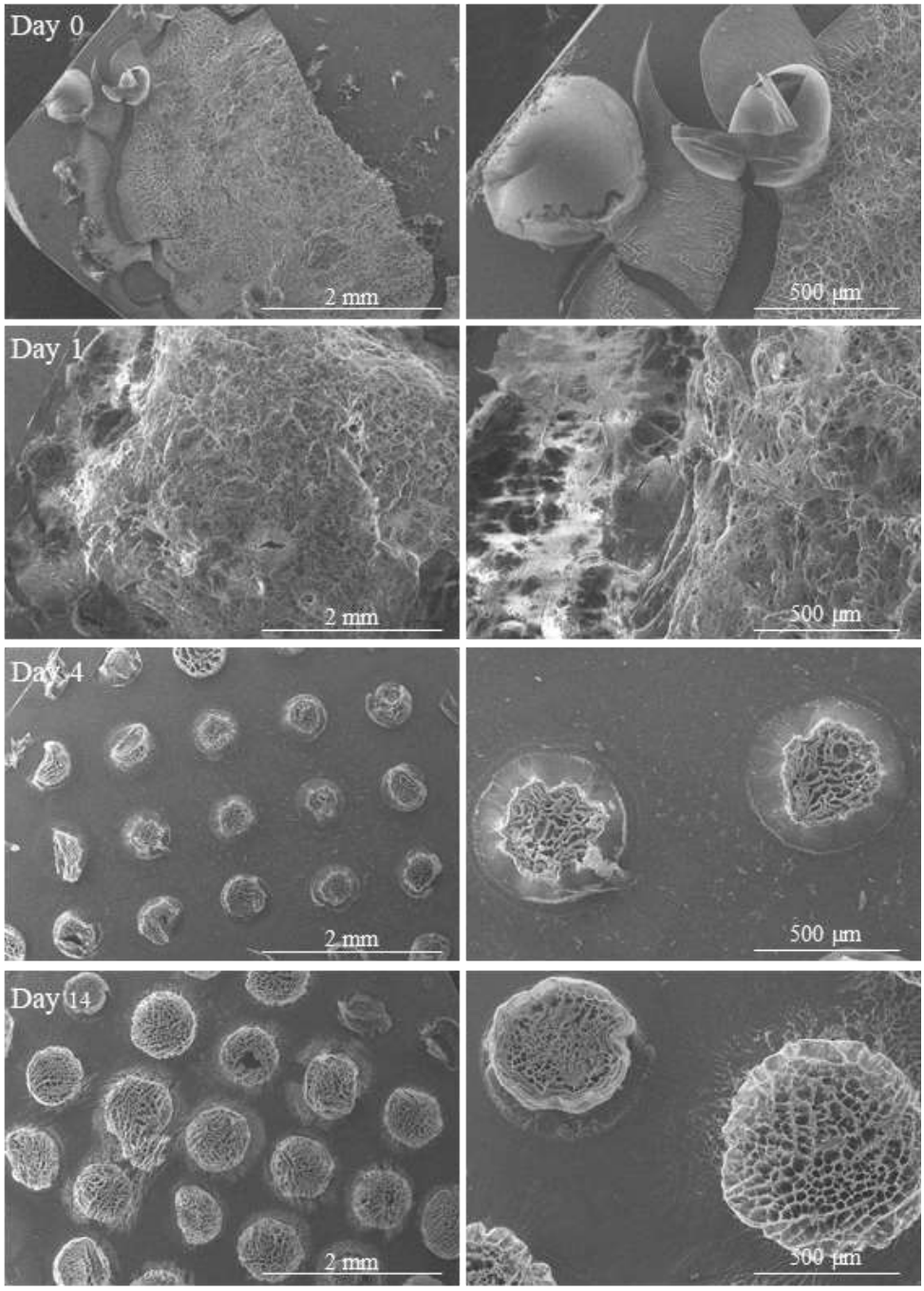

Figure 36 - Top-view SEM image of VA-CNTs micropillars covered on a thin GelMA layer for degradation studies, for 14 days.

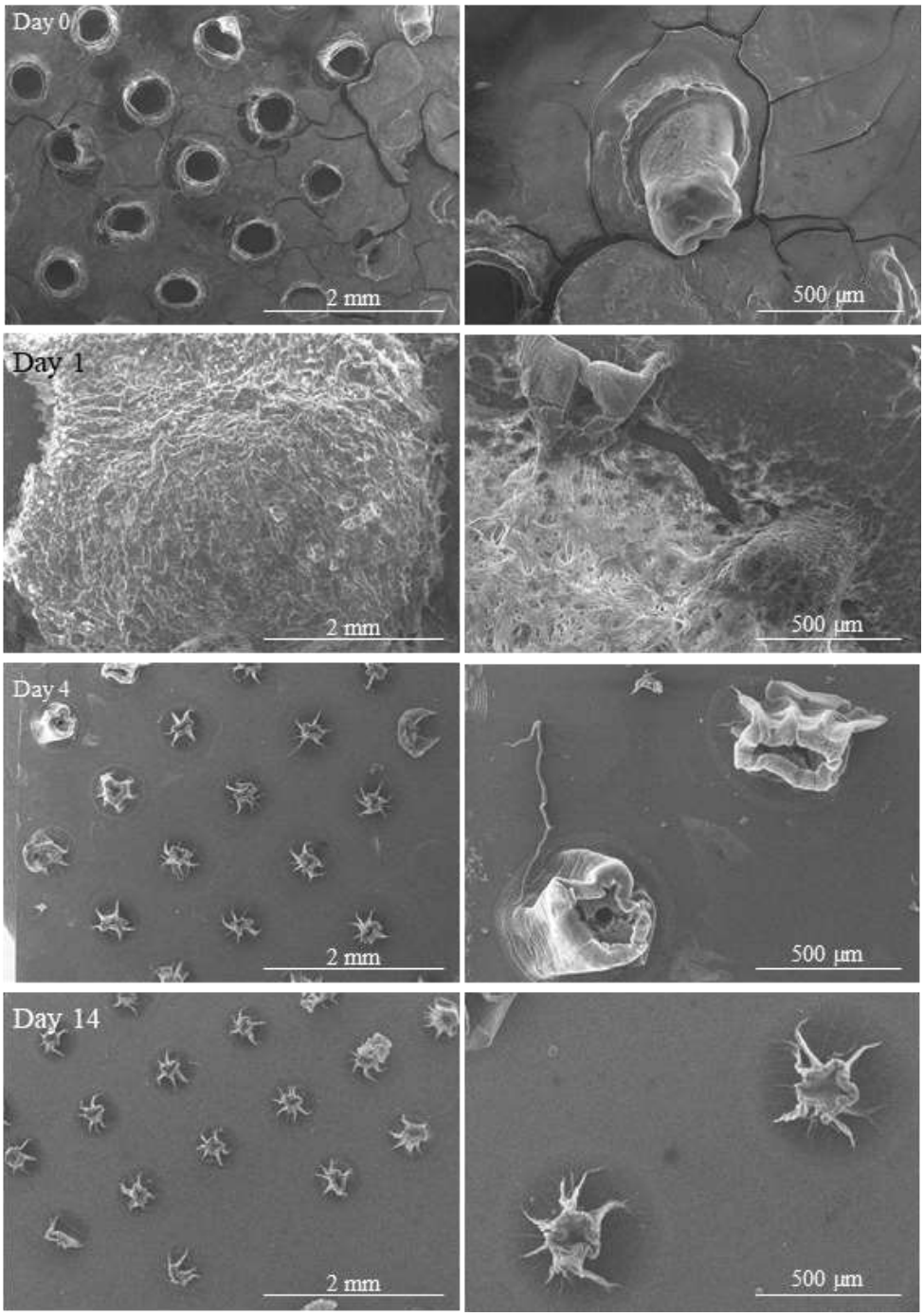

Figure 37 - SEM images of the degradation of GelMA on the patterned capillary driven CNTs micropillars, over 14 days.

To further verify the lack of hydrogel dimensional stability demonstrated by the SEM images on the different CNTs morphologies, the interaction between the VA-CNTs and the GelMA hydrogel was investigated by means of FTIR measurements (Figure 38). FTIR

reveals information about the chemical bonds on the material, since each chemical bond emits a specific frequency, related to their energy level [110].

In the FTIR spectra, t=0 and t=1 CNTs/GelMA spectra (referred as the liofilized CNTs/GelMA samples before PBS and 1 day after emerged in PBS, respectively) shows some GelMA characteristic peaks between 1100 and 1700 cm^{-1}, related to C=O stretching groups and C−N−H bending. In addition, t=0 d and t=1 d spectra present broad peaks at around 3000 and 3300 cm^{-1} representing the C−H stretching groups and the presence of peptide bonds (mainly N−H stretching) respectively, indicating the presence of GelMA on the two samples correspondent to the t=0 d and t=1 d spectra [111]. In opposition, as ATR-FTIR results shows, the spectra for t=4 d and t=14 d, exhibits no characteristic peaks for the presence of GelMA. As verified in previous studies [112], the CNTs spectrum usually show their bands around 3400 cm^{-1} due to the vibrations of the elongation of the hydroxyl groups (O−H) and around 1650 cm^{-1}, representing the elongation vibration of the group C=O. As both materials exhibit some characteristic peaks on the same wavelength, it is possible to occur a band overlap, making it impossible to identify CNTs peaks.

Therefore, the resulting ATR-FTIR spectrum suggests that physical blending of GelMA to the VA-CNTs changes chemical composition and leads to the mass loss of the polymer over time, especially after day 4 (t=4 d).

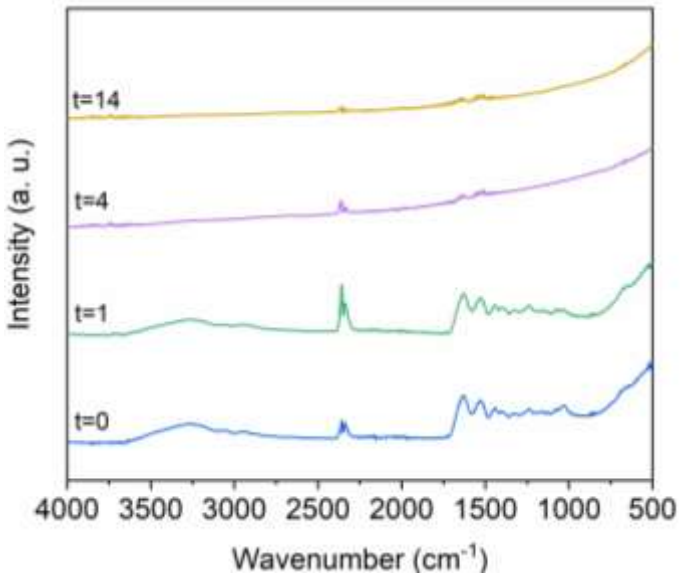

Figure 38 - FTIR pattern of VA-CNTs/GelMA hybrids.

3. Conclusion

In this work, three approaches were developed to integrate the synthesized GelMA hydrogel on the VA-CNTs substrates. The dimensional stability of the VA-CNTs biohybrids under simulated biological conditions were characterized in agreement with the different approaches.

SEM images demonstrated that the hydrogel overly degraded over time and that they could not serve as niches where neural stem cells can proliferate, interact, and benefit from a continuous intake of cell nutrients. FTIR results initially indicate the presence of GelMA on the studied VA-CNTs patterns, however after 4 days of immersion in PBS the hydrogel had degraded completely for all the biohybrid tested.

The results demonstrated that the use of the biohybrid methodology using GelMA specifically would not be viable and therefore, the work progressed without its integration on the different VA-CNTs substrates.

Chapter 5 – Cytocompatibility of VA-CNTs structures with neural stem cells

1. Experimental

1.1.Cell Culture, propagation and seeding

An individual cell line (NE-4C) was used to assess the suitability of the various VA-CNTs based structures to be explored as stimulus responsive platforms for neuronal growth. The NE-4C neuronal cell line obtained from the American Type Culture Collection (ATCC) was grown in cell culture flasks using Eagle's Minimum Essential Medium (EMEM, Sigma-Aldrich) with 10% (v/v) Fetal Bovine Serum (FBS, Sigma-Aldrich) and 1% (v/v) penicillin/streptomycin (P/S, Sigma Aldrich).

Before seeding the cells on the different patterned VA-CNTs patterns, cells were grown to confluency. Therefore, about three days after establishing the primary cell culture in 75 cm^2 flasks, stem cells were confluent. At this time, the culture medium was aspirated, and the cells washed with PBS. Then, the cells were incubated with 3 mL of Trypsin-EDTA (Ethylenediamine tetraacetic acid) solution (0.05%, Sigma Aldrich) for 15 minutes at 37 ˚C to detach them from the culture flask. To stop the trypsin action, 8 mL of complete growing medium were then added to the culture flask. Culture medium with the resuspended stem cells was then transferred by gently pipetting to tubes that were centrifuged at 300 xg for 5 minutes. After removing the supernatant, the cells pellet was resuspended in fresh culture medium.

VA-CNTs substrates were UV sterilized and transferred into sterile wells of 24-well plates. Then, 5×10^4 cells in culture medium were seeded on 5x5 mm substrates, and cultured for different time periods, ranging from 1 to 14 days. After 24h in culture, all-trans retinoic acid (RA, Sigma Aldrich) was added to the complete medium on a reserved set of samples from each morphology, to induce neuronal differentiation. After 48h, the medium was changed to a RA and serum-free neuronal medium: Dulbecco's modified Eagle's/F-12 nutrient medium supplement with 1% (v/v) B27 (Thermo Fisher Scientific) and 1% (v/v) insulin-transferrin-selenium (ITS, Sigma Aldrich). 1% (v/v) P/S was added as antibiotics.

The control samples in all experiments were glass coverslips for cell culture. All cultures were grown in a humidified atmosphere containing 5% CO_2 incubator at 37 °C and the culture and differentiation medium totally renewed every 2 days.

1.2.Characterization

1.2.1. Cell viability and proliferation

To evaluate the ability of different VA-CNTs substrates to support cell growth and proliferation, resazurin viability and Live/Dead assays were performed.

For resazurin viability assay, the sterilized VA-CNTs substrates patterns were placed on 24-well plates. A total of 5×10^4 NE-4C cells/scaffold were subsequently seeded on the substrates and on the coverslips ("control"). At determined time points (1st, 3rd, 7th, and 14th day) cells were incubated for 4h in the dark with fresh medium containing 10% (v/v) of a 0.1 mg/mL resazurin (ACROS Organics) in PBS, after which 100 µL per well was transferred to a 96-well plate. Resazurin reduction to resorufin was thereafter measured in a microplate reader by spectrophotometry (Synergy HTX, BioTek) at 570 nm (resazurin maximum absorbance) and 600 nm (resorufin maximum absorbance) (*n*=3 for each group). For each day, a final optical density value (O.D.f) was calculated as follows:

$$\mathrm{ODf} = \mathrm{Sample}\left(\frac{\mathrm{OD}_{570\mathrm{m}}}{\mathrm{OD}_{600\mathrm{m}}}\right) - \mathrm{Negative\ Control}\left(\frac{\mathrm{OD}_{570\mathrm{m}}}{\mathrm{OD}_{600\mathrm{m}}}\right)$$

where the negative control is the O.D. of resazurin in the absence of cells.

To evaluate the cells viability/proliferation through the Live/Dead assay, medium was removed from the NE-4C cells and replaced by live/dead viability/cytotoxicity solutions at day 1, 7 and 14 of the culture. The LIVE/DEAD™ Viability/Cytotoxicity Kit for mammalian cells from Thermo Fisher Scientific was used. The VA-CNTs structures were washed twice with PBS. A live/dead solution was prepared by adding 4µL of ethidium homodimer-1 (EthD-1, Thermo Fisher Scientific) stock solution to 2 mL of sterile PBS and, after mixing thoroughly, 1 µL of calcein AM (Thermo Fisher Scientific) solution was added to the 2 mL EthD-1 solution. The solution was directly added to the CNTs structures in order to cover the whole sample and was left for 45 minutes at RT. Finally, the cells were washed once with PBS, and fluorescent images were obtained by fluorescence microscope

(Axioimager M2, Zeiss). The number of NE-4C cells that were grown on the various VA-CNTs substrates were determined by counting cell nuclei stained with calcein. Nuclei number was assessed with ImageJ (cell counting plug-in), using 3 images of the various morphologies on an area of $1{,}54\times10^{-3}$ cm^2.

1.2.2. Scanning Electron Microscopy (SEM)

The NE-4C neuronal stem cells cultured on the patterned VA-CNTs surfaces were observed by SEM. After culturing (1^{st}, $7^{th,}$ and 14^{th} day), the cells were washed twice with 0.1 M sodium cacodylate buffer (SCB, Sigma Aldrich) and fixed with solution 2.5% PFA + 2.5% GDA in SCB for 20 min at RT. All surfaces were then washed three times with 0.1 M SCB and dehydrated by immersion with (v/v) 30%, 50%, 70% 90%, 100% ethanol. Finally, the samples were dried using hexamethyldisilazane:ethanol at 1:2, 1:1, 2:1 and followed by 100% hexamethyldisilazane (HDMS, TCI. Japan). Finally, the samples were left to dry at RT overnight. SEM analysis was performed on a tabletop SEM (Hitachi TM4000Plus, Japan), operated in back-scattered electrons (BSE) mode at 15 kV, equipped with EDS.

1.2.3. Immunocytochemical Staining

Immunocytochemical staining allows to visualize if the stem cells have differentiated into neurons or astrocytes.

Neuronal cell differentiation was induced by the addition of all-trans RA to the culture medium, after 24h in culture and the change to a RA and serum-free neuronal medium within 48h hours.

After the 10^{th} day of culture, the culture medium was aspirated from the culture wells and the cells grown on the CNTs substrates were fixed with 4% paraformaldehyde in PBS for 20 minutes. After that period the cell were washed multiple times with PBS and permeabilized at RT with 0.1% Triton X-100 (Fisher Scientific) in PBS for 5 minutes. After the fixation of cells and their permeabilization, the nonspecific binding sites were blocked with 2% bovine serum albumin (BSA, Thermo Fisher Scientific) in PBS for 30 minutes.

The cells were then incubated with the primary antibody solution diluted in 0.1% BSA + 0.1% Triton in PBS, followed by 1 hour incubation at RT. Two sets of samples were prepared in order to identify different elements on the four different morphologies. On the first set, neurites were stained with purified anti-tubulin β 3 (Anti-Tuj1, 1:1000), while astrocytes were stained with anti-glial fibrillary acidic protein (Anti-GFAP, 1:500), while the second set of samples resorted to Anti-Tuj1 (1:1000) to stain neurons and synaptophysin [YE269] (1:200) to stain synapses. The primary antibodies were removed by washing three times with PBS. Finally, secondary antibody (anti-mouse 1:500 with anti-chicken 1:1000 for the first set, and anti-mouse 1:500 with anti-rabbit 1:1000 for the second set) was added in the dark for 45 minutes at RT. The cells were rinsed and stored in PBS in the dark. The cells were then nuclei counterstained with SlowFade™ Diamond Antifade Mountant with DAPI (4',6-diamidino-2-phenylindole, Sigma).

1.2.4. Statistical Analysis

All the quantitative data are expressed as mean ± standard deviation (SD). Statistical significance was determined, using OriginLab, by performing One-way analysis of variance (ANOVA), followed by post hoc Tukey's test, except for VA-CNTs forest morphology for cell quantification, where a Kruskal-Wallis ANOVA was used, followed by post hoc analysis for non-parametric tests. Significance was accepted at *p*-values inferior to 0.05.

2. Results and Discussion

2.1.1. Cell Viability assay

i. Resazurin Assay

Living cells are metabolically active and are able to reduce via mitochondrial reductase, the nonfluorescent dye resazurin to the strongly fluorescent dye resorufin. This reduction is proportional to the metabolic activity of a cell population and therefore resazurin assay is a valuable and noninvasive tool to measure live cell number as it is non-toxic for the cells which can then return to culture or be used for other purposes [113].

To observe whether the presence of VA-CNTs and their different patterning morphologies inhibited viability of the NSC used, the cells were submitted to the resazurin viability assay (Figure 39 and Figure 40). It was determined that neither the CNTs nor their various organizations inhibit cell viability of NE-4C cells over a 14 days culture time period.

Figure 39 shows the growth behavior of the stem cells when cultured on the control. Cells exhibit a high proliferation rate up to 7 days. Afterwards, their growth seems to slow down or even become stagnant. This is most likely due to the cells approaching confluence and their growth become contact inhibited and subsequently their metabolism may slow down. Moreover, it is also possible that some cells are dying as a natural process for developing stem cell derived neuronal cultures, whereas the cell maturation process includes some cells apoptosis while others continue to mature freely. Regarding the various VA-CNTs patterns, all present a similar profile compared to the control, *i.e.*, a significant proliferative rate up to 7 days followed by a stagnant-like growth.

Since the micropillars based morphologies do not present as much VA-CNTs as the forest-based ones that cover all the Si substrates, comparisons between these morphologies are deemed not useful to do in terms of percentage of cells presenting a metabolic activity throughout the entire samples. Overall, these results indicated that VA-CNTs are favorable platforms for NE-4C neural stem cells to proliferate, regardless the morphology and organization given to the CNTs.

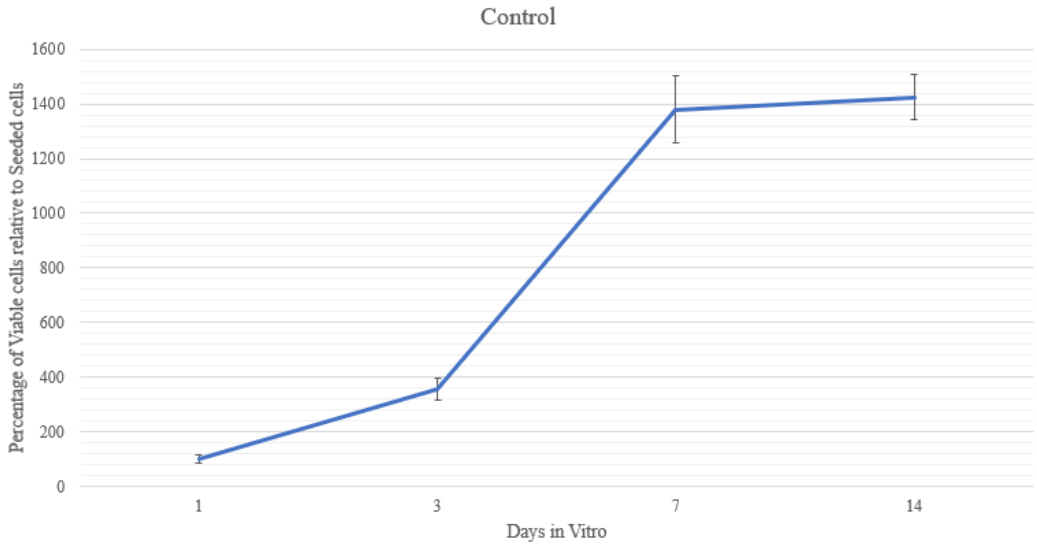

Figure 39 - NE-4C cell viability by resazurin assay (control).

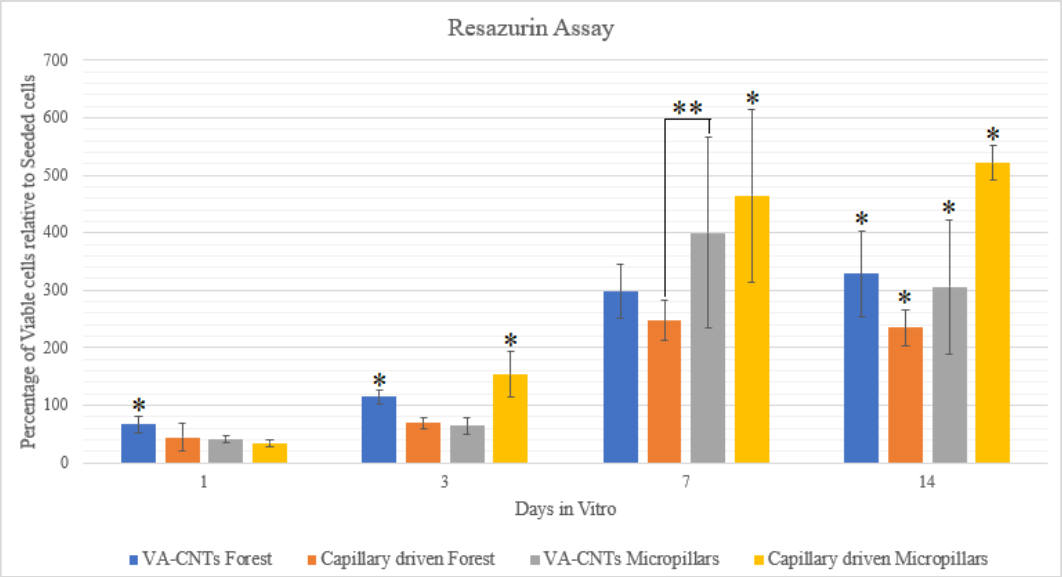

Figure 40 - VA-CNTs on NE-4C cell viability by resazurin assay. Statistical analysis by One-way ANOVA followed by post hoc Tukey's test: *p <0.05, n=6, where * denotes statistical significant difference between morphologies for each day; **p <0.05, n=6, where ** denotes statistical significant difference between two morphologies for each day.

ii. Live/Dead Assay: Fluorescence microscopy and live cells quantification

The cytotoxicity was also examined via the Live/Dead assay (Figure 41). This experiment came to confirm the increasing cell proliferation of the NE-4C cell line with increasing culture time, as observed by the resazurin assay. The quasi-absence of dead cells and the considerable cell proliferation on the VA-CNTs platforms over the 14 days of culture demonstrate that the carbon nanomaterial support the survival and proliferation of NSCs. The small number of dead cells present on the samples can still be explained as the natural process for developing stem cell derived neuronal cultures, the cell maturation process, which consists on the death of some cells while others continue to mature freely [99]. Initially, at shorter times of culture (up to 7 days), there was no apparent lack of adhesion from the cells to any of the various morphologies, neither on the CNTs based structures nor the Si substrates. However, after 14 days, the cells seem to present a decreased presence on the Si substrate of the VA-CNTs micropillars samples, in opposition to the micropillars walls. The reduction of the live cells at the 14th day of the cultured, reflected particularly on the CNTs micropillar substrates, might be associated with the fact that cells seem to have

adhered more strongly to the VA-CNTs walls, while the cells deposited on the Si substrate have died and disappeared over time (with the medium replacement every 2 days and the several washes associated to the live/dead assay). This led to the apparent reduction of the live cells present on this morphology sample, as the cells where adhered to the sidewalls of the carbon nanotubes and could not be accounted by top view images.

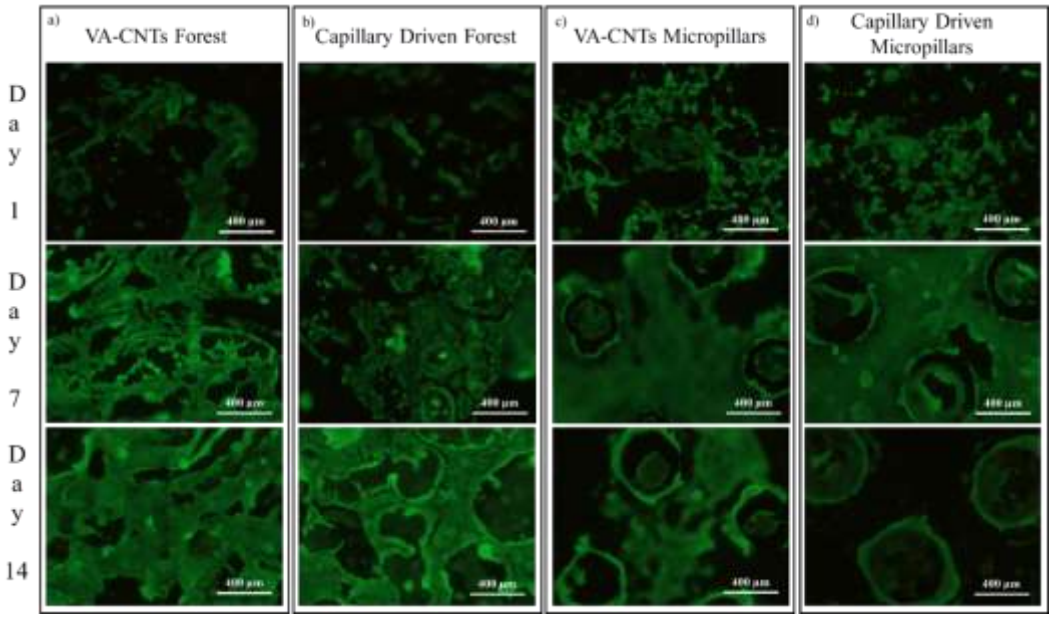

Figure 41 - Live/Dead images of NE-4C cells on different substrate morphologies, after culturing for 14 days.

The percentage of the live cells evaluated from the data obtained via fluorescence microscopy (Figure 42), showed that CNTs forest morphology induced slow but continuous cell proliferation increase over the 14 cell culture days, while the micropillars morphology exhibited a striking increase of the percentage of viable cells (~40-50%) from day 1 to day 7, followed by an abrupt decrease on the 14th day of cell culture, in a statistically significant percentage of cells (~35-40%). However, this quantification of the viable cells is related to both the CNTs structures and the Si substrate, so the interpretation must rely on the concomitant observation of the fluorescence microscopy (Figure 41). Thus, the live cells decrease observed on the VA-CNTs micropillars substrates can be associated with the morphology of the platform, since the NSCs exhibited preference for the carbon structures

to adhere and proliferate, rather than the Si substrate, for longer culture periods. So, the calculated decrease of live cells for the micropillars based morphologies are representative of the lack of adhesion and loss of cells in the Si substrate part of these samples and the angle of the results visualization interfering with the counting of the cells on the sidewalls.

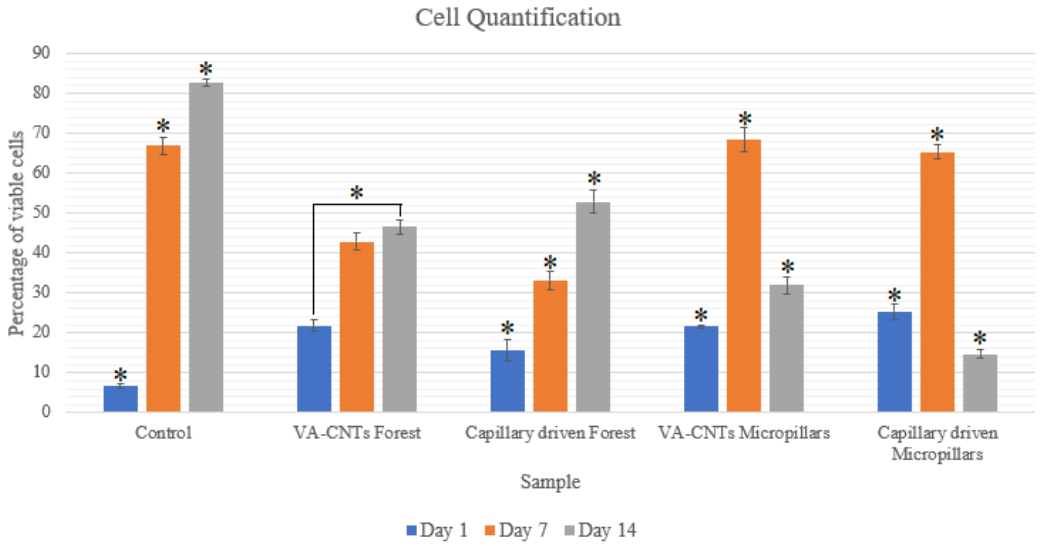

Figure 42 - Percentage of Live cells challenged with different CNTs morphologies, analyzed under fluorescent microscopy. Statistical analysis by One-way ANOVA followed by post hoc Tukey's test: $*p$ <0.05, n=3, where * denotes statistical significant difference in between days for each morphology; on VA-CNTs Forest morphology, statistical analysis was performed by a Kruskal-Wallis ANOVA test, followed by a post-hoc analysis for non-parametric tests: $^{\#}p < 0.05$, n=3, where # denotes significant difference between days of culture.

2.1.2. Scanning Electron Microscopy (SEM)

Figure 43 and Figure 44, show the SEM analysis of the seeding and proliferation of the NE-4C cell line on the VA-CNTs forests, which presented a smoother surface. In this morphology the cells have exhibited an intimate contact with the CNTs forest and display a clear proliferation progress through the 14 days of cell culture, with a higher concentration on the superior zones of the CNTs forest and filaments, as already visualized by fluorescence microscopy images. Between the two forest pattern substrates, no significant difference can be considered. Yet, a slight preference for the capillary driven substrate is noted, as cells seem to proliferate in a higher range.

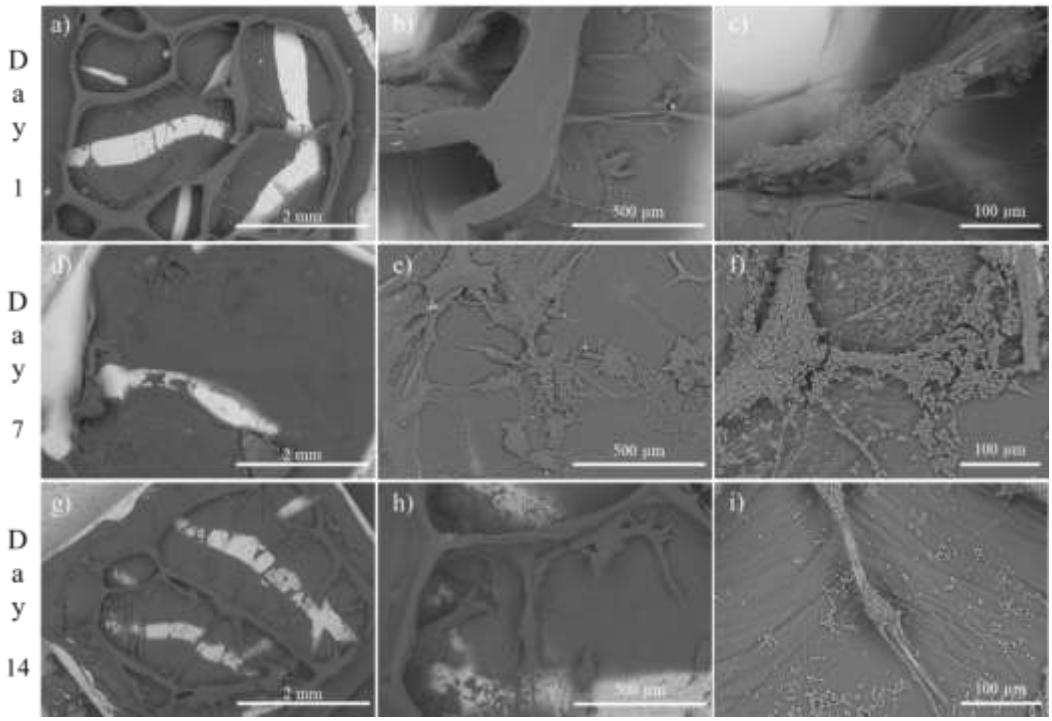

Figure 43 - Top-view SEM images after NSCs were seeded and cultured for 1 (a to c), 7 (d to f) and 14 (g to i) days on the VA-CNTs forest.

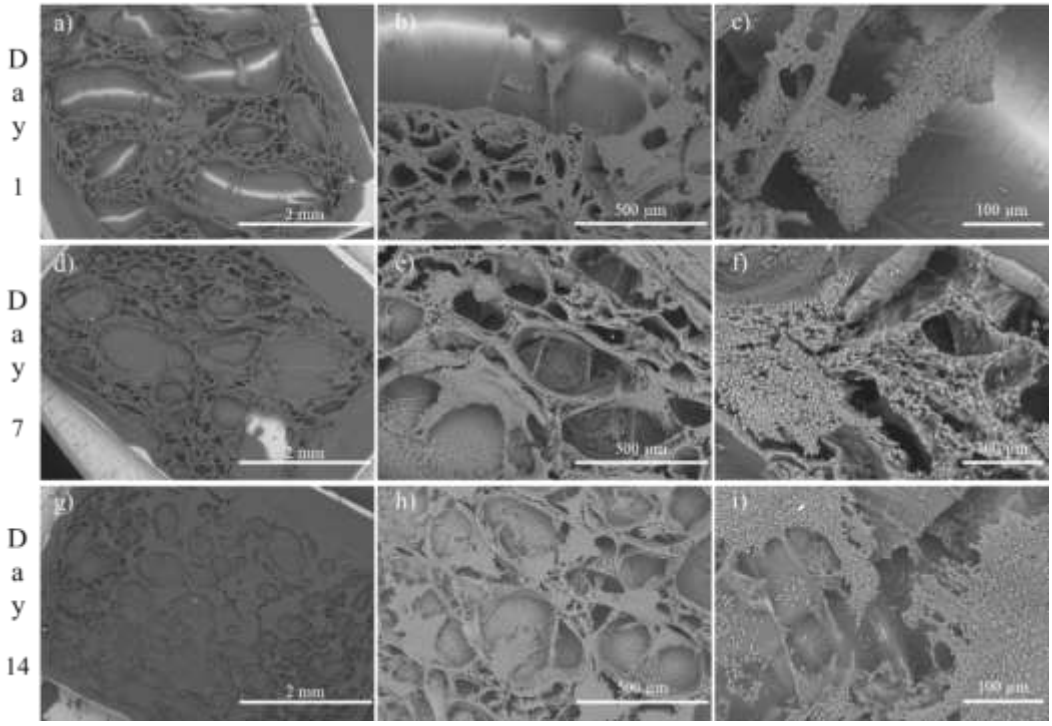

Figure 44 - Top-view SEM image of capillary driven CNTs forest as support for NSCs survival and neurite outgrowth. Images taken after cell line were seeded and cultured for 1 (a to c), 7 (d to f) and 14 (g to i) days.

On the VA-CNTs micropillars templates Figure 45 and Figure 46, once again results show clearly the preference of the seeded neural stem cells for the VA-CNTs micropillars walls in comparison to the Si substrate, over the 14-culture days, agreeing with the results from the Live/Dead assay. This behavior is related to the NSCs need to adhere in order to proliferate, therefore even if the cells attach to the Si substrate instead of the VA-CNTs micropillars on day 1, by day 7 the cells can have proliferated in bundles and attached to the carbon structures, while the cells on the Si substrate may undergo apoptosis and/or have been removed by washes and medium changes. After 7 days it was expected to find neurites of several millimeters long connecting the micropillar. However due to the large interspacing of 400 µm, in opposition to the ideal 10 µm pointed by *Gabriela S. et al.* [99], neurite network formation was not achieved. Instead, it is perceived the formation of large bundles (fasciculation) connecting the micropillars arrays, as it can be observed either on the VA-CNTs micropillars substrate (Figure 45 (g to i)) and the capillary driven micropillars pattern (Figure 46 (e and h)). Although the bundles are involving the micropillars, they appear to have a random organization when forming the neurite network. The noticeable cell substrate

preference also suggests that NSCs sense and actively respond to surface roughness, selecting the uneven micropillars walls in opposition to the plain Si substrate surface [114].

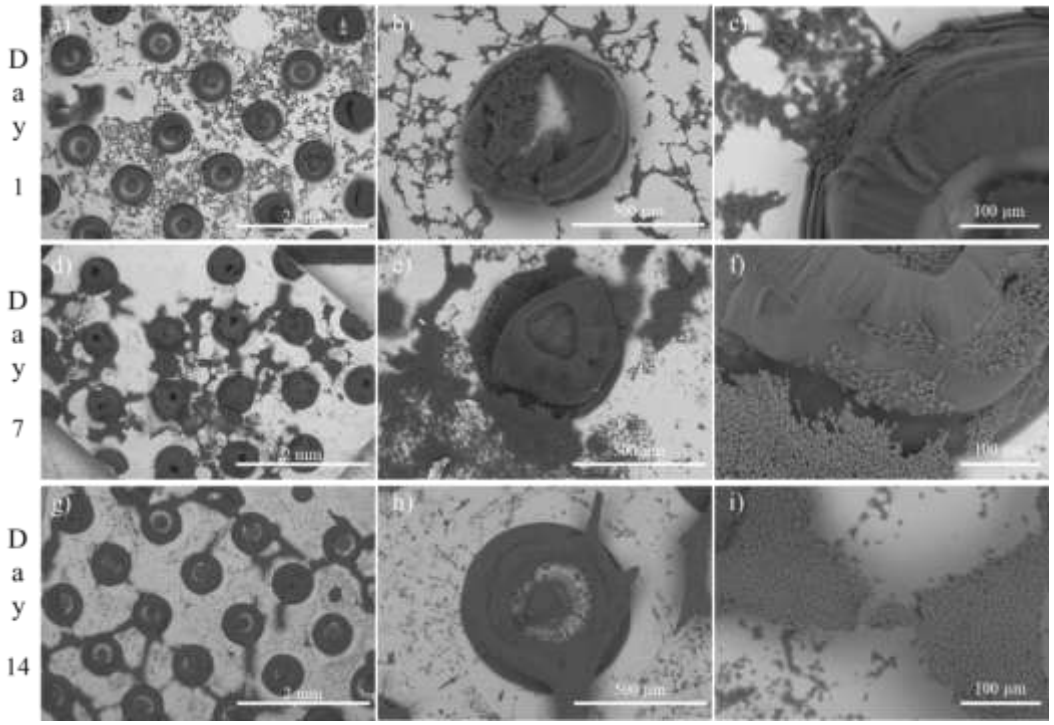

Figure 45 - Top-view SEM images after NSCs were seeded and cultured for 1 (a to c), 7 (d to f) and 14 (g to i) days the patterned VA-CNTs micropillars.

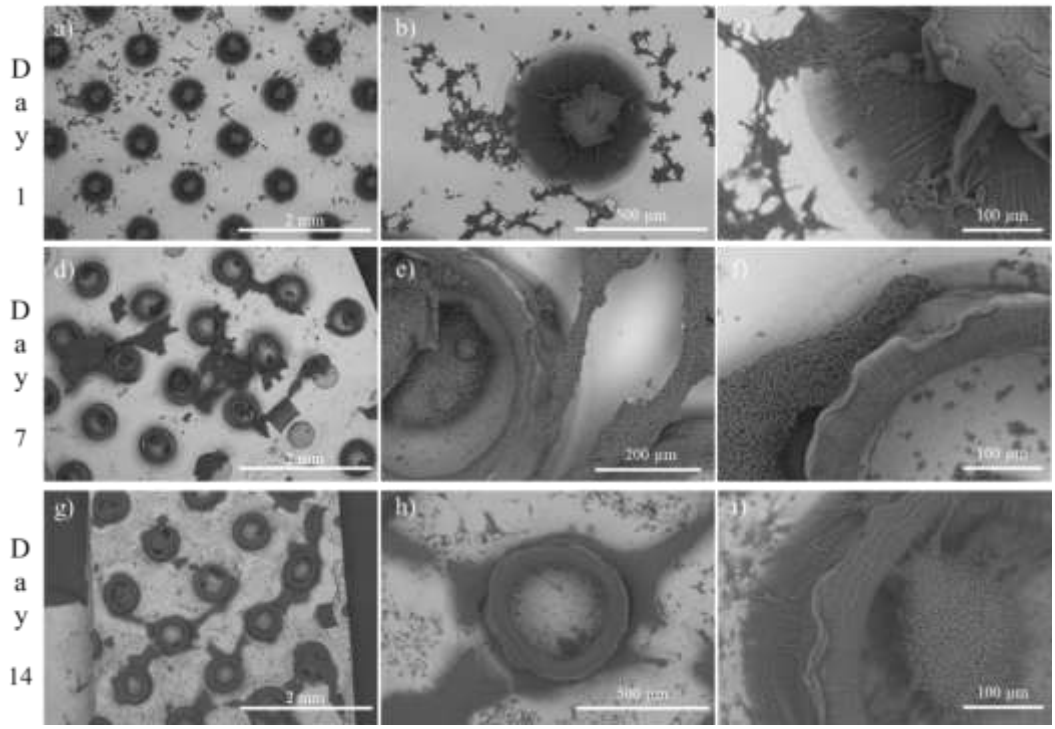

Figure 46 - SEM images of the neuronal network of cells (NE-4C cell line) seeded and cultured for 1 (a to c), 7 (d to f) and 14 (g to i) days the capillary driven patterned VA-CNTs micropillars.

2.1.3. Immunocytochemical Staining

In order to obtain a VA-CNTs platform capable of replicating the development of neurogenesis, NE-4C cell line was seeded on the different prepared CNTs patterns to study their capacity to proliferate and differentiate. Previous experiments report have already investigated neural differentiation on CNTs forests and micropillars and determined that CNTs/stem cells interaction have potential for aiding neuron differentiation [115][116].

Although NSCs proliferated in all the VA-CNTs patterns (Figure 47), the forest morphology transmitted a weak signal for Anti-Tuj1 positive (green), while the CNTs micropillars show strong Anti-Tuj1 expression that signals the NSCs differentiation into neurons. Furthermore, the GFAP staining (red) that marks the presence of astrocytes is scarcely seen, which suggest that NSCs have almost completely differentiate into neurons, making the CNTs platforms potentially favorable neuronal regeneration. The scarce presence of astrocytes, although known for the formation of scar tissue that is prejudicial for regeneration [117], it is not troubling as astrocytes have also the capability of secreting neurotrophic factors, providing support and guidance for axonal growth and an improved functional recovery of the SCI, while the glia scar is still in formation [118][119]. Within

this context, further studies should focus on the effect of VA-CNTs on the phenotype of astrocytes.

Immunofluorescence images revealed also an evident tendency of the neuronal cells to adhere and proliferate on the periphery/edges of the VA-CNTs forests and on the sidewalls of the nanotubes micropillars, as can be observed on Figure 47b and Figure 48e, as the cells seem to create thick bundles in those areas. Besides the neurons demonstrating the ability of directly attaching to the VA-CNTs forest and pillars and outgrow, they did not appear to exhibit preferential orientated growth over the CNTs patterns. Thus, neurites grew randomly across the nanotube's morphologies arranged in various directions.

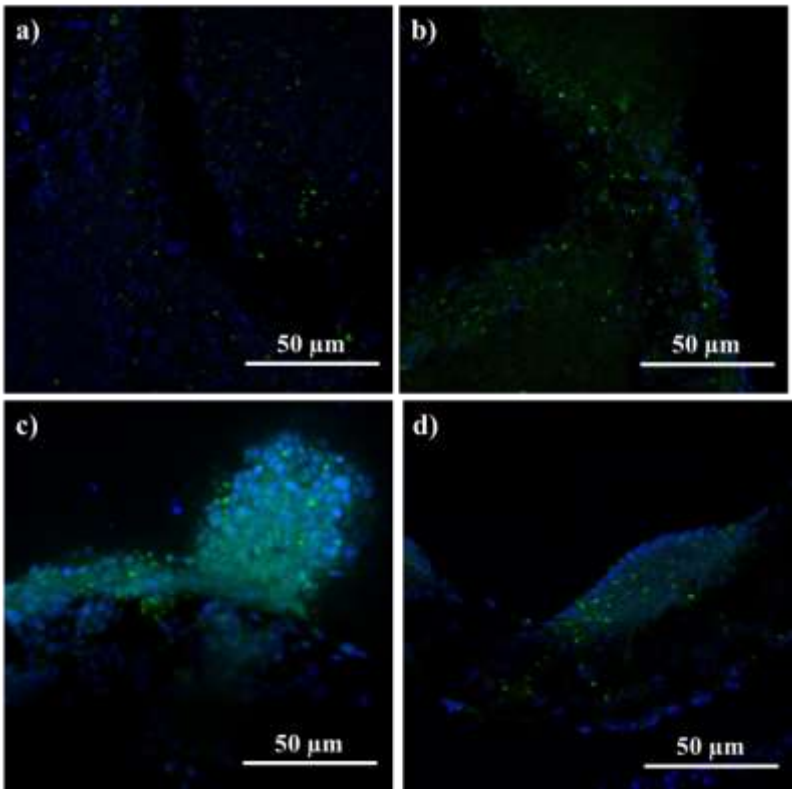

Figure 47 - Immunocytochemical merge images of NSCs cultures on CNTs platforms, labeled with Anti-Tuj1 (green) and GFAP antibody (red); a) VA-CNTs forest, b) capillary-driven CNTs forest, c) VA-CNTs micropillars and d) capillary driven CNTs micropillars.

Figure 48 displays the samples stained with Anti-Tuj1 and synaptophysin. In conjunction with differentiation, synaptogenesis is another critical aspect of the nervous

system function. In order to study synapse formation, the differentiated NSCs were stained for synaptophysin, an integral membrane glycoprotein that occurs in the presynaptic vesicles of neurons.

In Figure 48a) and c), it can be noted from the Anti-Tuj1 deposition marking for differentiation into neurons (green) and nuclei staining (blue), that although these samples, *i.e*., the forests and the micropillars, showed a good proliferation of the neural stem cells (blue), little differentiation can be visualized (green). This can be related to the formation of cell bundles inhibiting cell maturation and affecting the dendrite elongation phase [120].

In opposition, capillary driven CNTs forest and micropillars (Figure 48b), d) and e)) show good adhesion, proliferation and most notably cell differentiation with the formation of dendrites. The factor that marks the difference between the capillary driven morphologies and the remaining is the surface nanoscale roughness, very suitable for cell support and directing neurite growth, even though it was not observed on the prepared samples [85]. Therefore, this bio-mimetic topography more similar to the *in vivo* conditions, coupled to the higher concentration of cell nutrients on the superficial regions of the substrates, resulted in increased cell proliferation and differentiation along the forest edges and micropillars tops, in resemblance to the previous study by Usmani S. *et al.* [121].

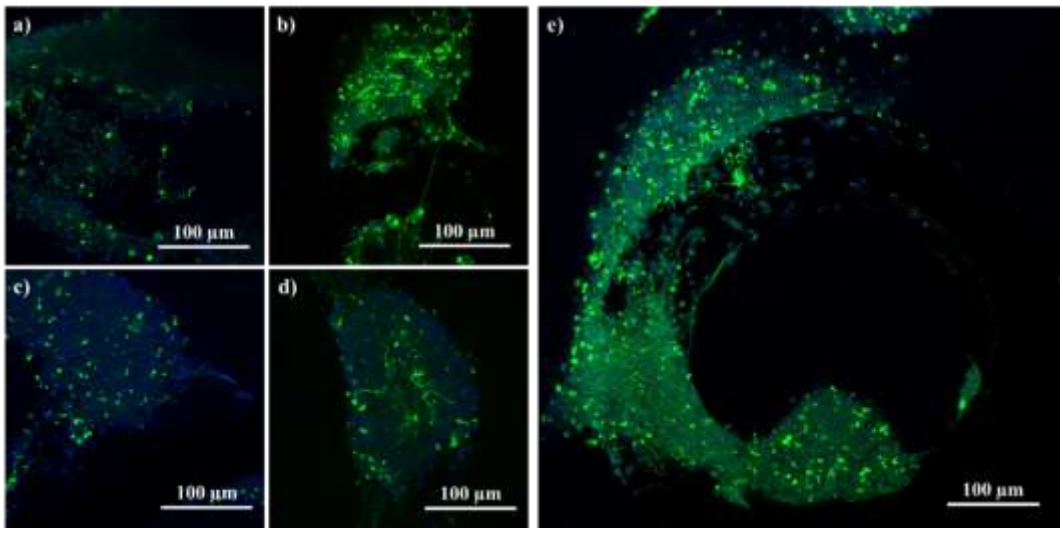

Figure 48 - Immunocytochemistry analysis at day 10 by Anti-Tuj1 (green) and synaptophysin (green) of the NE-4C neuronal cell line in four different CNTs morphologies; a) VA-CNTs forest, b) capillary-driven CNTs forest, c) VA-CNTs micropillars and (d and e) capillary driven CNTs micropillars.

3. Conclusion

In closing, it was demonstrated that all the prepared VA-CNTs patterns provided a suitable substrate for NE-4C cells adhesion, growth, and proliferation.

The viability results indicate that all the unmodified VA-CNTs samples were adequate for cell attachment and thereby growth or proliferation. Still, the neural stem cells demonstrated preference for particular patterns.

Overall, the sample with the highest cell viability is the capillary-driven VA-CNTs platform. NE-4C cells shown good proliferation and allocation uniquely to the micropillars walls and the outgrowth of neurites (also verified on the capillary driven VA-CNTs forest). This is justified by the physicochemical profiles of the capillary driven substrates, including their smaller hydrophobicity (Figure 32) and surface roughness, which resulted on a more suitable substrate for cell attachment, growth, and neurite formation.

Chapter 6 – Conclusions and future remarks

This master dissertation focused on the study and preparation of a biomimetic three-dimensional scaffold, comprising VA-CNTs and a GelMA-based hydrogel, for NSCs proliferation and differentiation. The aim to develop a platform that allows the regeneration of damaged spinal cord.

Continuous and patterned (micropillars) VA-CNTs forests were successfully grown by a T-CVD technique by using a multilayer catalyst ($Fe/SiO_2/Si$). The prepared samples were later submitted to a capillary driven process which resulted on twisted VA-CNTs micropillars and honeycomb-like morphologies on the CNTs forest substrate. A clear feature of these morphologies is their nanorough surface.

To assure the creation of a suitable environment for cells proliferation it was developed a photopolymerized GelMA solution. After some characterization assays, the hydrogel showed high degradation rate, due to the VA-CNTs presence on the biohybrid. This behavior can be attributed to the high ability of the CNTs to act as a radical scavengers interfering in this way with the process of photopolymerization [122].

Nonetheless, the alternative VA-CNTs platform without hydrogel, shown to be adequate for cell proliferation and differentiation. The characterization of the cell viability and morphology seeded on the CNTs forest and micropillars revealed the suitability of the substrate. Cell behavior determined differences between the substrate patterns and the morphologies processed by driven capillarity, revealing an overall preference for the capillary driven CNTs micropillars, where the formation of dendrites is achieved.

On further work, the use of free-standing VA-CNTs forests would grant a great advantage on the study of cell behavior on the prepared VA-CNTs. The thin carbon film is achieved by its controlled detachment from the $Fe/SiO_2/Si$ substrate, as illustrated on Figure 49. The alternative to the scaffolds used on this work would be that it allows the preparation of a platform for cell seeding without the presence of the Si wafer (that showed detrimental effects for neuronal cell adhesion and proliferation). This enables the possibility to create a conductive scaffold capable of electrically stimulate the seeded NSCs. Previous studies have already made evidence of this method, as Salehi M. *et al* [123] proven by the use of an

"electrically conductive biodegradable porous neural guidance conduit for transplantation of allogeneic Schwann cells", resulting a conduit with comparable nerve regeneration ability to the autograft. Mooney E. *et al* [124] has also studied the same effect on MSCs, and proven that by providing a biomimetic electroactive cue, the manipulation of the MSCs differentiation can be achieved by using carbon nanotubes properties as a medium or scaffold.

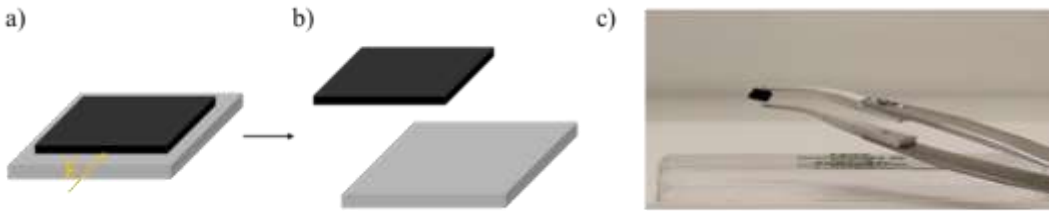

Figure 49 - Free-standing VA-CNTs forest.

Another alternative for the use of the GelMA based hydrogel, would be the use of alginate. This natural polymer brings the favorable characteristics such as biocompatibility, and biodegradability, tunable mechanical properties but also undergoes crosslinking in the presence of divalent Ca^{2+} ions, circumventing in this way the use of photo-crosslinkable hydrogels, not mentioning the fact that it has been broadly used for cell culture, combined with MWCNTs, due to their reinforcing capability [125].

Bibliography

[1] W. C. W. Chan, *Bio-Applications of Nanoparticles*, vol. 620. New York, NY: Springer New York, 2007.

[2] L. Dai, "From conventional technology to carbon nanotechnology. The fourth industrial revolution and the discoveries of C_{60}, carbon nanotube and nanodiamond.," in *Carbon Nanotechnology*, Elsevier, 2006, pp. 3–11.

[3] A. G. Mamalis, L. O. G. Vogtländer, and A. Markopoulos, "Nanotechnology and nanostructured materials: Trends in carbon nanotubes," *Precis. Eng.*, vol. 28, no. 1, pp. 16–30, 2004, doi: 10.1016/j.precisioneng.2002.11.002.

[4] "About Nanotechnology | National Nanotechnology Initiative." [Online]. Available: https://www.nano.gov/about-nanotechnology. [Accessed: 28-Oct-2021].

[5] H. Kroto, J. Heath, and S. O'Brien, "C60: Buckminsterfullerene," *Nature*, vol. 318, pp. 162–163, 1985, doi: 10.1038/318162a0.

[6] K. S. Novoselov *et al.*, "Electric field effect in atomically thin carbon films," *Science*, vol. 306, no. 5696, pp. 666–669, 2004, doi: 10.1126/SCIENCE.1102896.

[7] P. Woods, "The discovery of cosmic fullerenes," *Nat. Astron.*, vol. 4, no. 4, pp. 299–305, 2020, doi: 10.1038/s41550-020-1076-5.

[8] T. R. Shojaei *et al.*, "Applications of nanotechnology and carbon nanoparticles in agriculture," in *Synthesis, Technology and Applications of Carbon Nanomaterials*, Elsevier, 2018, pp. 247–277.

[9] J. R. Siqueira and O. N. Oliveira, "Carbon-based nanomaterials," in *Nanostructures*, Elsevier Inc., 2017, pp. 233–249.

[10] F. Ghaemi, M. Ali, R. Yunus, and R. N. Othman, "Synthesis of carbon nanomaterials using catalytic chemical vapor deposition technique," in *Synthesis, Technology and Applications of Carbon Nanomaterials*, Elsevier, 2018, pp. 1–27.

[11] J. Simon, E. Flahaut, and M. Golzio, "Overview of carbon nanotubes for biomedical applications," *Materials (Basel).*, vol. 12, no. 4, p. 624, 2019, doi: 10.3390/ma12040624.

[12] N. Choudhary, S. Hwang, and W. Choi, "Carbon Nanomaterials: A Review," in *Handbook of Nanomaterials Properties*, Springer Berlin Heidelberg, 2014, pp. 709–769.

[13] Y. Segawa, H. Ito, and K. Itami, "Structurally uniform and atomically precise carbon nanostructures," *Nat. Rev. Mater.*, vol. 1, no. 1, pp. 1–14, 2016, doi: 10.1038/natrevmats.2015.2.

[14] H. W. Kroto, "C_{60}: Buckminsterfullerene, The Celestial Sphere that Fell to Earth," *Angew. Chemie Int. Ed. English*, vol. 31, no. 2, pp. 111–129, Feb. 1992, doi: 10.1002/ANIE.199201113.

[15] P. Schwerdtfeger, L. N. Wirz, and J. Avery, "The topology of fullerenes," *Wiley*

Interdiscip. Rev. Comput. Mol. Sci., vol. 5, no. 1, pp. 96–145, 2015, doi: 10.1002/WCMS.1207.

[16] C. Redondo-Gómez, R. Leandro-Mora, D. Blanch-Bermúdez, C. Espinoza-Araya, D. Hidalgo-Barrantes, and J. Vega-Baudrit, "Recent Advances in Carbon Nanotubes for Nervous Tissue Regeneration," *Adv. Polym. Technol.*, vol. 2020, pp. 1–16, 2020, doi: 10.1155/2020/6861205.

[17] A. K. Geim and K. S. Novoselov, "The rise of graphene," *Nat. Mater.*, vol. 6, no. 3, pp. 183–191, 2007, doi: 10.1038/nmat1849.

[18] E. P. Randviir, D. A. C. Brownson, and C. E. Banks, "A decade of graphene research: production, applications and outlook," *Mater. Today*, vol. 17, no. 9, pp. 426–432, Nov. 2014, doi: 10.1016/J.MATTOD.2014.06.001.

[19] M. Pumera, "Graphene-based nanomaterials and their electrochemistry," *Chem. Soc. Rev.*, vol. 39, no. 11, pp. 4146–4157, 2010, doi: 10.1039/c002690p.

[20] C. Soldano, A. Mahmood, and E. Dujardin, "Production, properties and potential of graphene," *Carbon N. Y.*, vol. 48, no. 8, pp. 2127–2150, 2010, doi: 10.1016/J.CARBON.2010.01.058.

[21] P. C. Ma, N. A. Siddiqui, G. Marom, and J. K. Kim, "Dispersion and functionalization of carbon nanotubes for polymer-based nanocomposites: A review," *Compos. Part A Appl. Sci. Manuf.*, vol. 41, no. 10, pp. 1345–1367, 2010, doi: 10.1016/j.compositesa.2010.07.003.

[22] G. Hills *et al.*, "Modern microprocessor built from complementary carbon nanotube transistors," *Nature*, vol. 572, no. 7771, pp. 595–602, 2019, doi: 10.1038/s41586-019-1493-8.

[23] X. He *et al.*, "Carbon nanotubes as emerging quantum-light sources," *Nat. Mater.*, vol. 17, no. 8, pp. 663–670, 2018, doi: 10.1038/s41563-018-0109-2.

[24] K. Hara *et al.*, "Evaluation of CNT toxicity by comparison to tattoo ink," *Mater. Today*, vol. 14, no. 9, pp. 434–440, 2011, doi: 10.1016/S1369-7021(11)70188-2.

[25] B. Fadeel and K. Kostarelos, "Grouping all carbon nanotubes into a single substance category is scientifically unjustified," *Nat. Nanotechnol.*, vol. 15, no. 3, pp. 164–164, 2020, doi: 10.1038/s41565-020-0654-0.

[26] A. Bianco, K. Kostarelos, and M. Prato, "Making carbon nanotubes biocompatible and biodegradable," *Chem. Commun.*, vol. 47, no. 37, pp. 10182–10188, 2011, doi: 10.1039/C1CC13011K.

[27] S. Iijima, "Helical microtubules of graphitic carbon," *Nature*, vol. 354, no. 6348, pp. 56–58, 1991, doi: 10.1038/354056a0.

[28] V. Choudhary and A. Gupt, "Polymer/Carbon Nanotube Nanocomposites," in *Carbon Nanotubes - Polymer Nanocomposites*, InTech, 2011.

[29] B. Huang, "Carbon nanotubes and their polymeric composites: the applications in tissue engineering," *Biomanufacturing Rev.*, vol. 5, no. 3, pp. 1–26, 2020, doi: 10.1007/s40898-020-00009-x.

[30] B. Peng, M. Loscacio, and P. Zapol, “Measurements of near-ultimate strength for multiwalled carbon nanotubes and irradiation-induced crosslinking improvements.,” *Nat. Nanotech*, vol. 3, pp. 626–631, 2008, doi: 10.1038/nnano.2008.211.

[31] B. R. C. De Menezes, K. F. Rodrigues, B. C. D. S. Fonseca, R. G. Ribas, T. L. D. A. Montanheiro, and G. P. Thim, “Recent advances in the use of carbon nanotubes as smart biomaterials,” *J. Mater. Chem. B*, vol. 7, no. 9, pp. 1343–1360, 2019, doi: 10.1039/c8tb02419g.

[32] R. Rafiee, Ed., *Carbon Nanotube-Reinforced Polymers: From Nanoscale to Macroscale*. Elsevier, 2017.

[33] D. F. Williams, *The Williams Dictionary of Biomaterials*. Liverpool, UK: Liverpool University Press, 1999.

[34] M. F. L. De Volder, S. H. Tawfick, R. H. Baughman, and A. J. Hart, “Carbon nanotubes: Present and future commercial applications,” *Science (80-.).*, vol. 339, no. 6119, pp. 535–539, 2013, doi: 10.1126/science.1222453.

[35] E. Bekyarova *et al.*, “Applications of Carbon Nanotubes in Biotechnology and Biomedicine,” *J. Biomed. Nanotechnol.*, vol. 1, no. 1, pp. 3–17, 2006, doi: 10.1166/jbn.2005.004.

[36] T. de los Arcos *et al.*, “Strong influence of buffer layer type on carbon nanotube characteristics,” *Carbon N. Y.*, vol. 42, pp. 187–190, 2004, doi: 10.1016/j.carbon.2003.10.020.

[37] A. Facciolà *et al.*, “Carbon nanotubes and central nervous system: Environmental risks, toxicological aspects and future perspectives,” *Environ. Toxicol. Pharmacol.*, vol. 65, pp. 23–30, 2019, doi: 10.1016/j.etap.2018.11.006.

[38] K. Koziol, B. O. Boskovic, and N. Yahya, “Synthesis of carbon nanostructures by CVD method,” *Adv. Struct. Mater.*, vol. 5, pp. 23–49, 2011, doi: 10.1007/8611_2010_12.

[39] B. Zhao, L. Zhang, X. Wang, and J. Yang, “Surface functionalization of vertically-aligned carbon nanotube forests by radio-frequency Ar/O_2 plasma,” *Carbon N. Y.*, vol. 50, no. 8, pp. 2710–2716, Jul. 2012, doi: 10.1016/j.carbon.2012.02.029.

[40] M. Ahmad and S. R. P. Silva, “Low temperature growth of carbon nanotubes – A review,” *Carbon N. Y.*, vol. 158, pp. 24–44, 2020, doi: 10.1016/j.carbon.2019.11.061.

[41] A. Venkataraman, E. V. Amadi, Y. Chen, and C. Papadopoulos, “Carbon Nanotube Assembly and Integration for Applications,” *Nanoscale Res. Lett.*, vol. 14, no. 1, pp. 1–47, 2019, doi: 10.1186/s11671-019-3046-3.

[42] L. Meng, C. Fu, and Q. Lu, “Advanced technology for functionalization of carbon nanotubes,” *Prog. Nat. Sci.*, vol. 19, no. 7, pp. 801–810, 2009, doi: 10.1016/j.pnsc.2008.08.011.

[43] A. C. P. de Vasconcelos *et al.*, “In situ photocrosslinkable formulation of nanocomposites based on multi-walled carbon nanotubes and formononetin for potential application in spinal cord injury treatment,” *Nanomedicine Nanotechnology, Biol. Med.*, vol. 29, p. 102272, 2020, doi: 10.1016/j.nano.2020.102272.

[44] K. Balasubramanian and M. Burghard, “Chemically Functionalized Carbon Nanotubes,” *Small*, vol. 1, no. 2, pp. 180–192, 2005, doi: 10.1002/smll.200400118.

[45] T. Torres, “Carbon Nanotubes and Related Structures. Synthesis, Characterization, Functionalization, and Applications. Edited by Dirk M. Guldi and Nazario Martín.,” *Angew. Chemie Int. Ed.*, vol. 50, no. 7, pp. 1473–1474, 2011, doi: 10.1002/anie.201006930.

[46] A. Vashist *et al.*, “Advances in Carbon Nanotubes–Hydrogel Hybrids in Nanomedicine for Therapeutics,” *Adv. Healthc. Mater.*, vol. 7, no. 9, 2018, doi: 10.1002/adhm.201701213.

[47] J. Saroia, W. Yanen, Q. Wei, K. Zhang, T. Lu, and B. Zhang, “A review on biocompatibility nature of hydrogels with 3D printing techniques, tissue engineering application and its future prospective,” *Bio-Design Manuf.*, vol. 1, no. 4, pp. 265–279, 2018, doi: 10.1007/s42242-018-0029-7.

[48] X. Yuan, X. Zhang, L. Sun, Y. Wei, and X. Wei, “Cellular Toxicity and Immunological Effects of Carbon-based Nanomaterials,” *Part. Fibre Toxicol.*, vol. 16, no. 1, pp. 1–27, 2019, doi: 10.1186/S12989-019-0299-Z.

[49] T. V. Galassi, M. Antman-Passig, Z. Yaari, J. Jessurun, R. E. Schwartz, and D. A. Heller, “Long-term in vivo biocompatibility of single-walled carbon nanotubes,” *PLoS One*, vol. 15, no. 5, p. 22, 2020, doi: 10.1371/JOURNAL.PONE.0226791.

[50] S. Fiorito, A. Serafino, F. Andreola, A. Togna, and G. Togna, “Toxicity and biocompatibility of carbon nanoparticles,” *J. Nanosci. Nanotechnol.*, vol. 6, no. 3, pp. 591–599, 2006, doi: 10.1166/jnn.2006.125.

[51] E. M, G. M, and H. K, “A review of toxicity studies of single-walled carbon nanotubes in laboratory animals,” *Regul. Toxicol. Pharmacol.*, vol. 74, pp. 42–63, 2016, doi: 10.1016/J.YRTPH.2015.11.015.

[52] A. Erdely *et al.*, “Identification of systemic markers from a pulmonary carbon nanotube exposure,” *J. Occup. Environ. Med.*, vol. 53, no. 6, 2011, doi: 10.1097/JOM.0B013E31821AD724.

[53] S. T. Yang *et al.*, “Long-term accumulation and low toxicity of single-walled carbon nanotubes in intravenously exposed mice,” *Toxicol. Lett.*, vol. 181, no. 3, pp. 182–189, 2008, doi: 10.1016/J.TOXLET.2008.07.020.

[54] E. A *et al.*, “Cross-talk between lung and systemic circulation during carbon nanotube respiratory exposure. Potential biomarkers,” *Nano Lett.*, vol. 9, no. 1, pp. 36–43, 2009, doi: 10.1021/NL801828Z.

[55] Y. Bai *et al.*, “Repeated administrations of carbon nanotubes in male mice cause reversible testis damage without affecting fertility,” *Nat. Nanotechnol.*, vol. 5, no. 9, pp. 683–689, 2010, doi: 10.1038/nnano.2010.153.

[56] E. Cruces, A. C. Barrios, Y. P. Cahue, B. Januszewski, L. M. Gilbertson, and F. Perreault, “Similar toxicity mechanisms between graphene oxide and oxidized multi-walled carbon nanotubes in Microcystis aeruginosa,” *Chemosphere*, vol. 265, p. 11, 2021, doi: 10.1016/j.chemosphere.2020.129137.

[57] D. W. Porter *et al.*, “Mouse pulmonary dose- and time course-responses induced by exposure to multi-walled carbon nanotubes,” *Toxicology*, vol. 269, no. 2–3, pp. 136–147, 2010, doi: 10.1016/j.tox.2009.10.017.

[58] N. Kobayashi, H. Izumi, and Y. Morimoto, “Review of toxicity studies of carbon nanotubes,” *J. Occup. Health*, vol. 59, no. 5, pp. 394–407, 2017, doi: 10.1539/joh.17-0089-RA.

[59] B. Ouyang *et al.*, “Toxicity and environmental impact of multi-walled carbon nanotubes to nitrogen-fixing bacterium Azotobacter chroococcum,” *J. Environ. Chem. Eng.*, vol. 9, no. 4, p. 105291, 2021, doi: 10.1016/j.jece.2021.105291.

[60] K. Donaldson, V. Stone, C. L. Tran, W. Kreyling, and P. J. A. Borm, “Nanotoxicology,” *Occup. Environ. Med.*, vol. 61, no. 9, pp. 727–728, 2004, doi: 10.1136/OEM.2004.013243.

[61] S. Alidori *et al.*, “Carbon nanotubes exhibit fibrillar pharmacology in primates,” *PLoS One*, vol. 12, no. 8, p. 183902, 2017, doi: 10.1371/JOURNAL.PONE.0183902.

[62] X. Lu *et al.*, “Long-term pulmonary exposure to multi-walled carbon nanotubes promotes breast cancer metastatic cascades,” *Nat. Nanotechnol.*, vol. 14, no. 7, pp. 719–727, 2019, doi: 10.1038/s41565-019-0472-4.

[63] “The risks of nanomaterial risk assessment,” *Nat. Nanotechnol.*, vol. 15, no. 3, pp. 163–163, 2020, doi: 10.1038/s41565-020-0658-9.

[64] A. J. Ryan *et al.*, “Electroconductive Biohybrid Collagen/Pristine Graphene Composite Biomaterials with Enhanced Biological Activity,” *Adv. Mater.*, vol. 30, no. 15, 2018, doi: 10.1002/adma.201706442.

[65] M. A. Correa-Duarte, N. Wagner, J. Rojas-Chapana, C. Morsczeck, M. Thie, and M. Giersig, “Fabrication and biocompatibility of carbon nanotube-based 3D networks as scaffolds for cell seeding and growth,” *Nano Lett.*, vol. 4, no. 11, pp. 2233–2236, 2004, doi: 10.1021/nl048574f.

[66] V. C. Bitirim, G. Kucukayan-Dogu, E. Bengu, and K. C. Akcali, “Patterned carbon nanotubes as a new three-dimensional scaffold for mesenchymal stem cells,” *Mater. Sci. Eng. C*, vol. 33, no. 5, pp. 3054–3060, 2013, doi: 10.1016/j.msec.2013.03.044.

[67] F. Wu, J. Zheng, Z. Li, and M. Liu, “Halloysite nanotubes coated 3D printed PLA pattern for guiding human mesenchymal stem cells (hMSCs) orientation,” *Chem. Eng. J.*, vol. 359, pp. 672–683, 2019, doi: 10.1016/j.cej.2018.11.145.

[68] M. De Volder *et al.*, “Diverse 3D microarchitectures made by capillary forming of carbon nanotubes,” *Adv. Mater.*, vol. 22, no. 39, pp. 4384–4389, 2010, doi: 10.1002/adma.201001893.

[69] T. Bedir, S. Ulag, C. B. Ustundag, and O. Gunduz, “3D bioprinting applications in neural tissue engineering for spinal cord injury repair,” *Mater. Sci. Eng. C*, vol. 110, p. 110741, 2020, doi: 10.1016/j.msec.2020.110741.

[70] S. R. Caliari and J. A. Burdick, “A practical guide to hydrogels for cell culture,” *Nat. Methods*, vol. 13, no. 5, pp. 405–414, 2016, doi: 10.1038/nmeth.3839.

[71] N. Ghane, M. H. Beigi, S. Labbaf, M. H. Nasr-Esfahani, and A. Kiani, “Design of hydrogel-based scaffolds for the treatment of spinal cord injuries,” *J. Mater. Chem. B*, vol. 8, no. 47, pp. 10712–10738, 2020, doi: 10.1039/d0tb01842b.

[72] W. J, T. L, C. N, R. S, and M. X, “The cellular response of nerve cells on poly-l-lysine coated PLGA-MWCNTs aligned nanofibers under electrical stimulation,” *Mater. Sci. Eng. C. Mater. Biol. Appl.*, vol. 91, pp. 715–726, 2018, doi: 10.1016/J.MSEC.2018.06.025.

[73] J. Li, C. Wu, P. K. Chu, and M. Gelinsky, “3D printing of hydrogels: Rational design strategies and emerging biomedical applications,” *Mater. Sci. Eng. R Reports*, vol. 140, p. 100543, 2020, doi: 10.1016/j.mser.2020.100543.

[74] H. Shirahama, B. H. Lee, L. P. Tan, and N. J. Cho, “Precise tuning of facile one-pot gelatin methacryloyl (GelMA) synthesis,” *Sci. Rep.*, vol. 6, no. 1, pp. 1–11, 2016, doi: 10.1038/srep31036.

[75] J. Saroia, W. Yanen, Q. Wei, K. Zhang, T. Lu, and B. Zhang, “A review on biocompatibility nature of hydrogels with 3D printing techniques, tissue engineering application and its future prospective,” *Bio-Design Manuf.*, vol. 1, no. 4, pp. 265–279, 2018, doi: 10.1007/s42242-018-0029-7.

[76] A. Sun *et al.*, “Current research progress of photopolymerized hydrogels in tissue engineering,” *Chinese Chem. Lett.*, vol. 32, no. 7, pp. 2117–2126, 2021, doi: 10.1016/J.CCLET.2021.01.048.

[77] W. Zhu, B. T. Harris, and L. G. Zhang, “Gelatin methacrylamide hydrogel with graphene nanoplatelets for neural cell-laden 3D bioprinting,” in *Proceedings of the Annual International Conference of the IEEE Engineering in Medicine and Biology Society, EMBS*, 2016, pp. 4185–4188, doi: 10.1109/EMBC.2016.7591649.

[78] K. K. Bokara, J. Y. Kim, Y. Il Lee, K. Yun, T. J. Webster, and J. E. Lee, “Biocompatability of carbon nanotubes with stem cells to treat CNS injuries,” *Anat. Cell Biol.*, vol. 46, no. 2, p. 85, 2013, doi: 10.5115/acb.2013.46.2.85.

[79] Y. Tang, P. Yu, and L. Cheng, “Current progress in the derivation & therapeutic application of neural stem cells,” *Cell Death Dis.*, vol. 8, no. 10, p. 3108, 2017, doi: 10.1038/cddis.2017.504.

[80] J. R. Lee, S. Ryu, S. Kim, and B. S. Kim, “Behaviors of stem cells on carbon nanotube,” *Biomater. Res.*, vol. 19, no. 1, 2015, doi: 10.1186/s40824-014-0024-9.

[81] M. MP, H. RC, and R. AM, “Molecular functionalization of carbon nanotubes and use as substrates for neuronal growth,” *J. Mol. Neurosci.*, vol. 14, no. 3, pp. 175–182, 2000, doi: 10.1385/JMN:14:3:175.

[82] H. N and T. R, “Molecular motors and mechanisms of directional transport in neurons,” *Nat. Rev. Neurosci.*, vol. 6, no. 3, pp. 201–214, 2005, doi: 10.1038/NRN1624.

[83] R. Sorkin *et al.*, “Process entanglement as a neuronal anchorage mechanism to rough surfaces,” *Nanotechnology*, vol. 20, no. 1, p. 015101, 2009, doi: 10.1088/0957-4484/20/1/015101.

[84] Z. Zhou *et al.*, “Effective nerve cell modulation by electrical stimulation of carbon nanotube embedded conductive polymeric scaffolds,” *Biomater. Sci.*, vol. 6, no. 9, pp. 2375–2385, 2018, doi: 10.1039/C8BM00553B.

[85] X. Zhang, S. Prasad, S. Niyogi, A. Morgan, M. Ozkan, and C. S. Ozkan, “Guided neurite growth on patterned carbon nanotubes,” *Sensors Actuators B Chem.*, vol. 106, no. 2, pp. 843–850, 2005, doi: 10.1016/J.SNB.2004.10.039.

[86] J. Groll *et al.*, “A definition of bioinks and their distinction from biomaterial inks,” *Biofabrication*, vol. 11, no. 1, p. 013001, 2018, doi: 10.1088/1758-5090/AAEC52.

[87] R. Nisticò, D. Scalarone, and G. Magnacca, “Sol-gel chemistry, templating and spin-coating deposition: A combined approach to control in a simple way the porosity of inorganic thin films/coatings,” *Microporous Mesoporous Mater.*, vol. 248, pp. 18–29, 2017, doi: 10.1016/J.MICROMESO.2017.04.017.

[88] C. Wang, X. Chen, F. Chen, and J. Shao, “Organic photodetectors based on copper phthalocyanine films prepared by a multiple drop casting method,” *Org. Electron.*, vol. 66, pp. 183–187, 2019, doi: 10.1016/J.ORGEL.2018.12.035.

[89] O. A. Hamid, H. M. Eltaher, V. Sottile, and J. Yang, “3D bioprinting of a stem cell-laden, multi-material tubular composite: An approach for spinal cord repair,” *Mater. Sci. Eng. C*, p. 111707, 2020, doi: 10.1016/j.msec.2020.111707.

[90] J. Koffler *et al.*, “Biomimetic 3D-printed scaffolds for spinal cord injury repair,” *Nat. Med.*, vol. 25, no. 2, pp. 263–269, 2019, doi: 10.1038/s41591-018-0296-z.

[91] H. Cui *et al.*, “Direct 3D printing of a tough hydrogel incorporated with carbon nanotubes for bone regeneration,” *J. Mater. Chem. B*, vol. 7, no. 45, pp. 7207–7217, 2019, doi: 10.1039/c9tb01494b.

[92] J. Malda *et al.*, “25th Anniversary Article: Engineering Hydrogels for Biofabrication,” *Adv. Mater.*, vol. 25, no. 36, pp. 5011–5028, Sep. 2013, doi: 10.1002/ADMA.201302042.

[93] V. Lovat *et al.*, “Carbon nanotube substrates boost neuronal electrical signaling,” *Nano Lett.*, vol. 5, no. 6, pp. 1107–1110, 2005, doi: 10.1021/nl050637m.

[94] W. C. Chang, M. Kliot, and D. W. Sretavan, “Microtechnology and nanotechnology in nerve repair,” *Neurol. Res.*, vol. 30, no. 10, pp. 1053–1062, 2008, doi: 10.1179/174313208X362532.

[95] N. B. Chauhan, H. M. Figlewicz, and T. Khan, “Carbon filaments direct the growth of postlesional plastic axons after spinal cord injury,” *Int. J. Dev. Neurosci.*, vol. 17, no. 3, pp. 255–264, 1999, doi: 10.1016/S0736-5748(99)00003-9.

[96] I. Calaresu *et al.*, “Polystyrene Nanopillars with Inbuilt Carbon Nanotubes Enable Synaptic Modulation and Stimulation in Interfaced Neuronal Networks,” *Adv. Mater. Interfaces*, vol. 8, no. 9, p. 2002121, 2021, doi: 10.1002/admi.202002121.

[97] P. NP *et al.*, “Transparent carbon nanotubes promote the outgrowth of enthorino-dentate projections in lesioned organ slice cultures,” *Dev. Neurobiol.*, vol. 80, no. 9–10, pp. 316–331, 2020, doi: 10.1002/DNEU.22711.

[98] S. Imani, Z. Zagari, S. R. Zarchi, M. Jorjani, and S. Nasri, “Functional Recovery of Carbon Nanotube/Nafion Nanocomposite in Rat Model of Spinal Cord Injury,” *Artif. Cells, Nanomedicine, Biotechnol.*, vol. 44, no. 1, pp. 144–149, 2015, doi: 10.3109/21691401.2015.1024844.

[99] G. S. Lorite *et al.*, “Carbon nanotube micropillars trigger guided growth of complex human neural stem cells networks,” *Nano Res.*, vol. 12, no. 11, pp. 2894–2899, 2019, doi: 10.1007/S12274-019-2533-2.

[100] F. Yang, C. Y. Xu, M. Kotaki, S. Wang, and S. Ramakrishna, “Characterization of neural stem cells on electrospun poly(L-lactic acid) nanofibrous scaffold,” *J. Biomater. Sci. Polym. Ed.*, vol. 15, no. 12, pp. 1483–1497, 2004, doi: 10.1163/1568562042459733.

[101] A. Subramanian, U. M. Krishnan, and S. Sethuraman, “Development of biomaterial scaffold for nerve tissue engineering: Biomaterial mediated neural regeneration.,” *J. Biomed. Sci.*, vol. 16, no. 1, p. 108, 2009, doi: 10.1186/1423-0127-16-108.

[102] X. Liu, J. C. Kim, A. L. Miller, B. E. Waletzki, and L. Lu, “Electrically conductive nanocomposite hydrogels embedded with functionalized carbon nanotubes for spinal cord injury,” *New J. Chem.*, vol. 42, no. 21, pp. 17671–17681, 2018, doi: 10.1039/C8NJ03038C.

[103] M. Imaninezhad, K. Pemberton, F. Xu, K. Kalinowski, R. Bera, and S. P. Zustiak, “Directed and enhanced neurite outgrowth following exogenous electrical stimulation on carbon nanotube-hydrogel composites,” *J. Neural Eng.*, vol. 15, no. 5, p. 056034, 2018, doi: 10.1088/1741-2552/aad65b.

[104] M. F. L. De Volder, S. J. Park, S. H. Tawfick, D. O. Vidaud, and A. J. Hart, “Fabrication and electrical integration of robust carbon nanotube micropillars by self-directed elastocapillary densification,” *J. Micromechanics Microengineering*, vol. 21, no. 4, 2011, doi: 10.1088/0960-1317/21/4/045033.

[105] N. Chakrapani, B. Wei, A. Carrillo, P. M. Ajayan, and R. S. Kane, “Capillarity-driven assembly of two-dimensional cellular carbon nanotube foams,” *Proc. Natl. Acad. Sci. U. S. A.*, vol. 101, no. 12, pp. 4009–4012, 2004, doi: 10.1073/pnas.0400734101.

[106] M. S. Dresselhaus, G. Dresselhaus, R. Saito, and A. Jorio, “Raman spectroscopy of carbon nanotubes,” *Phys. Rep.*, vol. 409, no. 2, pp. 47–99, 2005, doi: 10.1016/J.PHYSREP.2004.10.006.

[107] J. Choo *et al.*, “Investigation on the temperature-dependent growth rate of carbon nanotubes using chemical vapor deposition of ferrocene and acetylene,” doi: 10.1016/j.cplett.2004.11.113.

[108] Z. Tao, P. Wang, F. Zhang, and J. Na, “Carbon Nanotube Thin Film-Supported Fibroblast and Pluripotent Stem Cell Growth,” *Bionanoscience*, vol. 4, no. 3, pp. 288–300, 2014, doi: 10.1007/S12668-014-0139-4.

[109] M. Pavese, S. Musso, S. Bianco, M. Giorcelli, and N. Pugno, “An analysis of carbon nanotube structure wettability before and after oxidation treatment,” *J. Phys. Condens. Matter*, vol. 20, no. 47, 2008, doi: 10.1088/0953-8984/20/47/474206.

[110] L. Martineau, H. T. Peng, and P. N. Shek, “Development of a novel biomaterial: Part II. Evaluation of a photo cross-linking method Defence R&D Canada-Toronto DEFENCE DÉFENSE &,” 2005.

[111] K. Rahali *et al.*, “Synthesis and Characterization of Nanofunctionalized Gelatin Methacrylate Hydrogels,” *Int. J. Mol. Sci.*, vol. 18, no. 12, p. 2675, 2017, doi: 10.3390/IJMS18122675.

[112] A. C. P. de Vasconcelos *et al.*, “In situ photocrosslinkable formulation of nanocomposites based on multi-walled carbon nanotubes and formononetin for potential application in spinal cord injury treatment,” *Nanomedicine Nanotechnology, Biol. Med.*, vol. 29, p. 102272, 2020, doi: 10.1016/J.NANO.2020.102272.

[113] U. JS, D. MD, W. JA, and M. WM, “Essential design considerations for the resazurin reduction assay to noninvasively quantify cell expansion within perfused extracellular matrix scaffolds,” *Biomaterials*, vol. 129, pp. 163–175, 2017, doi: 10.1016/J.BIOMATERIALS.2017.02.015.

[114] X. Xie *et al.*, “Enhancing the Nanomaterial Bio-Interface by Addition of Mesoscale Secondary Features: Crinkling of Carbon Nanotube Films To Create Subcellular Ridges,” *ACS Nano*, vol. 8, no. 12, pp. 11958–11965, 2014, doi: 10.1021/NN504898P.

[115] Y. Nho, J. Y. Kim, D. Khang, T. J. Webster, and J. E. Lee, “Adsorption of mesenchymal stem cells and cortical neural stem cells on carbon nanotube/polycarbonate urethane,” *Nanomedicine*, vol. 5, no. 3, pp. 409–417, 2010, doi: 10.2217/NNM.10.16.

[116] S. U. Moon *et al.*, “Carbon nanotubes impregnated with subventricular zone neural progenitor cells promotes recovery from stroke,” *Int. J. Nanomedicine*, vol. 7, pp. 2751–2765, 2012, doi: 10.2147/IJN.S30273.

[117] G. Courtine and M. V. Sofroniew, “Spinal cord repair: advances in biology and technology,” *Nat. Med. 2019 256*, vol. 25, no. 6, pp. 898–908, 2019, doi: 10.1038/s41591-019-0475-6.

[118] R. White, E., L. Jakeman, and B., “Don’t fence me in: Harnessing the beneficial roles of astrocytes for spinal cord repair,” *Restor. Neurol. Neurosci.*, vol. 26, no. 2–3, pp. 197–214, 2008.

[119] S. Okada, M. Hara, K. Kobayakawa, Y. Matsumoto, and Y. Nakashima, “Astrocyte reactivity and astrogliosis after spinal cord injury,” *Neurosci. Res.*, vol. 126, pp. 39–43, 2018, doi: 10.1016/J.NEURES.2017.10.004.

[120] G. M. Cooper, “Cell Proliferation in Development and Differentiation,” in *The Cell: A Molecular Approach. 2nd edition*, Sinauer Associates, 2000.

[121] S. Usmani *et al.*, “3D meshes of carbon nanotubes guide functional reconnection of segregated spinal explants,” *Sci. Adv.*, vol. 2, no. 7, 2016, doi: 10.1126/SCIADV.1600087.

[122] G. Gonçalves, S. M. A. Cruz, A. Ramalho, J. Grácio, and P. A. A. P. Marques, “Graphene oxide versus functionalized carbon nanotubes as a reinforcing agent in a

PMMA/HA bone cement," *Nanoscale*, vol. 4, no. 9, pp. 2937–2945, 2012, doi: 10.1039/C2NR30303E.

[123] M. Salehi *et al.*, "Sciatic nerve regeneration by transplantation of Schwann cells via erythropoietin controlled-releasing polylactic acid/multiwalled carbon nanotubes/gelatin nanofibrils neural guidance conduit," *J. Biomed. Mater. Res. - Part B Appl. Biomater.*, vol. 106, no. 4, pp. 1463–1476, 2018, doi: 10.1002/JBM.B.33952.

[124] E. Mooney *et al.*, "The electrical stimulation of carbon nanotubes to provide a cardiomimetic cue to MSCs," *Biomaterials*, vol. 33, pp. 6132–6139, 2012, doi: 10.1016/j.biomaterials.2012.05.032.

[125] B. Joddar, E. Garcia, A. Casas, and C. M. Stewart, "Development of functionalized multi-walled carbon-nanotube-based alginate hydrogels for enabling biomimetic technologies," *Sci. Reports 2016 61*, vol. 6, no. 1, pp. 1–12, 2016, doi: 10.1038/srep32456.